ISSN 1220-8434 VOLUME 17, 2009

ACTA TRIBOLOGICA

University of Suceava, Romania

ACTA TRIBOLOGICA

Volume 17, 2009

ACTA TRIBOLOGICA

A Journal on the Science of Contact Mechanics, Friction, Lubrication, Wear, Micro/Nano Tribology, and Biotribology

Volume 17, 2009

University of Suceava, Romania

Published by the Applied Mechanics Section of the University of Suceava

University "Stefan cel Mare" of Suceava Publishing House

13th University Street, Suceava, 720229, Suceava, ROMANIA
Phone: (40) – 0230 – 216 – 147 int. 273, E-mail: editura@usv.ro

ACTA TRIBOLOGICA VOLUME 17, 2009

CONTENTS

ISSN 1220 - 8434

ACTA TRIBOLOGICA
Volume 17, (2009), 1-5

Emanuel DIACONESCU

Vlad – Flaviu ZEGREAN
email: *zegrean@fim.usv.ro*

Marilena GLOVNEA

Department of Applied Mechanics,
University "Stefan cel Mare" of Suceava,
ROMANIA

SHEAR PROPERTIES OF MOLECULAR LIQUID NEAR A METALLIC WALL

Although the thickness of EHD oil films should vanish at very low rolling speeds, experimental investigations indicate that often this thickness does not fall below a remnant value of 10-30 nm. Initially, this phenomenon was attributed to a much higher viscosity near the wall than in the bulk, according to an empirical formula. Recently, theoretical physical background of the phenomenon was advanced by means of molecule-wall interaction potential. It was shown that, besides viscosity, shear modulus and limiting shear stress are enhanced in the neighborhood of the wall. These theoretical findings predict correctly experimentally found thin film thickness. New experimental evidence is needed to support theoretical results. This paper provides experimental results concerning the evaluation of structural flow units, minimum intermolecular potential and limiting shear stress in thin layers.
Keywords: liquid-wall interaction, viscosity, shear modulus, limiting shear stress, molecular layer

1. INTRODUCTION

EHL theory predicts that if the relative rolling speed of two surfaces tends towards zero, the film thickness formed between them must vanish. Experimental results obtained by Johnson, Waite and Spikes [1], Cann and Spikes [2], Luo and Wen [3], and others show that a lubricant film of about 10…30 nm or thicker is preserved between the surfaces at very low speeds. Zhang, Luo and Wen [4,5] attributed this phenomenon to the existence of an ordered lubricant film, caused by the interaction between liquid molecules and the metallic surface, which is placed between central EHD film and the adsorbed layer. To predict theoretically the thickness of this layer, they used an empirical equation for the viscosity and a numerical program written for one-dimensional flow. They carried out experimental investigations of thin film thickness using a ball on disk apparatus and they found a good agreement with the numerical results.

By noting the insufficiency of an empirical formula for the viscosity in the neighborhood of the wall, Diaconescu [6,7] approached the subject by using the molecule-wall interaction potential and a general theoretical viscosity equation. The viscosity is found to decrease exponentially with the distance from the wall as shown in Figure 1. This distance is expressed by the number of molecular layers from the wall and the dimensionless viscosity is referenced by the bulk viscosity.

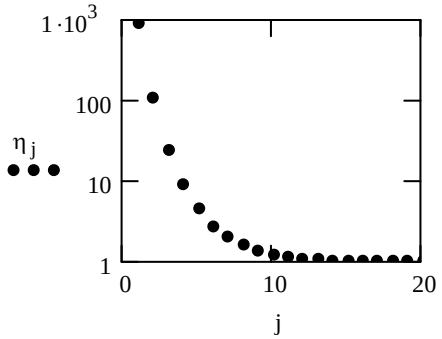

Figure 1. The dependence of viscosity on the number of molecular layer from the metallic surface

Using a molecular theory previously advanced for the solid like properties of molecular substances, [8], and the molecule-wall interaction potential, [6], Diaconescu, [7] found that both shear modulus and limiting shear stress increase in the wall vicinity with respect to their bulk values in the same fashion, as shown in Figure 2.

Again, the distance from the wall is indicated by the number of the molecular layers, whereas dimensionless shear modulus g, is referenced to its bulk value.

The advanced theory shows that the wall viscosity is hundred times higher that in the bulk, whereas the wall shear modulus as well as the wall limiting shear stress exceed by a few times their corresponding values in the bulk.

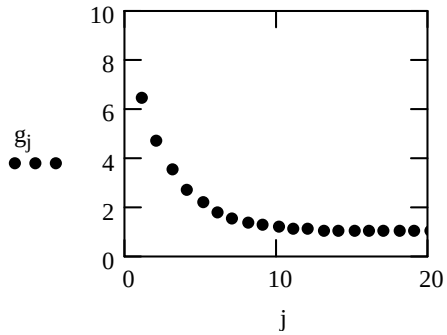

Figure 2. Dimensionless variation of shear modulus and limiting shear stress with the number of molecular layer from the metallic surface

These values show that, compared to the bulk, the liquid flow is impeded in the neighborhood of the wall, as well as its elastic or plastic shear. This suggests that the supplementary attraction in the wall neighborhood generates a thin attached layer on each wall, measuring 6 to 14 molecular layers. These attached layers are responsible for remnant oil film. At very low rolling speeds, the thickness of this film is the sum of the thicknesses of the layers attached to the wall. If the speed is high enough, an EHD film is formed between attached layers. Consequently, total film thickness is the sum of remnant and EHD film thicknesses. The effects of pressure and temperature upon nanometric film thickness enter by their influence upon bulk shear properties of the liquid. This conclusion and the predicted dependence of thin EHD oil films on rolling speed agree very well with the experimental results of Zhang, Luo, and Wen [4,5]. This agreement suggests that the advanced theory is qualitatively correct. Nevertheless, supplementary experimental confirmation is needed, especially concerning the shear properties of molecular liquids in the neighborhood of a metallic wall. This paper aims to provide new experimental evidence into the subject, as well as corresponding experimental procedures.

2. EXPERIMENTAL RESULTS

2.1 Evaluation of structural flow units

A unanimous point of view upon the structural flow units in EHD oil films was not achieved yet. These may be single molecules, molecular clusters or molecular segments. According to Hirst and Moore, [9], molecular clustering occurs at low temperatures, which dissociate into molecules as the temperature rises. When the liquid possesses branched molecules, at certain moments, some of these branches can flow individually. To clarify the subject, new evidence is needed.

Experimental investigations on an atomic force microscope (AFM) were performed to identify the flow units in liquid paraffin, as well as their average dimension.

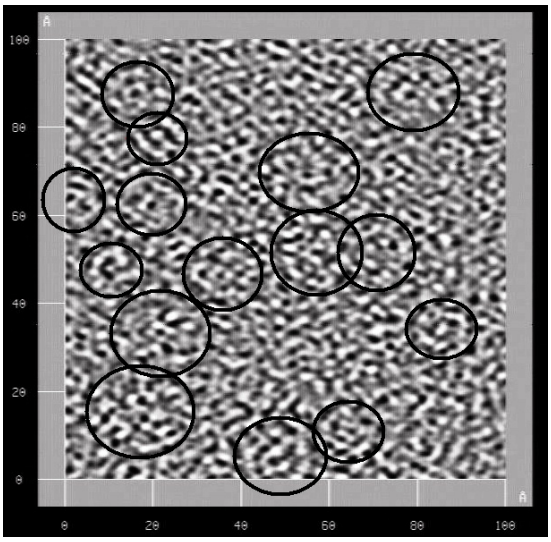

Figure 3. Typical scanned image of solid paraffin film

To this end, a tiny amount of melted paraffin was let to drop on a cooled mica surface, thus freezing rapidly while preserving the flow structural units. In its turn, the mica layer was fixed on a cool metallic surface. Then, the surface of solid paraffin film was scanned by aid of a non-contact AFM. A typical example for obtained images is depicted in Figure 3.

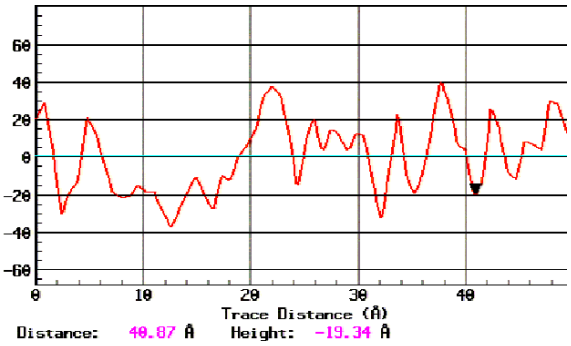

Figure 4. Paraffin surface profile

It can be seen that paraffin molecules and their branches tend to pack into nearly spherical clusters having a diameter of 20…25 Å. For a better view, some of these are circled by black lines. Nevertheless, individual molecules fill the space between the clusters. A 40 Å long surface profile, shown in Figure 4, allows assessment of the average value the diameter of structural flow unit. This was found to be 4.47 Å.

2.2 Evaluation of minimum intermolecular potential

The minimum intermolecular potential, a key parameter for liquid behavior, can be determined

either by measuring the maximum intermolecular force or by determining the oil surface tension.

The maximum intermolecular forces depend on the parameters of intermolecular potential. It occurs when the intermolecular distance reaches the following value:

$$r_m = r_{pT}\sqrt[6]{\frac{13}{7}}, \quad (1)$$

where r_{pT} is the equilibrium intermolecular distance at pressure p and temperature T. Maximum value of intermolecular force is:

$$f_{max} = 2.6899 k_e k_{pT} \frac{\varepsilon}{r_m}, \quad (2)$$

in which ε is the minimum value of intermolecular potential and k_e, k_{pT} are coefficients defined in [8]. It is obvious that the knowledge of maximum intermolecular force f_{max} yields the minimum intermolecular potential ε if r_m is known.

A very simple experiment illustrated in Figure 5 was used to find f_{max}. A flat glass disk has its lower face in contact with the investigated oil.

A very slowly increasing force is applied upwards on the disk via an accurate AMETEK micro-dynamometer. This is able to record the peak value of the transmitted force. This force is the sum of maximum intermolecular forces acting upon all structural units. After the average diameter of these units and the disk diameter are known, f_{max} can be easily assessed.

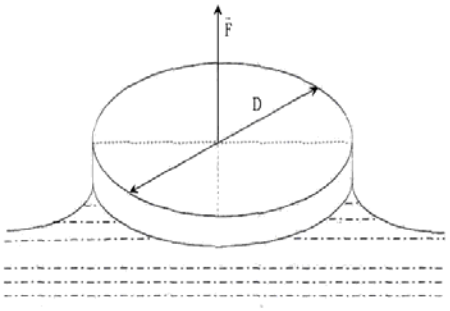

Figure 5. A simple experiment to measure maximum intermolecular force

The experiments are carried out at atmospheric pressure and at several temperatures, on two lubricating oils, namely T90EP2 (diamonds in Figure 6) and 20W40 (squares in Figure 6). The results show that the maximum value of intermolecular forces has an order of magnitude of $(4\ldots4.5)10^{-18}$N, depending on oil and temperature. As shown in Figure 6, maximum intermolecular force decreases nearly linearly with temperature.

The second procedure for finding the minimum intermolecular potential is the measurement of surface tension. To this end, oil surface tension was measured under constant temperature by using successively two parallel glass plates, separated by various small distances (0.02 mm, 0.126 mm, 0.2 mm and 0.28mm) and measuring accurately the height of raising column. For instance, in the case of the oil T90EP2 at 22ºC, all measurements supplied the same surface tension, σ=47.88 N/m. The minimum value of intermolecular potential is found in terms of surface tension from Stefan's formula:

$$\varepsilon = C_s \cdot \sigma \cdot \omega^{\frac{2}{3}}, \quad (3)$$

where C_s=6.97 is Stefan's constant and ω is the molar volume, found from the intermolecular distance.

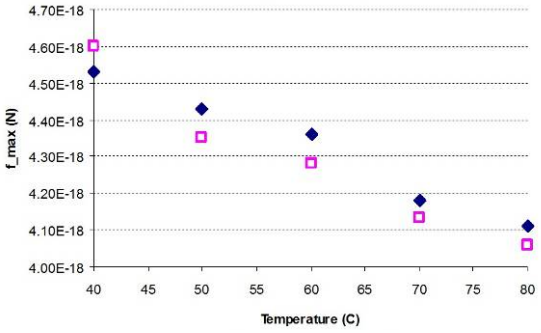

Figure 6. Dependence of maximum intermolecular force on temperature for two oils

Resulting value of minimum intermolecular potential is $\varepsilon=8.343\cdot10^{-17}$ J for T90EP2 and $\varepsilon=8.158\cdot10^{-17}$ J for 20W40. These values seem to be correct when compared to known values for simple hydrocarbons.

2.2 Evaluation of limiting shear stress in thin layers

Two sets of experiments were carried out to find the limiting shear stress of lubricating oils in thin layers. The first seeks to find the dependence of this stress on pressure at constant temperature, whereas the second operates at various temperatures, but under atmospheric pressure.

In the first case, schematically shown in Figure 7, a very thin uniformly thick layer of oil is entrapped between two thick flat glass plates pressed by dead-weights. The ratio between this load and nominal contact area yields the pressure acting between the plates. The upper plate is connected by a thin string to the sensor of a fixed micro-dynamometer. The bottom plate can move along a fixed sliding guide. A slowly increasing force is

applied to the lower plate. The dynamometer records the peak value of the tangential force transmitted through the oil. By dividing this maximum force to contact area, one finds the average value of limiting shear stress. The experimental results are plotted in Figure 8. It is obvious that the limiting shear stress increases linearly with pressure, as in the bulk:

$$\tau_\ell = a + b \cdot p \,. \qquad (4)$$

Dimensionless slope of the straight line is 0.267. This is 4.4 times higher than the 0.06 value obtained for T90EP2, in satisfactory agreement with theoretical values shown in Figure 2.

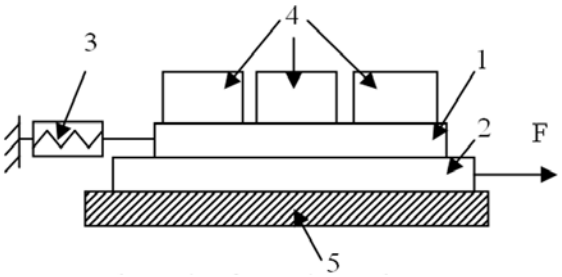

Figure 7. Schematic of experimental setup: 1-upper plate, 2-lower plate, 3-dynamometer, 4- dead weights, 5-sliding guide

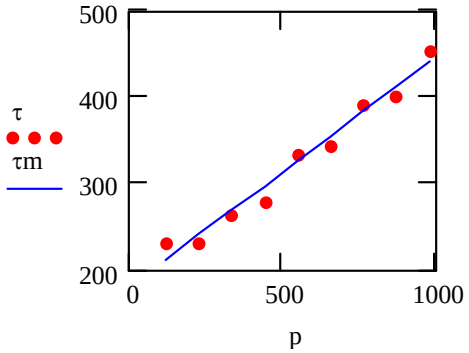

Figure 8. The dependence of limiting shear stress on pressure in thin layers (both pressure and limiting shear stress are expressed in Pa)

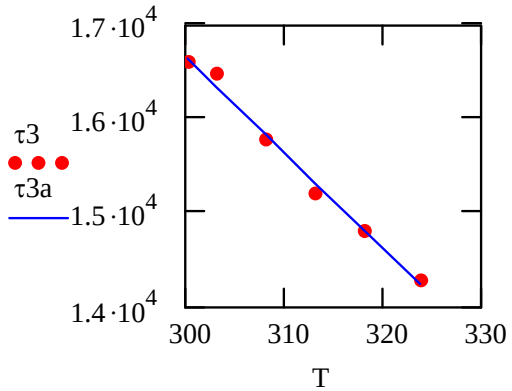

Figure 9. Effect of temperature upon limiting shear stress in thin oil film

In the second case, a fuel injection element having a clearance of 1.5 μm was used as tester. A radial film thickness of 0.75 mm may be high compared to molecular dimension, but thin with respect to clusters diameter.

The cylinder was fixed on the sensor of the dynamometer, and the plunger was pulled by a slowly increasing force, generating a sliding speed of 0.035 m/s. The dynamometer records the maximum force at onset of sliding. The ratio of this force to the contact area between the plunger and the cylinder yields the limiting shear stress.

The temperature is set by heating the assembly via warm air and it is measured by aid of thermocouple fixed on outside surface of the cylinder. The results are plotted in Figure 9. This behavior is similar to that in the bulk on small temperature interval.

The slope of the straight line, of -102Pa/K, is smaller than in the bulk, as the result of a more rigid structure in the neighborhood of the wall.

3. CONCLUSIONS

This paper leads to following conclusions.

- Theoretical investigations show that lubricating oils have different properties in the neighborhood of a metallic surface than in the bulk. All shear properties take much higher values than in the bulk due to the supplementary interaction arising between molecules and the wall.
- These enhanced properties generate an attached layer to each wall, which does not shear. In full EHD lubrication, the oil film thickness is the sum of thicknesses of these two attached layers and of that formed by hydrodynamic effects at sufficiently high rolling speeds. A good agreement between these predictions and measured thin oil film thickness was found [4,5].
- New experimental evidence upon molecular liquids properties in the wall vicinity is needed. The paper brings evidence upon structural flow units, minimum intermolecular potential and limiting shear stress.
- The typical structural flow units and their dimensions in melted paraffin are determined by aid of atomic force microscopy. It is found that both individual molecules and clusters coexist in an amorphous solid.
- The minimum intermolecular potential is determined either by measuring maximum intermolecular force or by assessing the surface tension. The experimental values thus determined are in good agreement.
- The experimental values of limiting shear stress in the wall neighborhood, as well as its dependence on pressure and temperature, match well the theoretical predictions.

REFERENCES

1. Jonhson G.J., Wayte R., Spikes H.A., 1991, "The Measurement and Study of Very Thin Lubricant Films in Concentrated Contact," *Tribology Transactions*, **34,** (2), pp. 187-194.

2. Cann, P.M., Spikes, H.A., 1994, "Thin Film Optical Interferometry in the Study of Grease Lubrication in a Rolling Point Contact," *Acta Tribologica*, **2** (1), pp. 45-50, (1994).

3. Luo, J. B., Wen, S. Z., 1996, "Mechanism and Characteristics of Thin Film Lubrication at Nanometer Scale," *Science in China (A)*, Vol. **39** (12), pp. 1312-1322.

4. Zhang, C., Luo, J., Wen, S., 2001, "A New Postulation of Viscosity and its Application in Computation of Film Thickness in Thin Film EHL," *Acta Tribologica*, 9 (1), pp. 35-40.

5. Zhang, C., Luo, J., Wen, S., 2002, "A New Postulation of Viscosity and its Application in Computation of Film Thickness in TFL," *ASME Journal of Tribology*, 124, pp. 811-814.

6. Diaconescu, E.N., 2006, "Nanometric Thickness EHL Oil Films," *Proceedings of IJTC, STLE/ASME International Joint Tribology Conference*, San Antonio, Texas, USA, October 22-25.

7. Diaconescu, E. N., 2007, "A Physical Approach to the Wall Effect in Elastohydrodynamic Lubrication," *ROTRIB 2007*.

8. Diaconescu, E.N., 2004, "Solid-like Properties of Molecular Liquids Subjected to EHD Conditions," *ASME/STLE International Joint Tribology Conference*, October 24-27, Long Beach, California, USA, 10 pp. on CD.

9. Hirst, W., Moore, A. J., 1981, "The Effect of Temperature on Traction in Elastohydrodynamic Lubrication," *Phil. Trans. of Roy. Soc. London*, vol. 298, A 1438, pp. 183-298.

ISSN 1220 - 8434

ACTA TRIBOLOGICA
Volume 17, (2009), 6-12

Laura PETRARU
e-mail: *Laura.Petraru@omv.com*

Franz NOVOTNY-FARKAS

Karin BAUMANN

OMV Refining & Marketing, Competence Center Lubes, 2320 Schwechat,
AUSTRIA

NEW APPROACH IN OXIDATION STABILITY TESTING OF THE GAS TURBINE OILS

The chemosorbic compounds with metal are composing after coating the surface with fluor-oligomeric material (FOM). Hardness, indentation and friction behavior of FOM coat were investigated. Scratch adhesion and friction tests show that the fluor-oligomeric film decreases the solid body micro-hardness and modifies contact rheology by reducing the shearing force at the local contact. FOM coat shows good elasticity in rough contacts, but with a higher hardness it may be more suitable for abrasive applications, i.e. reduced plasticity in a given tribo-contact.
Keywords: gas turbine oils, antioxidants, thermo-oxidative stability

1. INTRODUCTION

Modern gas turbine oils are designed to meet an exceptional high thermo-oxidative stability due to the development of more efficient power plants. Even in so called “high performance” gas turbine oils, oxidation causes sludge, deposits and varnish formation. These thermo-oxidation stability related problems lead to early breakdowns, wear, filter plugging and other operation failures [1].

For a better understanding of the phenomena, extensive studies of the given thermo-oxidation stability problems are required.

2. TURBO-MACHINES AND THEIR LUBRICATION

The worldwide energy demand is growing continuously and the electrical power consumption is hardly covered by newly established production plants and capacities.

In the power generation, there are three main principal types of turbo-machinery that gained their major role and importance, widespread acceptance and common popularity: water, steam and gas turbines.

Due to their high efficiency and flexibility in heavy-duty operation regimes, a greater than ever market share has been achieved, especially by gas and combined cycle turbines.

A representative layout and typical scheme of the combined cycle turbine operation is shown in Figure 1.

These different turbo-machines are characterized by a wide variety of speeds, mechanical loads and thermal stresses.

The turbo-machinery design and construction, the operating conditions, such as loads, operating temperatures, oil makeup and contaminants, belong to the main factors that determine turbine oil performance requirements and its service life [4-6,8].

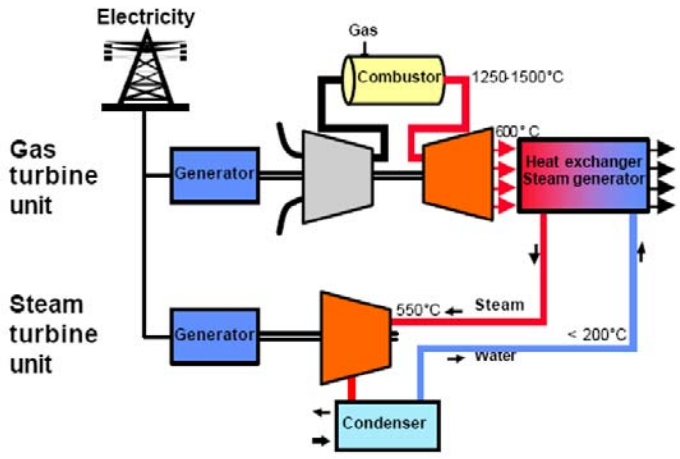

Figure 1. Steam, gas and combined cycle turbines

3. DEMANDS ON TURBINE OILS

The demands on turbine oils are defined by the turbines themselves and their specific operating conditions. The oil in the lubricating and control circuits of steam and gas turbines has to fulfill several objectives [7]:

- hydrodynamic lubrication of all bearings and the lubrication of gearboxes,
- heat dissipation,
- functional fluid for control and safety circuits,
- avoidance of friction and wear on gear tooth flanks in turbine gearboxes and when the turbine is spooled-up.

Apart from these mechanical-dynamic requirements, the following physical-chemical specifications also have to be fulfilled by turbine oils [7]:

- aging stability for long operating periods,
- hydrolytic stability,
- corrosion protection, even if water, steam and/or condensation is present,
- reliable separation of water (vapor and separation of condensed water),
- rapid air release and low foaming,
- good filterability and purity.

The general overview of turbine oil operation conditions is shown in Table 1 [2].

Gas turbine applications have the most severe operation conditions for turbine oil (see Table 1).

Elevated sump temperature and high hot spot peaks represent the uniqueness of overall gas turbine oil challenges.

This unfavorable impact of much higher operation temperatures call for distinguishing oils with much higher thermal and oxidation resistance and robustness.

Table 1. Overview of turbine oil operation conditions

	Water	Steam	Gas
Critical turbine components	bearings guide vanes control system	bearings control system	bearings gear control system
Speed, rpm	50…600	>3000	3000…7000
Oil sump temp., ºC	40…60	45…65	50…95
Hot spot peaks, ºC	75…90	80…150	150…180
Unfavourable impact	(water) air	(steam) air	air high temp.
Oil service life, thousand hours	100…250	50…150	20…30

Furthermore, there are strong efforts to ensure a longer, more extended, but trouble-free operation of gas turbines. An adequate lubricating oil quality should be responsible to ensure and perform that desired longer service life and the reliability of the gas turbines operation.

These more challenging operation conditions dictate the use of gas turbine oils with special performance level regarding their thermo-oxidation stability.

4. TURBINE LUBRICANTS – SPECIFICATIONS

For matching these severe operation requirements, in recent time, new or revised industrial standards and turbine oil specifications have been introduced.

DIN 51515 lubricants and Governor Fluids for Turbines were revised in 2001 (Part 1-L-TD formal service, specifications) and new, so-called "high temperature turbine oils" were defined in DIN 51515 part 2 (Part 2-L-TG, Lubricants and governor Fluids for turbines for higher temperature service specifications).

Table 2 presents the specifications highlighted in the German standard DIN 51515-1/2 [3].

Table 2. German Specification: DIN 51515-1/2.

- **DIN 51515 -1 (June 2001) TD (Turbine "Dampf" = Steam)**
  Normal duty, typical tests are
  - TOST life: 2000 h
  - Copper corrosion, rust method A, foam, air release, water separation
  - The foaming requirements are very low: 450/0 -450/0 - 450/0 to emphasize the importance of the air release. (Negatively affected from Antifoam agents)

- **DIN 51515 – 2 (November 2004) TG (Turbine, gas)**
  For higher temperature services, typical tests are
  - RPVOT: 800 min
  - TOST life: 3000h
  - RPVOT modified: 85% retention
  - Copper corrosion, rust method A, foam, air release, water separation

5. OEM SPECIFICATIONS

The development and the progress of standardization activities have not been stopped with the creation of international and national specifications.

In the meantime there have been also introduced or revised several new Original Equipment Manufacturers (OEM) specifications and guidelines for turbine oils. Especially the gas turbine oils have been recently specified in distinctive product standard with individual performance requirements for thermo -oxidation stability. An overview of the main OEM specifications is listed in Table 3.

Table 3. OEM specifications

OEM/Organization	Specification	Turbine Type	Comments
Alstom	HTGD 90117	Gas/Steam	With and without FZG requirement; D2272 minimum of 300 minutes. D943 of 2000 h; Zinc max 5 ppm.
General Electric	GEK 101941A	Gas, Frame 6F	FZG requirement of 8 fail (minimum); D2272 minimum of 500 minutes
General Electric	GEK 107395A	Gas/Steam, Class H	D943 minimum of 7000 hours ; D2272 minimum of 1000 minutes ; modified D2272 test
General Electric	GEK 27070	Steam	
General Electric	GEK 28143A	Gas, Frame 3, 5, & 6B	With and without antiwear additives
General Electric	GEK 32568f	Gas, Frame 7/9	D2272 minimum of 500 minutes; modified D2272 test
General Electric	GEK 46506D	Steam	D2272 minimum of 250 minutes
Mitsubishi Heavy Industries	MS04-MA-CL001	Gas/Steam	"Dry TOST" specification; low temperatures; D943 of 2000 h;
Mitsubishi Heavy Industries	MS04-MA-CL002	Gas/Steam	"Dry TOST" specification; high temperature; D2272 minimum of 700 minutes
Mitsubishi Heavy Industries	MS04-MA-CL003	Gas	"Dry TOST" specification; high temperature with EP; D2272 minimum of 700 minutes; D943 of 4000 h
Siemens	TLV 9013 04	Gas/Steam	With and without FZG requirement
Siemens Westinghouse	M spec 55125Z3	Gas	D2272 minimum of 350 minutes

5.1 Gas turbine oil formulation trends and bench testing

In order for a turbine oil to fulfill its fundamental functions, it must possess different chemical and physical features. These features and the performance level of turbine oils is a function of the type, character and quality of base stocks used in their formulations.

The chemical structure and composition of base stocks can determine the finished oil properties, as the thermo - oxidation stability, aging characteristics, solubility of aging products, efficiency of antioxidants and other functional additives.

Turbine oil formulators and manufacturers responded by using non-conventional base stocks with extremely increased antioxidant additive treat-rates [9].

Correspondingly, enhanced types of turbine oils appeared and were commercialized to satisfy these lately specified demands on better thermo – oxidation stability.

As main test criteria for thermo-oxidation stability were employed, same bench test methods as measured by ASTM D 2272 Rotating Pressure Vessel Oxidation Test (RPVOT) and ASTM D 943 Turbine Oil Stability Test (TOST) as in evaluation of the traditional R&O and conventional formulated turbine oils.

Industrial representatives still believe that thermo-oxidation stability, evaluated even by RPVOT/TOST values, is a priority and extremely important. So, they have prescribed and listed firstly those two old bench tests in their new more severe specifications for gas turbine oils (Tables 4 and 5).

Table 4. Comparison of main physical and chemical characteristics in specifications of gas turbine oils (I)

Parameter		Test method	DIN 51515-2 L-TG	ASTM D 4304 TYP III (draft)	ISO/DIS 8086 TGB/TGSB
Viscosity class		ISO 3448	32/46	32/46	32/46/66
Viscosity index		ISO 2909	---	---	90
Air release, min		ISO 9120	5	5	5/5/6
Foming(tendency/stability)	max	ISO 6247			
-Seq. I °C @ 24°C, ml/ml			450/0	50/0	450/0
-Seq. II°C @ 93°C, ml/ml			100/0	---	50/0
-Seq. III°C @ 24°C after 93°C, ml/ml			450/0	---	450/0
Water content, m%		ISO 12937	0,015	0,02	0,02
Water separability		ISO 6614			
-time to 3ml emulsion@ 54°C,min	max	DIN 51589-1	---	30	30
-separation (steam), sec,	max		300	---	---
TAN, mgKOH/g	max	ISO 6618	report	0,2	report
Cleanliness at delivery state, class	max	ISO 4406	20/17/14	-/17/14	-/17/14
Flash point(COC), °C	max	ISO 2719	160/185	200/200	200/200/200

Table 5. Comparison of thermo -oxidation test requirements in specification of gas turbine oils (II)

Parameter		Test method	DIN 51515-2 L-TG	ASTM D 4304 TYP III (draft)	ISO/DIS 8086 TGB/TGSB
Oxidation stability @ high temp (72h @ 175°C)		ASTM D 4636 according to	...		...
-viscosity change		"alternative		report	
max		procedure2"		report	
-acid number change	max				
Metal specimen weight change, mg/cm²					
-steal				±0,250	
-aluminium				±0,250	
-cadmium				±0,250	
-copper				±0,250	
-magnesium				±0,250	
Oxidation stability ("TOST")					
-time for TAN to 2 mg KOH/g	min	ISO 4263-1	3000	3500/3000/2500	3500/3000/2000
-1000h TOST sludge, mg	max	ASTM D 4310	...	...	report
-1000h TOST TAN, mgKOH/g	max	ASTM D 4310	...	...	
RPVOT, min	min	ASTM D 2272	800	750	500
Modified RPVOT, %	min	ASTM D 2272	85	85	85

In fact, recent gas turbine oil developments of oil companies concentrated on the satisfaction and fulfillment of the required extremely high RPVOT/TOST values only, but not under real-life operating conditions. The methodology validations and the evaluation of fleet discrepancies have not been taken into account.

6. OIL FORMULATION CONSIDERATIONS

6.1 How to balance the oil formulation?

Oil's molecular composition influences its physical and chemical properties, particularly the thermo–oxidation resistance and aging characteristics. Nitrogen heterocycles and aromatic compounds have a negative influence on base oil stability. Some sulphur containing compounds are viewed as desirable since they inhibit hydrocarbon autocatalytic oxidation through free-radical chain termination pathways. Therefore, the solvent refined base stocks Group I can hardly fulfill modern heavy-duty gas turbine performance requirements.

Without an effective antioxidant, which is non-volatile and thermally stable, even the non-conventional base stocks will be oxidized quite rapidly.

Part of antioxidants can be lost by vaporization or become ineffective as a result of high temperatures. The proper treat rate and chemical selection of antioxidants are key issues for the design of the thermal stability and aging resistance [10].

6.2 Dilemma of using non-conventional base stocks

The non-conventional base stocks are advantageous because of much higher oxidation and thermo–oxidation stability, by comparison to conventional base stocks Group I.

They have a quite homogenous hydrocarbon structure (Figure 2), with nearly full absence of aromatic, and/or heteroaromatic constituents.

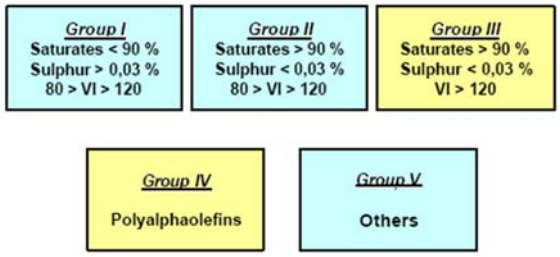

Figure 2. Basestock categories according to ATIEL/API

Non-conventional base stocks have an excellent additive response for a comparable performance level, and a lower additive treat rate is required.

Nevertheless, all these non-conventional base stocks have lower solvency, resulting in earlier sludge formation and additive dropout if commonly high treat rates and antioxidant types are used.

6.3 Selection and proper balance of antioxidants

There are a huge number of different chemical sorts of antioxidants that can be selected and employed for gas turbine oils.

A proper formulation balance requires a selection of two or more chemical type of antioxidants with synergetic potential and multifunctional character, finding out the ways to reduce overall additive treat rates.

Lower treat rates of antioxidants can decrease the additive solubility weakness in highly non-polar base stocks, and also minimize the probability for additive dropout, sludge and deposit formation.

The individual components of employed antioxidant additives and their chemistry must be carefully selected and have low volatility, good thermal stability and adequate solubility in the base stocks used in the desired gas turbine oil formulations.

Primary antioxidants, the hindered phenolic antioxidants, are very effective types at moderate sump oil temperatures (Figure 3). Nevertheless they have high sublimation and volatility potential.

This type of antioxidant is not effective enough as a single antioxidant, to control the high temperature stability of the gas turbine oils.

The aminic antioxidants are very effective types to boost RPVOT / TOST values, especially for non-conventional base stocks. Therefore, they are widely used and represent definitive constituents in current turbine oil formulations.

Nevertheless, at higher treat rates, they can cause additive dropout and form insolubles at elevated temperatures (Figure 4).

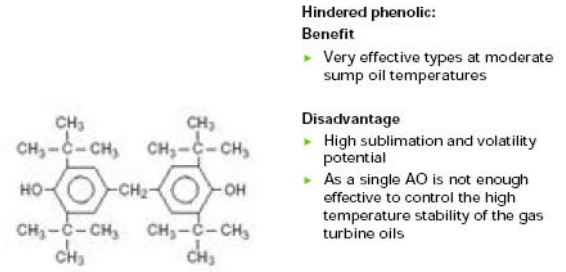

Figure 3. Hindered phenolic type of antioxidants

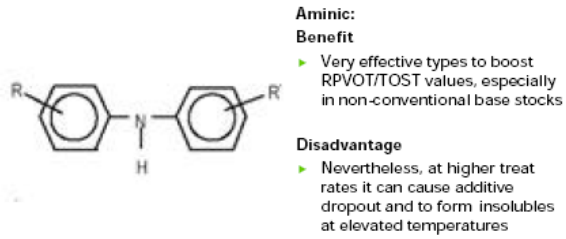

Figure 4. Aminic type of antioxidants

The antioxidant system used for gas turbine oil is based on a unique, synergetic combination of primary and secondary antioxidants, which exhibit good solubility and allow the use of lower treat rates.

Synergies have been found when optimal ratios of primary antioxidant or free radical scavengers are added to the combination of hindered phenols and alkylated diphenylamine antioxidants.

6.4 Using mixed antioxidant additive systems

Further optimization can be achieved with the addition of phosphorus or sulphur type secondary antioxidants or peroxide decomposers. This synergetic antioxidant effects differ from base stock to base stock.

It should be noted that in industrial practice, rather the ready-made turbine oil packages will be employed, offered by different additive suppliers. The formulations, based on such full packages gained a broad use. Only a few lubricant manufacturers make extra efforts in regard to optimizing the chemical composition of additive ingredients and using single components.

However, a balanced, self-tailored and optimal ratio or component combination is important in reducing additive treat rates and in the design of a correct turbine oil composition [11,12].

7. NECESSITY OF NEW BENCH TESTING PROCEDURES

7.1 Shortcomings of the current bench testing

All used and specified key bench test methods are required to correlate with real-life operating condition or they have to be even more severe.

The current turbine oil thermo-oxidation bench testing methods are shown in Table 6.

The test method ASTM D 2070 was introduced earlier for evaluation of hydraulic fluids. The test temperature of 135°C does not seem to be high enough to evaluate the extremely high stresses on gas turbine oils.

The other two tests, TOST / RVPOT used for gas turbine oils, as they were introduced for the water and steam turbine application. Nevertheless, the operation regimes and performance requirements of these turbine oils are very different.

Table 6. Turbine oil thermo-oxidation bench testing methods

Test method	CM-A ASTM D 2070	TOST ASTM-D 943	RPVOT ASTM D 2272
Oil sample volume	200 g	300 ml	50 g
Water content	none	60 ml	5 ml
Metal catalyst	Cu rod Fe rod	Cu coil Fe coil	Cu coil
Air/Oxigen	air (no flow)	oxygen, 3L/H	90 PSI oxygen
Temperature	135°C	95°C	150°C
Test duration	168 h	3000–10000+ h	10 - 40+ h
Evaluation criteria	sludge rod rating	dTAN	pressure drop

Currently, in case of “high performance” gas turbine oils the TOST test procedure takes a long time (e.g. more than 10.000 hours) and it does not cover the critical temperature and required performance range. Some antioxidants have their performance disadvantages and weaknesses (intense volatility, dropout, thermal instability), even above the specified values of TOST (95°C) and that of RPVOT (150°C). It is in the range of 150-190°C.

The gas turbine oils should have distinctively high thermo-oxidation stability, at rightly elevated temperatures and without presence of water.

The currently used higher antioxidant (or additive package) levels generate not only higher TOST / RPVOT values, but as side effect, they also induce a higher sludge formation potential.

These critical features cannot be simulated and evaluated with the current praxis.

7.2 New recommended bench testing

The currently used bench tests are unable to fulfill the state-of-the-art bench testing requirements, in evaluation of sludge and varnish formation tendency. The adequate bench test procedures of thermo-oxidation stability should have to simulate the real operation conditions and their results should have to correlate with real-life turbine oil conditions.

Table 7. New recommended bench testing

Test method	MAN-Turbo in-house	Modified Baader DIN 51554	in-house HTOST (CEC-L-48-A-00)
Oil sample volume	150 ml	60 ml	100 ml
Water content	-	-	-
Metal catalyst	-	Cu coil	-
Air/Oxigen	-	air (no flow)	Air, 5L/h
Temperature	120/150/180°C	150°C	160°C
Test duration	48 h	168 h	96 -192 h
Evaluation criteria	sludge	sludge, dTAN, dSaponification, Cu coil	dKV, dTAN, FTIR (oxidation, AO)

The current real-life needs require that the desired bench test procedures should be focused on evaluation of the solubility of base stocks, thermal stability of functional additives at elevated temperatures, as well as the overall sludge and varnish formation potential of gas turbine oils.

In order to correlate with real-life operating condition new testing procedures have been applied and evaluated in our laboratory (see Table 7):

- A rapid screening test of thermal stability, solvency and AO dropout – MAN Turbo in-house test [13];
- An evaluation of sludge formation potential in presence of copper coil – BAADER aging test adopting DIN 51554 [3];
- A high temperature oxidation stability test – modified CEC-L-48-A-00 in-house, method B test apparatus [14].

Involving several industrial partners, there are broad ongoing studies and running experimental programs, aimed at developing new qualifying methods. A large number of test series will be carried out and experimental data base will be generated.

8. CONCLUSIONS

The gas turbines have an important role in market share in modern power generation.

The thermo-oxidative stability of gas turbine oils is a key performance parameter.

Advanced gas turbine oil formulations should be based in future on non-conventional base stocks Group II/III.

Balanced mixtures of hindered phenolic and aminic antioxidants should be used to control oxidative degradation and aging either at moderate elevated and high oil temperatures.

The total treat rate of antioxidants should be reduced and optimized to the base stock performance level and its solubility.

New testing procedures should be introduced and tailored to the distinctive performance requirements of gas turbine oils, depending on severity of operational conditions.

Solving thermo-oxidation problems of gas turbine oils is furthermore a challenge for oil formulators, OEMs, and machinery operators as well.

REFERENCES

1. (a) **Mang, T., Dresel, W.,** 2006, Lubricants and Lubrication, Wiley-VCH, Weinheim; (b) **Gatto, V.J., Moehle, W.E., Cobb, T.W., Schneller, E.R**. - *J. of ASTM International*, 4, 3, pp. 1-20. (c) **Livingstone, G.J., Thompson, B.T., Okazaki, M.E.,** 2007, *J. of ASTM International*, 4, 1, pp. 1-18.

2. *** ASTM D 4378 – 03.

3. *** German Standard DIN 51554.

4. Quick, L., 2005, "New Turbine and Lubricant Technology Requires New Customer Focused Oil

Monitoring Methods," *ASTM Symposium*, December 5th, Norfolk, VA.

5. Habereder T., 2006, "Ashless Additive Technology for Modern Turbine Oils," *Lubricants Russia*, WTC, Moscow.

6. Bloch, H.P., 2000, *Practical Lubrication for Industrial Facilities*, Marcel Dekker.

7. Mang, T., Dresel W., 2001, *Lubricants and Lubrications*, Wiley-VCH.

8. Sweeney P.J., 2001, *Lubrication of Steam, Gas and Water Turbines in Power Generation – A Chevron Texaco Experience*, Sydney NSW.

9. Lopopolo V., 2005, "Development and Testing of an Antiwear Gas Turbine Lubricant in Challenging Offshore Environment," *IAGT Symposium*, Banff, October.

10. Rudnick L.R.., 2003, *Lubricant Additives – Chemistry and Applications*, Marcel Dekker.

11. Denis, J. et al., 2000, *Lubricant Property Analysis & Testing*, Editions Technip Paris.

12. Gatto, V., et al., 2005, "Oxidation Fundamentals & its Application to Turbine Oil Testing," *ASTM Symposium*, Dec. 5th (2005), Norfolk, VA.

13. *** MAN Turbomaschinen AG AA-10-217/A-C.

14. *** International Standard CEC-L-48-A-00.

ISSN 1220 - 8434 **ACTA TRIBOLOGICA**
Volume 17, (2009), 13-16

Liana BOGATU[1]
email: *lianabogatu@icerp.ro*

Ion PETRE[1]
Anca MARIN[1]
Constantin TĂNĂSESCU[2]
Diana PETRE[2]
Niculae Napoleon ANTONESCU[3]
Liviu MIRCI[3]

[1] SC ICERP SA Ploieşti, **ROMANIA**

[2] Petroleum and Gas University of Ploieşti, **ROMANIA**

[3] Politehnica University of Timisoara,, **ROMANIA**

HYDRAULIC OILS FROM REGENERABLE FEED STOCKS WITH A LOW ENVIRONMENTAL IMPACT

The aim of this research study is to obtain biodegradable hydraulic oils characterized in accordance with European standard regarding the quality and environmental impact. The formulation of this type of lubricant is based on vegetable oils or mixtures of vegetable oils with more stable base oils and appropriate additives. The study evaluates the laboratory testing results regarding vegetable oil-based lubricating characteristics and hydraulic oils obtained from base oil mixture and suitable additives.

Keywords: hydraulic oils, vegetable oil-based lubricants, biodegradable lubricating oils, vegetable oils oxidation stability

1. INTRODUCTION

The monitoring and observing studies conducted in Europe and in the USA on the lubricating oils' life cycle have proved that over 50% of used oils get in the ecosystem. Due to the fact that 95% of lubricating oils are obtained from petroleum resources that have a low grade of biodegradability, these uncontrolled losses of used oils have, from the environmental point of view, an alarming impact.

In the international context there is an important experience in problems regarding lubricating oils environmental impact. In the last years, remarkable interests were identified in the Nordic countries and, also, in other European countries. Thus, the following organizations were created: Nordic Swan (Nordic Countries), Swedish Standard (Sweden), Blue Angel (Germany), NF-Environment Mark (France), Austrian Ecol-Label (Austria), VAMIL regulation (The Netherlands), ISO 15380 (International Standard) [1].

Significant results have been obtained on the international level, especially in the Nordic countries that advanced concerns in the environmental aspects of legislations field, results in elaborating a regulation for renewable feed stocks requirements. Therefore, the Swedish Standard for greases fabrication (SS 15570 Greases) includes requirements for renewable feed stocks. Also, the Nordic Swan includes requirements for lubricating oils.

Among the viable solutions for ecological lubricating oils fabrication, significant results have been obtained in vegetable lube base oils using field, because these are characterized by a high biodegradable grade, a lower toxicity level and are obtained from renewable feed stocks. Thus, it can be achieved simultaneously both the objective regarding the biodegradability of the obtained lubricating oils and the natural resources savings objective, respectively oilfields protection (very difficult to renew) that are continuously decreasing both as number and as exploitation potential.

Vegetable oil-based lubricants are emerging as an environmentally preferable alternative to existing petroleum oil products. Users are finding that vegetable oils can offer even better performance than petroleum oils in some applications, with the added benefits of being less toxic, renewable and biodegradable.

The lubricants include a large and various types of oils, such as: engine oils, hydraulic oils, compressor oils, turbine oils, slide way oils, transmission oils, greases, metal working fluids, preservative fluids and so on. After engine oils, the hydraulic oils are the most used type of lubricant. Different types of vegetable oil-based biodegradable hydraulic fluids for use in heavy equipment are moving toward commercialization [2].

In the last years, the authors have made research studies regarding the use of vegetable base oils to lubricant formulations [3-8].

2. HYDRAULIC OILS CHARACTERISTICS

The most important characteristics required by the hydraulic oils are the adequate fluid viscosity and antiwear properties.

Other significant characteristics include:

- oxidation resistance – important with a growing tendency for bulk oil temperatures to increase in many hydraulic systems;

- thermal stability – to resist degradation and attack of metals at high temperatures;
- corrosion resistance to avoid harmful attack on the variety of metals used in hydraulic systems;
- extreme pressure properties;
- water separation – to avoid problems of emulsification with small quantities of water entering the system through condensation;
- air-release and antifoam properties – to avoid cavitation effects and increased compressibility.

The specific values of these characteristics are regulated by standards as DIN 51524, NFE 48603, DENISON HF-O, CINCINNATI MILACRON etc.

3. COMPARISON BETWEEN VEGETABLE OILS AND OTHER BASE OILS

Nowadays, the lubricants market is divided like this:

- Mineral oils (92…94%);
- Synthetic oils (5…6%);
- Vegetable oils (1.5…2%).

The data about such type of oils, concerning the lubricating properties, environmental impact and extent, emphasize the following aspects (Table 1).

Evaluating these results it can be noticed the indication "very good" for mineral type as regards the extent, for vegetable type concerning biodegradability and renewability and for synthetic referring to quality.

Vegetable oils have a promising potential to be used for lubricants fabrication, according with the actual regulations regarding biodegradability, the renewability and toxicity. But, the environmental impact and human safety represent only a part of the imposed requirements of lubricant oils. For specific applications of the lubricants we have to consider a lot of aspects referring to the working conditions.

To satisfy these requirements, the feed stock for lubricating oils fabrication, respectively lube base oils and additives, have to accomplish some important characteristics as:

- viscosity corresponding to the designed working parameters;
- high viscosity index;
- low pour point;
- high flash point;
- high oxidation resistance;
- high biodegradability grade;
- others (corrosion resistance, wear protection, extreme pressure resistance, foaming tendency, desemulsification etc).

Referring to these properties, Table 2 shows the characteristic average values for three representative base oil types: vegetable oil, mineral oil and synthetic oil.

As it can be noticed, vegetable oils have remarkable viscosity index, flash point and biodegradability, but poor acidity, pour point and completely unsatisfactory oxidation resistance.

Mineral oils have a good viscosity index, flash point, pour point, acidity and oxidation resistance, but a low biodegradability capacity.

The synthetic oils as polyalphaolefins have a very good viscosity index and pour point, good flash point, acidity and oxidation resistance and an acceptable biodegradability capacity, the only problem being their higher price.

Referring to vegetable oils, the application of this type of base oils at lubricant fabrication is conditioned by improving oxidation resistance.

Considering these facts, the idea of the research study was to mix the vegetable oils with appropriate base oils and additives that have the needed performance.

Table 1. Lubricants comparison

Oil type	**Lubricating properties**	**Biodegradability**	**Renewability**	**Extent**	**Price**
Mineral	good	low	low	very good	good
Vegetable	acceptable	very good	very good	low	acceptable
Synthetic	very good	partial	-	low	high

Table 2. Tested characteristics

Characteristics		**Vegetable oil** Sunflower	**Mineral oil** ISO-VG 32	**Synthetic oil** PAO 6	**Test method**
Kinematics Viscosity	at 100°C, cSt	31.85	29.50	31.16	ISO 3104
	at 40°C, cSt	7.62	4.93	5.78	
Viscosity Index		222	92	129	ASTM 2270
Pour Point °C		-9	-12	-40	ISO 3016
Flash Point, °C		260	210	210	ISO 2592
Oxidation stability RBOT, minutes		10	60	100	ASTM 2272
Acidity, mg KOH/g		6	0.005	0.03	ASTM 974
Biodegradability, %		>90	<50	>70	CEC L-33-A-934

The study was developed taking into account the following base oils: mineral oil – SAE 20 and vegetable oil – Sunflower. The main characteristics of these components, tested in the ICERP laboratory, are presented in Table 3.

To accomplish the whole range of hydraulic oils characteristics (wear resistance, extreme pressure resistance, foam tendency, corrosion prevention etc.), the quality of the base oils had to be improved by adding specific compounds. Generally, for obtaining a lubricant with high performances it is necessary to use:

- antioxidant additives;
- anti-wear and extreme pressure additives;
- antifoam additives;
- antirust and anticorrosion additives.

For our research study we have used the following additives, having the mentioned functions:

- A1 – zinc alkyl-dithiophosphates and calcium sulfonate (multifunctional additive);
- A2 - zinc alkyl-dithiophosphates (multifunctional additive);
- A3 – alkylphenol, alkyl diaryl amine, tri-n-butyl phosphate, (an ashless multifunctional oxidation and rust inhibiting additive package);
- DS – polymethacrylate with pour point depressant function;
- AF – silicon polymer with antifoaming function.

The tested oils composition and characteristics are detailed in Table 4.

Table 3. Base oils characteristics

Characteristics	Mineral oil SAE 20	Sunflower	Test method
Viscosity at 40ºC, cSt	53.10	32.6	ISO 3104
Viscosity at 100ºC, cSt	7.20	7.64	ISO 3104
IV	92	216	ASTM 2270
Pour point, ºC	-15	-9	ISO 3016
TAN, mg KOH/g	-	2.0	ASTM 974
RBOT, minutes	65	5	ASTM 2272

Table 4. Tested oils composition and characteristics

Specifications	Tested oils			
Base-oil composition, weight %				
Sunflower oil	100	100	70	30
Mineral oil SAE 20	-	-	30	70
Additives type and concentration, % weight				
A1	0.6	-	0.6	-
A2	-	1.0	-	1.0
A3	-	0.3	-	0.3
DS, pour point depressant	0.5	0.5	0.5	0.5
AF, antifoaming	0.002	0.002	0.003	0.003
Tested oils characteristics				
Kinematics viscosity at 40°C, mm^2/s at 100°C, mm^2/s	 32.6 7.64	 34.54 7.80	 42.22 7.70	 49.89 7.69
Viscosity Index	216	207	153	126
Pour Point, °C	-9	-15	-33	-36
Flash Point, °C	264	265	246	220
Copper Corrosion (3 hours at 100°C)	1a	1a	1b	1b
Rust Test	pass	pass	pass	pass
Rotary Bomb Oxidation, minutes	10	15	20	65
Four Ball Test Scar Diameter (300N, 60 min) mm	0.40	0.40	0.40	0.38
Foam Test, Stability, ml Sequence I Sequence II Sequence III	 0 0 0	 0 0 0	 0 0 0	 0 0 0
Biodegradability, % weight	85	82	70	51

4. CONCLUSIONS

Using only vegetable oils for biodegradable hydraulic oils formulation, a high biodegradability grade is obtained, but it doesn't accomplish all the quality conditions required for such a lubricant type.

The additives used frequently in mineral and synthetic oils based lubricants fabrication (anti-oxidant, antiwear, anticorrosion, depressant, anti-foaming additives) are not as efficient for vegetable oils.

Good results were obtained using mixtures between vegetable oils, mineral oils and specific additives. Thus, the required performance level for all the characteristics is obtained.

The vegetable oils could be an approachable solution for hydraulic lubricants fabrication and an alternative for the mineral base oil.

The mixtures between vegetable oils, mineral oils and suitable additives provide adequate characteristics for the formulated lubricants.

Most convenient mixtures (with smaller dosage of mineral oils) could be obtained using new and more efficient additives.

REFERENCES

1. Norrby, T., Kopp, M., 2000, "Environmentally Adapted Lubri-cants in Swedish Forest Industry. A Critical Review and Case Study," *Tribology 2000-Plus, 12th International Colloquium Esslingen*, January 11-13, pp. 161-168.

2. McGraw, L., 2000, Biodegradable Hydraulic Fluid Nears Market, USA Agricultural Research Service, April 19.

3. Bogatu, L., Tănăsescu, C., 2005, „Uleiuri lubrifiante biodegra-dabile", *Buletinul Universităţii Petrol-Gaze din Ploieşti, Seria Tehnică*, 57, 2, pp. 53-56.

4. Bogatu, L., Tănăsescu, C., 2005, "Biodegradable lubricating oils," *2nd Intern. Conf. on Manufacturing Engineering ICMEN*, Proc., ed. Bouzakis, K.D., 5-7 October, Chalkidiki, Greece, pp. 591-595.

5. Tănăsescu, C., Petre, D., Jugănaru, T., Ciuparu, D., Bogatu, L., 2007, "Increasing the Oxidation Stabi-lity of Vegetable Oil by Catalytic Hydrogenation for Application in Lubrication," *10th Intern. Conf. on Tribology*, SERBIATRIB-07, Kragujevac, Serbia, 19-21 June.

6. Bogatu, L., Petre, I., Marin, A., Amira, C., 2007, „Biodegradable hydraulic lubricants based on modified vegetable oils," *10th Intern. Conf. on Tribology*, SERBIATRIB-07, Kragujevac, Serbia, 19-21 June.

7. Mirci, L.E., Boran, S., Herdan, J.M., 2000, "New Synthetic Ester Type Base Oils (with Biodegra-dability Potential)," *Tribology 2000-Plus, 12th Intern. Colloquium Esslingen*, January 11-13, pp. 135-141.

8. Mirci, L.E., Boran, S., Pode, V., Resiga, D., 2007, "Synthetic lubricants based on sebacic complex esters," *J. of Synthetic Lubrication*, 24, 1, pp. 51-63.

ISSN 1220 - 8434

ACTA TRIBOLOGICA
Volume 17, (2009), 17-20

Carmen BUJOREANU
email: *bujor1000@yahoo.com*

Viorel PALEU

Dept. of Machine Elements & Mechatronics,
"Gh. Asachi" Technical University of Iasi,
ROMANIA

IMPACT PARAMETERS IN ROLLING CONTACT LUBRICATION

The EHD mechanism is the "miracle mechanism" for life and durability. The key to unlock the mysteries behind oil physical properties and chemical attributes is the identification of the functional regions of a lubricated contact. Some experiments related to a severe wear leading to contact catastrophic damage are presented and emphasize the mean parameters controlling lubrication and failure mechanisms. The test method invokes tribological interactions measured in terms of friction, gentle polishing wear of surface features, adhesive wear events and scuffing. With respect to lubrication and failure mechanisms for a given tribo-contact system, we propose that the key performance parameters are the entraining velocity, the sliding velocity, and temperature.
Keywords: lubrication, rolling contact, scuffing, sliding, temperature

1. INTRODUCTION

The EHD contact can be divided into three regions. The inlet region is the convergent section upstream of the high pressure Hertzian contact region. The inlet region is the functional region for EHD pressure generation, which has rigorous mathematical foundations for predicting film thickness within the Hertzian region. The dynamic motions within the inlet region pump the film up. The Hertzian region rides the film, and the exit region discharges the film. The decoupling of these functional regions is the secret behind testing machines and testing methods.

Oil and its viscosity, as well as pressure-viscosity properties within the convergent inlet region control EHD film thickness in a reliable and predictable fashion. The shear and traction of the pressurized film within the Hertzian contact region gives rise to heat generation, which is dissipated within the contacting bodies. For surface life and durability, the preservation of the EHD or micro-EHD mechanism is essential [1].

The primary purpose of oil chemical attributes is to preserve the EHD mechanisms as much as possible. Loss of "surface integrity" is the first step toward wear and scuffing failure mechanisms. While EHD mechanisms are essential for life and durability, chemical attributes for boundary lubrication mechanisms are equally essential. Chemical attributes play a critical role in preserving surface integrity. The processes of physical adsorption and chemical reaction heal and protect against local adhesion and disruption of the surface topography.

Tribo-contact systems, which have oil properties for EHD film-forming capability and chemical attributes for film-forming ability working together, can achieve remarkable levels durability.

2. IMPACT FACTORS

The decoupling of the inlet region EHD lubrication functions from the Hertzian region boundary and micro-EHD mechanisms provides means to identify the *impact parameters* associated with lubrication and failure.

Failure mechanisms of wear, scuffing and surface initiated fatigue are the result of micro-scale events associated with roughness features [2]. If roughness features do not "run-in" or have exhibited plastic flow, high normal stresses with repeated contact cycles can result in surface initiated fatigue or "frosting". Since EHD film thickness is a function of viscous properties in the inlet region and the entraining velocity, *the entraining velocity becomes an impact performance factor.*

The sliding velocity within the Hertzian region determines the shear strain at asperity sites. The shear stress at these sites is directly connected to the frictional conditions created at asperity sites.

Since sliding velocity controls the strain at asperity sites, as well as frictional heating, *sliding velocity becomes an impact factor*.

We recognized that contact load or stress is an important engineering parameter. It certainly is with respect to subsurface initiated fatigue, where material fatigue is directly related to shear stresses below the surface. From a tribological perspective of processes at the surface interface under high-speed lubricated conditions, load is translated into contact size, heat generation, and to some degree, asperity stress and strain. While engineers like to work in terms of load and stress, the critical phenomena within the contact is really seen to a greater degree as temperature or tangential stress and strain. Temperature can be viewed as the sum of bulk temperature from the contacting bodies and contact temperature within the contact itself. The bulk temperature controls the viscous properties in the inlet region for EHD film thickness. The contact temperature controls the bulk fluid traction coefficient in the Hertzian region. It is also a major contributor to oil and material chemical reactivity within the Hertzian region. So, *the temperature is an impact factor* associated with lubrication and failure mechanisms.

With respect to lubrication and failure mechanisms for a given tribo-contact system, we propose that the key performance parameters are the entraining velocity, the sliding velocity and temperature.

3. FAILURE EVALUTION

Tangential stress and strain under high-speed conditions, and without sufficient chemical response at the interface, can lead to scuffing failure. In some contact situations, wear, scuffing and fatigue may occur simultaneously. The dominant failure mode will depend upon the impact parameters above mentioned.

One can categorize surface deterioration into three basic modes: wear, scuffing and fatigue.

The term “adhesive wear” is commonly used when failed surfaces appear to have undergone plastic flow due to local “adhesion” at the interface. When attempting surface fatigue simulation tests with advanced bearing materials having corrosion resistant properties, local adhesive events have been found to prevent operation when the EHD film thickness is small relative to surface roughness height. If the chemistry of the material does not allow the formation of surface films from reactions with the oil, adhesive wear can supersede surface deterioration due to surface initiated fatigue. In addition, material properties that affect plastic flow, like hardness, seem to influence the onset of adhesive wear [3].

The mechanisms that control the ability of a surface to handle high normal and shear stress and to recover subsequent to local damaging events are a mystery. Testing for these mechanisms and associated surface durability attributes is essential for material development and assurance of performance in service.

It was found that surface failure by adhesive wear is initiated at microscopic sites of insufficient surface film lubrication or at sites of debris encounters. With limited chemical reactivity between lubricating oil and some corrosion resistant materials, local adhesion events, which are not able to recover, propagate into broad patches of adhesive wear damage. With sufficient sliding velocity and contact stress, adhesive wear can transition into a major scuffing event. A scuffing event is characterized by a rapid rise in friction and temperature.

Some scuffing tests have been carried out on the high-speed twin-disk machine (see Figure 1) available at LMC-INSA Lyon facilities, using the disc specimens (see Figure 2).

The test protocol described below is an attempt to simulate the adhesive wear mechanisms that believed to occur in rolling element bearings.

In the experimental procedure the scuffing limit is reached by increasing progressively the sliding speed, other operating conditions such nor-mal load and the rolling speed being kept constant.

The evidence of disk scuffing is a sudden increase of friction force, which stops automatically the machine at an earlier stage of damage process.

The contacting disks, presented in Figure 1, were arched performed in order to reproduce the ball-inner ring contact from 7206 ball bearing (the ellipticity factor k=8.964). A total of 16 tests have been carried out.

The lubricant used in these tests is a mineral oil, ELF 154 NS. Its rheological behaviour is estimated from experimental traction curves obtained on the twin-disk machine.

Scuffing limits for mean rolling speed of 40 m/s, three maximum Hertzian pressures (0.8, 1.0 and 1.2 GPa) and three oil feed temperatures (40, 70, 100 ^{0}C) have been studied on the twin-disk machine.

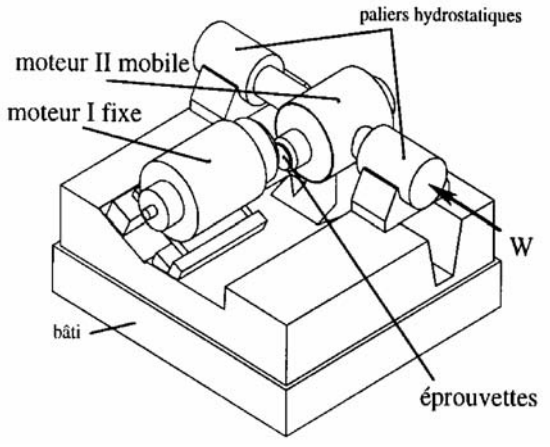

Figure 1. High-speed twin-disk machine

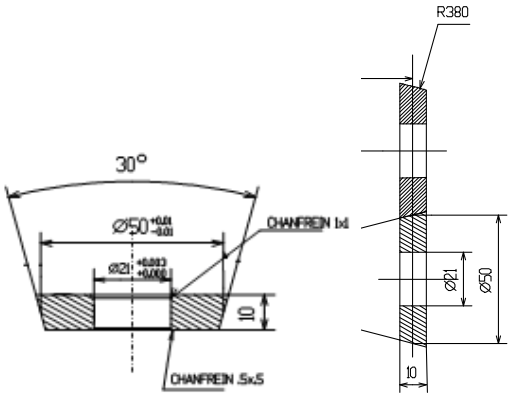

Figure 2. Disk specimens

For this simulative tribotesting, the simulation criteria reefer to material, geometrical characteristics and the lubrication regime of the practical system, that is 7206 angular ball-bearing.

4. RESULTS

The scuffing approaches analysis and our original experiments on rolling contacts have been detached the idea that, any scuffing mechanism considered, there is an energetically unbalance in the rolling contact. This unbalance generates disruptions in lubrication conditions and the scuffing risk appears. So, we consider the most adequate model to estimate the scuffing limits an energetically one. A dependence between contact pressure, sliding speed and critical level of energy dissipated can be settle for any operating conditions in a ball bearing which contact geometry and lubricant properties are known.

To estimate the scuffing failure for an angular contact ball bearing an algorithm have been proposed, as is presented in Appendix.

According to lubrication regime, the amount of heat is related to the oil film parameter λ. Also we consider the calculated and also measured contact temperature T as a supplementary criterion that reinforces the scuffing limits evaluation.

It was calculated the energy dissipated in contact and the onset of scuffing was estimated around $2 \cdot 10^{14}$ $W \cdot m^{-3}$.

Scuffing areas are corresponding to scuffing criterion:

$$\mu \cdot p \cdot V^{0.8} = \text{constant} \qquad (1)$$

Corroboration between all these experimental results allows a scuffing criterion to estimate this type of damage in angular contact ball bearing (7206C).

Figure 3 presents some scuffing experimental results obtained on specimens, using the test protocol above described and scuffing appearance on specimen surface.

Sliding speed and contact pressure with scuffing risk were found in antagonist coexistence, as follows:

- scuffing sliding speed has critical value up to 9 m/s (for specified testing conditions and a complete EHL regime);
- increasing the contact pressure and also the oil temperature impose the decreasing of critical sliding speed leading to scuffing.

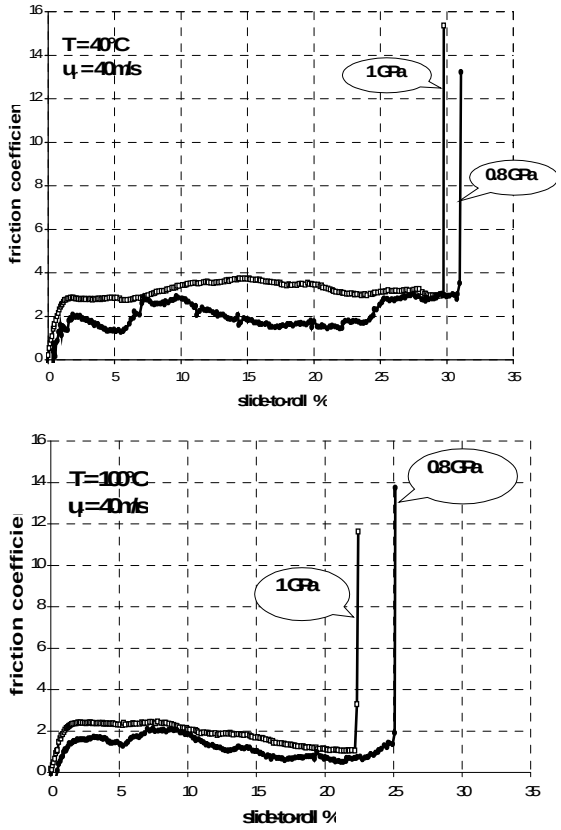

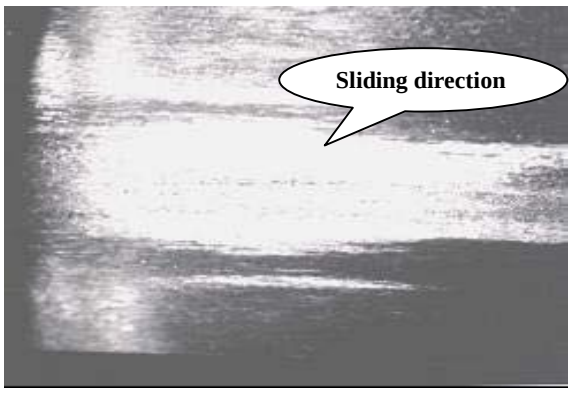

Figure 3. Scuffing onset

5. CONCLUSIONS

The test method invokes tribological inter-actions, which are measured in terms of friction,

gentle polishing wear of surface features, adhesive wear events and scuffing.

With respect to lubrication and failure mechanisms for a given tribo-contact system, we propose that the impact performance factors are the entraining velocity, the sliding velocity and temperature.

To make tests relevant to service performance, the impact parameters and their domain of operation must be understood. The lubrication and failure mechanisms that these ones invoke must then be properly simulated.

An experimental tool development must be devoted to this task.

REFERENCES

1. Lee S. C., Cheng H. S., 1998, "Scuffing Theory Modelling and Experimental Correlations," *ASME J. of Tribology*, 113, 3, pp.327-334.

2. Nélias D., Nassare F., Flamand L., 1999, « Etude experimentale et theorique du microgrippage dans les contacts elasto-hydrodynamiques, » *Rev. Gen. Therm.*, 36, pp. 26-39.

3. Bujoreanu C., Creţu S.S., 2005, "An Investigation of Scuffing in Angular Contact Ball-Bearings," *J. of the Balkan Tribological Association*, vol. II, 4, pp. 521-528.

APPENDIX

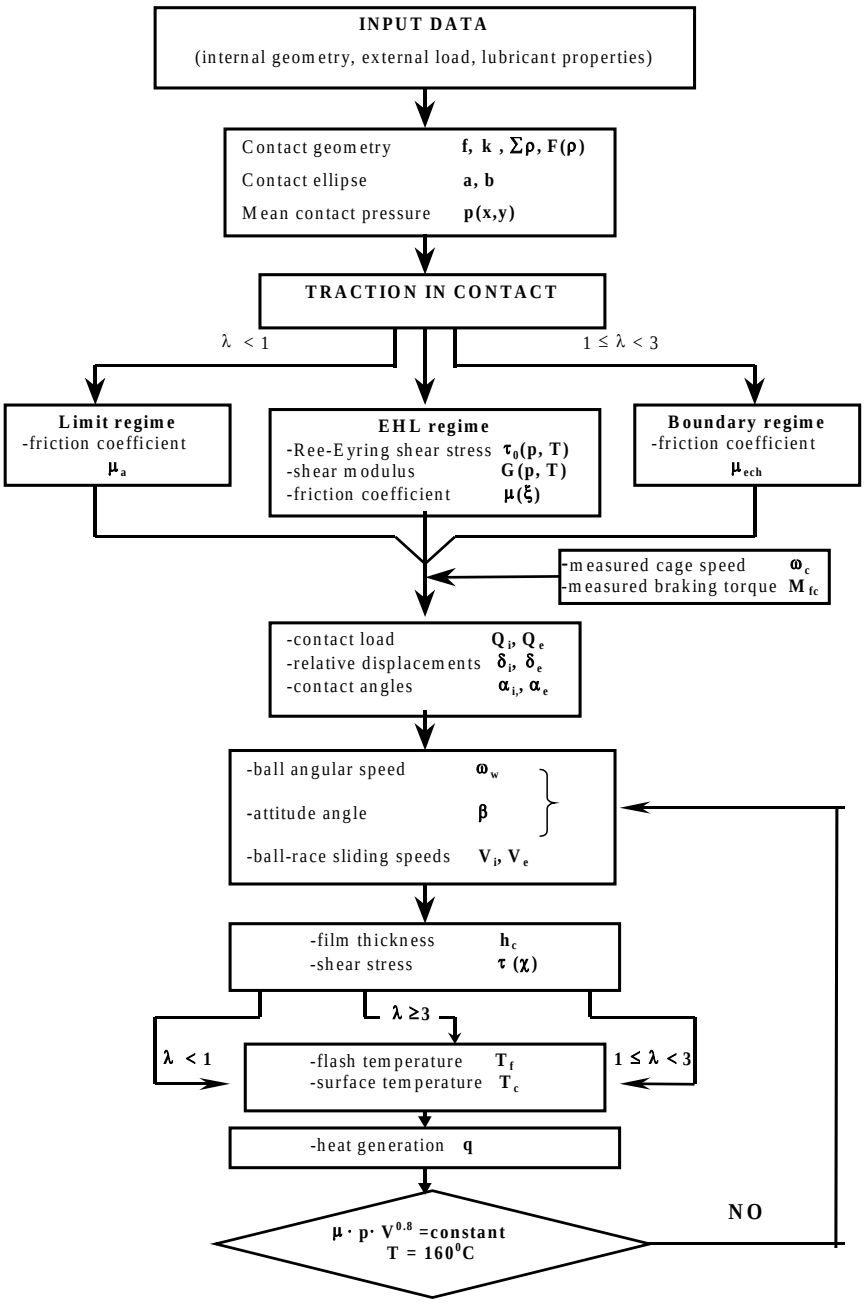

Algorithm for scuffing failure estimation in angular contact ball-bearing

ISSN 1220 - 8434

ACTA TRIBOLOGICA
Volume 17, (2009), 21-24

Gelu IANUŞ[1]

Dumitru OLARU[1]
e-mail: *dumitru_olaru@yahoo.com*

Peter LORENZ[2]

[1] Technical University "Gh. Asachi" Iasi, Dept. of Machine Design & Mechatronics, **ROMANIA**

[2] Hochschule fur Technik und Wirtshaft des Saarlandes HTW, **GERMANY**

ADHESION IN BALL ON FLAT MICROSYSTEMS

In the field of microsystems, adhesion force between the two contact surfaces has an important contribution to the friction losses. Two adhesion models have been presented and compared with the classical Hertzian model: the Johnson–Kendall–Roberts (JKR) model and the Derjaguin-Muller-Toporov (DMT) model. Using the above adhesion mentioned models, friction coefficient in a micro balls linear system has been analytical investigated.
Keywords: adhesion, adhesive contacts, contact mechanics, sphere–plane contact

1. INTRODUCTION

The influence of adhesion between solid surfaces on their mechanical performance becomes increasingly important with smoother surfaces, smaller length scales, and lighter loads. Nanotribological studies aim at explaining the frictional behavior of solid contacts by analyzing the mechanical properties of nanometer-sized asperities. Moreover, the advent of scanning probe techniques, particularly the scanning force microscope, has lead to a growing interest in theories describing the elastic deformation of small contacts under light load considering attractive forces [1].

If applied to arbitrary contact geometries, such theories easily become very complex. One of the mathematically simplest descriptions is obtained by assuming a sphere with radius R that is in contact with a flat surface. This geometry represents the perhaps most universal approximation of actual arbitrary single asperity contacts by any model geometry. However, easily applicable analytic theories that would describe its full mechanical contact behavior have not yet been reported even for this idealized model geometry [2-4].

Several continuum mechanics models have been developed which are able to predict the contact area between two elastic bodies. The first one of these models is due to Hertz and concerns two elastic spheres in the absence of adhesion. However, at small scales, such as the case of the tip–sample interaction in atomic force microscopy (AFM), the surface-to-bulk ratio becomes significant. Other models including the adhesion in the description of the contact area developed: the Johnson–Kendall–Roberts (JKR) model, the Derjaguin–Muller–Toporov (DMT) model, the Maugis–Dugdale (MD) and the Generalized Analytical Model [1].

Three of the above mentioned models was analyzed by the authors to obtain the best model for adhesion in a micro rolling linear system.

2. ANALYTICAL MODELS FOR ADHESIVE CONTACT

For a ball-plane contact presented in Figure 1, following assumptions can be made:

1. Deformations are assumed to be purely elastic, governed by linear equations of classical continuum elasticity according to the Hooke's law;
2. The contacting materials are elastically isotropic;
3. Neither Young's modulus E or Poisson's ratio **ν** changes under load;
4. The atomic structure is not taken into account;
5. The contact radius a is small compared to the radius R of the sphere (see Figure 1);
6. The curvature of the sphere in the contact area is described by a parabolic. This assumption works well as long as a <<R.

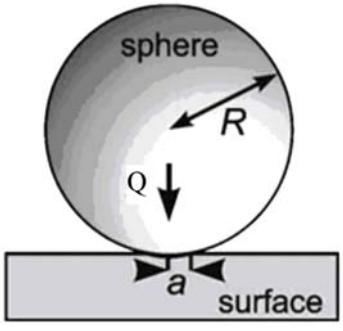

Figure 1. Geometry of a contact between a sphere and a flat surface: R - radius of the sphere: a- radius of the contact area; Q - externally applied loading force

Table 1 summarizes the relations for the radius of the contact area and the adhesion force for a spherical tip on a plane surface according to the three most used adhesion theories.

In the Table 1 following notations was made:

- F_{ad} – adhesive force between a sphere and a flat surface in N;
- R – radius of the sphere in m;
- Q – externally applied force in N;
- W- work of adhesion in N/m,
- E_{tot} – reduced Young's modulus determined by the relation:

$$E_{tot} = \frac{4}{3}\left[\frac{1-\nu_1^2}{E_1} + \frac{1-\nu_2^2}{E_2}\right]^{-1}, \quad (1)$$

where E_1 and E_2 are Young's modulus of sphere and surface in N/m^2, ν_1 and ν_2 are Poisson coefficients of sphere and surface; a - radius of contact zone between sphere and surface, in m.

In Hertz model the adhesion of the sample is neglected, whereas the two other theories take account of it outside (DMT) or inside (JKR) the contact area. Hence, Hertz theory can only be applied when the adhesion force is much smaller than the maximum load. In the two other theories, the work of adhesion W can be calculated from the jump-off-contact, if the sphere radius R is known. Then it is possible to calculate a as a function of the reduced Young's modulus E_{tot}. The JKR theory can be applied in the case of soft samples with a large adhesion, the DMT theory in the case of stiff samples with a small adhesion [2].

Table 1. Relations for the contact radius a and the adhesion force F_{ad} for a sphere on a flat surface [1]

	F_{ad}	a
Hertz	0	$\sqrt[3]{\frac{RQ}{E_{tot}}}$
DMT	$2\pi RW$	$\sqrt[3]{\frac{R}{E_{tot}}(Q+2\pi RW)}$
JKR	$\frac{(3\pi RW)}{2}$	$\sqrt[3]{\frac{R}{E_{tot}}(Q+3\pi RW+\sqrt{6\pi RWQ+(3\pi RW)^2})}$

3. EVALUATION OF FRICTION LOSSES IN A MICRO LINEAR BALL BEARING

The adhesion models presented in Table 1 was applied to a micro linear ball rolling system experimentally studied in [5]. Also, for this linear system, Olaru et al. developed an analytical model to evaluate the friction forces, model presented in detail in [6]. In Figure 2 is presented the geometry of a micro linear ball bearing.

The slider is in relative linear motion from the stator with the linear speed v and the ball has a angular velocity ω_b .

The geometrical characteristics of the micro linear systems are [8]:

- 4 stainless steel balls without contact between balls with diameter d=285 μm;
- silicon slider and stator with two V – groves realized at an angle $\theta = 54.7^o$;
- mass of the slider G =0.9 grams.

For these dimensions the adhesion between balls and silicon contact surfaces must be considered. Under the external load G all the four contacts of the ball with slider and stator are loaded with a normal force Q_0 given by relation:

$$Q_0 = \frac{G}{2 \cdot z \cdot \cos\theta}, \quad (2)$$

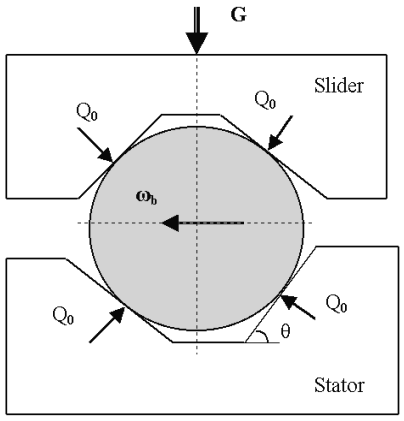

Figure 2. The geometry of the micro-linear ball-bearing [8]

According to the adhesion models presented in Table 1 the normal force for every ball – race contact Q will be determined by equations:

- Hertz model:

$$Q = Q_0; \quad (3)$$

- DMT model:

$$Q = Q_0 + 2\pi RW; \quad (4)$$

- JKR model:

$$Q = \left(Q_0 + 3\pi WR + \sqrt{6\pi WRQ_0 + (3\pi WR)^2} \right). \quad (5)$$

Considering dry contact on the surfaces of balls and races, in all four contacts are developed sliding contact forces FS as in Figure 3.

The moments acting on the ball are presented in Figure 4.

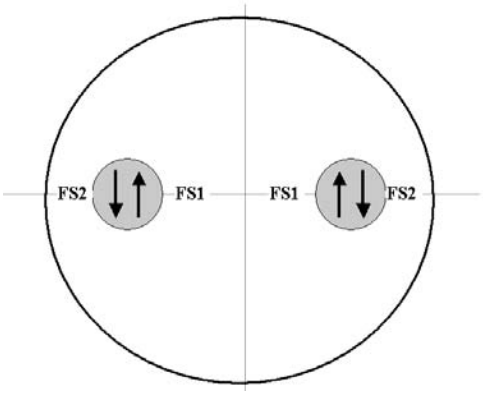

Figure 3. Sliding contact forces

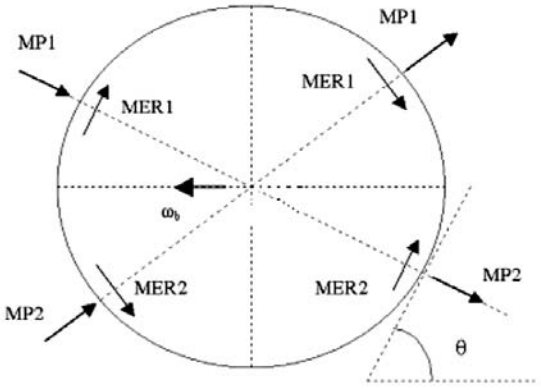

Figure 4. The moments acting on the ball

Based on the equilibrium of the forces and moments acting on the ball, the friction forces FS1 and FS2 can be determined as result of all the other forces and moments acting on the ball.

In each ball-race contact, two resistance moments are developed: the elastic resistance moments MER1 and MER2 and the pivoting moments MP1, MP2. The elastic resistance moment MER can be computed with relation:

$$MER = 7.48 \cdot 10^{-7} \left(\frac{d}{2} \right)^{0.33} \cdot Q^{1.33}. \quad (6)$$

Considering a constant friction coefficient for the sliding motion in a ball-race contact μ_s, the pivoting moment MP can be evaluated by relation:

$$MP = \frac{3}{8} \cdot \mu_s \cdot Q \cdot a. \quad (7)$$

The semi-major contact ellipse axis a is computed considering both normal load Q_0 and adhesion, according to the adhesion models as is indicated in Table 1.

To determine the friction forces FS1 and FS2, following two equilibrium equation are written: the equilibrium of the forces and of the moments acting of the ball. As result of symmetry the torques and the friction forces in contacts 1 and 2 are equal. Results the friction force FS as a function of the two torques: pivoting torque MP and elastic resistance moment MER:

$$FS = \frac{2}{d} \cdot \left[(MP) \cdot tg(\theta) + (MER) \right]. \quad (8)$$

Considering that every ball acts on the slider or stator in two contact points and for the same normal load in every contact, it can be obtained the total tangential resistance force given by a ball in rolling motion:

$$F_{ball-race} = \frac{1}{d} \cdot \left[4MP \cdot tg(\theta) + 4MER \right]. \quad (9)$$

For a system with z balls on the slider or on the stator acts a total tangential force F_{total} given by relation:

$$F_{total} = z \cdot F_{ball-race}. \quad (10)$$

A global friction coefficient can be obtained by dividing the total tangential resistance of the slider by the load G:

$$\mu_{global} = \frac{z \cdot F_{ball-race}}{G}. \quad (11)$$

4. NUMERICAL RESULTS AND CONCLUSIONS

The numerical results are performed for the condition used in the paper [5]:

- The geometrical parameters were mentioned above and the elastic properties of the ball and races were: $E_{steel} = 2.1 \cdot 10^{11}$ Pa, $E_{silicon} = 1.5 \cdot 10^{11}$ Pa, $\nu_{steel} = 0.3$, $\nu_{silicon} = 0.3$.
- The adhesion work for a steel ball and a silicon surface was considered to be W=0.07 N/m.
- The selection of the friction coefficient values for the pivoting moment between ball ad races μ_s was made according to the friction measurements realized with the various devices at the micro scale. The friction coefficient was computed for two values of the friction coefficient in pivoting motion, so for μ_s=0.5 and for μ_s=1.

The numerical results of global friction coefficient determined both for μ_s=0.5 and for μ_s=1

are presented in Figure 5 for all three adhesion models (non adhesion – Hertz, GMT and JKR models). For every model was computed the radius of contact area a and contact load Q according to the relations given in Table 1.

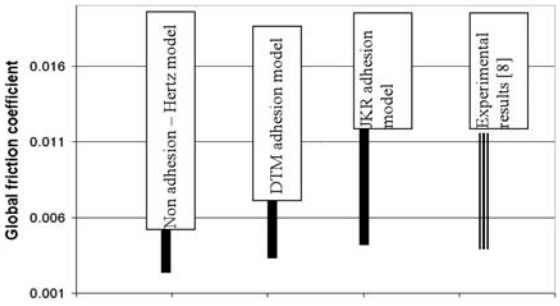

Figure 5. Numerical values of global friction coefficient determined by proposed model and experimental results obtained in [8]

If it was neglected the adhesion between ball and race according to Hertz model, was obtained values for the global friction coefficient μ_{global} between 0.003 and 0.006, as in Figure 5.

Including the adhesion effect was obtained increasing of the global friction coefficient. Small increasing of the friction coefficient was obtained with DMT adhesion model, with about 10% higher that Hertz model.

Including JKR adhesion model important increasing of global friction coefficient was obtained with values between 0.006 and 0.013 as is presented in Figure 5. The experimental results obtained in [5] indicate the global friction coefficient with values between 0.005 and 0.012.

Two important conclusions can be obtained:

- According to our analytical model it can be obtained global friction coefficient with and without considering adhesion effect between ball and rolling surface.
- The numerical results indicate that for micro steel ball and silicon plates used for a micro linear ball bearing the JKR adhesion model lead to the global friction coefficient compared with experimental results realized by [5].

ACKNOWLEDGMENT

This work was supported by CNCSIS Grant ID_607, NO. 381/4.10.2007.

REFERENCES

1. Schwarz, U.D., 2003, "A Generalized Analytical Model for the Elastic Deformation of an Adhesive Contact Between a Sphere and a Flat Surface," *J. of Colloid and Interface Science*, 261 (2003) 99–106.

2. Butt H.J., Cappella, B., Kappl M., 2005, "Force Measurements with the Atomic Force Microscope: Technique, Interpretation and Applications," *Surface Science Reports* 59, 1–152.

3. Sridhar, I., Sivashanker, S., 2003, "On the Adhesion Mechanics of Multi-Layer Elastic Systems," *Surface and Coatings Technology*, 167, pp. 181–187.

4. Johnson K. L., Greenwood J. A., 1997, "An Adhesion Map for the Contact of Elastic Spheres," *Journal of Colloid and Interface Science*, 192, pp. 326– 333, article no. cs974984

5. Lin T.W., Modafe A., Shapiro, B., Ghodssi, R., 2004, "Characterization of Dynamic Friction in MEMS – Based Microball Bearings," *IEE Transaction of Instrumentation and Measurement*, vol.53, no.3, June, pp.839-845.

6. Olaru D.N., Lorenz P., Rudy, D., 2004, "Frictioni in the Micro-Rolling Linear Systems for MEMS Applications," *VAREHD 12*, Suceava, 8-9 October.

ISSN 1220 - 8434

ACTA TRIBOLOGICA
Volume 17, (2009), 25-29

George V. PUIU[1]

Dumitru OLARU[2]
e-mail: *dumitru_olaru@yahoo.com*

Vasile PUIU[2]

[1] University of Bacau, Dept. of Machine Design,
ROMANIA
[2] Technical University "Gh. Asachi" Iasi, Dept. of Machine Design and Mechatronics,
ROMANIA

FRICTION TORQUE AND EFFICIENCY IN BALL - SCREW SYSTEMS

Complex relations for the friction torque and efficiency in a ball-screw system has been developed. The relations were adapted for a ball-screw system and influence of the speed and load on total friction torque were investigated. The efficiency of the system was computed and good agreement with the literature results was obtained. Also, a relation for the global friction coefficient in a ball screw system has been proposed.
Keywords: ball screw system, rolling friction, efficiency

1. INTRODUCTION

In a ball screw system the total friction consist of rolling and sliding friction in rolling contacts, friction in the return zones and recirculation channels, friction generated by lubricant and friction generated by sealing systems. The total friction torque generated in a ball screw system can be approximate by some empirical formulas depending of load and preload, rotational speed, lubricant, lubrication regimes, temperatures, sealing systems etc. In many applications it is necessary to accuracy estimate the friction torque acting on the nut or on the screw, for various operating conditions.

Based on the friction models for rolling bearings and for linear rolling guidance systems, the authors developed a new analytical model to evaluate the friction torque and efficiency in a ball screw system considering only the friction losses between the balls and races and between the balls. The numerical results were compared with experimental results obtained in literature [4,6] and good agreement was obtained.

2. FRICTION FORCES AND MOMENTS IN A BALL SCREW SYSTEM

In Figure 1 it is presented the position of a ball and the position of the normal load *Q* in a ball screw system, when the screw is rotating with an angular speed ω and the nut is moving with an axial speed ***v***.

2.1 Tangential forces on ball-race contact ellipses

The tangential forces developed between the balls and the races of screw and of the nut are presented in Figure 2. So, between ball and nut act the following forces: hydrodynamic rolling forces FRn, pressure forces FPn and FPnb, friction forces FSn. Also, between ball and screw acts the following forces: hydrodynamic rolling forces FRs, pressure forces FPs and FPsb, friction forces FSs. Between the balls acts the force FB. The directions of all above-mentioned forces are presented in Figure 2.

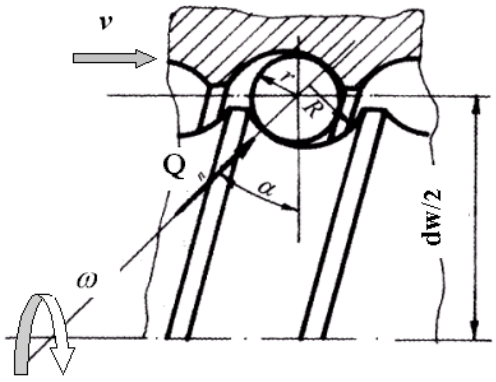

Figure 1. The contacts between ball and the two races in a ball screw system

FR is hydrodynamic rolling force due to Poiseuille flow of the lubricant contact. In the EHD lubrication condition this force can be computed by relationship [1-3]:

$$F_R = 2.86 \cdot E \cdot Rx^2 \cdot k^{0.348} \cdot G^{0.022} \cdot U^{0.66} \cdot W^{0.47}, \quad (1)$$

where E is the equivalent Young's modulus of the materials in contact, R_X is the equivalent radius in the rolling direction, k is the radii ratio, G, U, W are the dimensionless material, speed and load parameters developed in [3] for a ball-screw system.

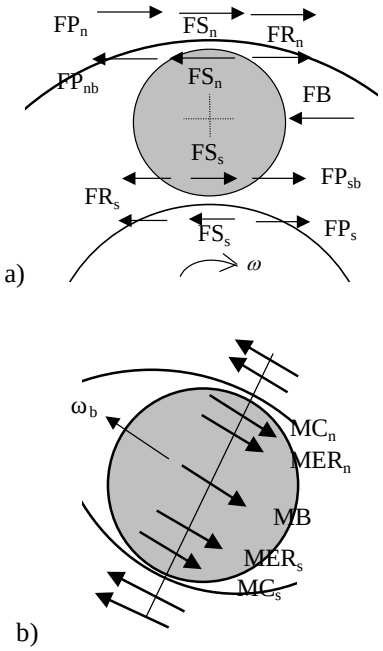

Figure 2. The forces (a) and the moments (b) acting on the ball and on the two races in a ball-screw system

FP is pressure forces due to the horizontal component of the lubricant pressure in the rolling direction. For a ball–ring contact, the pressure force acting on the center of the ball can be expressed as a function of hydrodynamic rolling force F_R [1-3]:

- for ball-nut contact:

$$FPnb = 2 \cdot FRn \cdot \left[1 + \frac{d_w \cdot \cos\alpha}{d_m} \right]; \tag{2}$$

- for ball-screw contact:

$$FPsb = 2 \cdot FRs \cdot \left[1 - \frac{d_w \cdot \cos\alpha}{d_m} \right]. \tag{3}$$

FB is the contact force between two balls. In this analysis FB is imposed.

The friction forces FSn and FSs on the two contacts are the sliding traction forces due to local micro-slip occurring in the contact, and can be calculated by the equilibrium of forces and moments acting on the ball.

2.2 The moments developed in the ball-race contact ellipses.

In the contact ellipses following two moments are developed: the moments due to elastic resistance generated in ball–races contacts MER and the moments generated by the curvature friction MC. Also, on the ball acting the resistance moment due to frictions between balls MB. In Figure 2 there are presented the moments which acts on the ball and are gene-rated on the contact ellipses: MCs, MERs are developed in the ball–screw race contact ellipse and MCn, MERn are developed in the ball–nut race contact ellipse.

MC is the curvature friction moment due to the local shear stresses developed in the slip region. Using a constant coefficient of friction μ_m depending of lubrication regime and a Hertzian distribution of the contact pressure, analytical relation for MC results [1,2,4]:

$$MC = 0.2 \cdot \mu_m \cdot \frac{Q \cdot a^2}{d_w} \cdot (1 - 5 \cdot Y^3 + 3 \cdot Y^5), \tag{4}$$

where Y is dimensionless distance between the point of pure rolling and the center of contact ellipse and can be considered 0.34, and a is semi major axis of contact ellipse.

MER is the elastic resistance of pure rolling and can be determined with relation of Snare [1-3]:

$$MER = 7.4 \cdot 10^{-7} \left(\frac{d_w}{2} \right)^{0.33} Q^{1.33} \times \left[1 - 3.519 \cdot 10^{-3} (k-1)^{0.806} \right]. \tag{5}$$

MB is a braking moment applied about the center of the rolling element:

$$MB = \mu_b \cdot \frac{d_w}{2} FB, \tag{6}$$

where μ_b is the friction coefficient between the contacted balls and FB is the contact force between the balls.

3. FRICTION TORQUE AND EFFICIENCY IN A BALL-SCREW SYSTEM

It is possible to express sliding forces FSs and FSn analytically to satisfy the equilibrium of forces and moments around the center of the ball. According to the forces and moments acting on the ball and presented in Figure 2 the following expressions for the forces FSs and FSn was developed:

$$FSs = \frac{MCn + MCs + MERn + MERs + MB}{d_w} + FRn + \frac{(FRs + FRn) \cdot d_w \cdot \cos\alpha}{d_m} + \frac{FB}{2}; \tag{7}$$

$$FSn = \frac{MCn + MCs + MERn + MERs + MB}{d_w} + FRs - \frac{(FRs + FRn) \cdot d_w \cdot \cos\alpha}{d_m} - \frac{FB}{2}. \tag{8}$$

According to Figure 2 the total tangential force between a ball and the screw Fs is the algebraic sum of the tangential contact forces in the rolling direction as $Fs = FRs + FSs$ and results:

$$Fs = \frac{MCn + MCs + MERn + MERs + MB}{d_w} + FRn + FRs + \frac{(FRs + FRn)\cdot d_w \cdot \cos\alpha}{d_m} + \frac{FB}{2}. \quad (9)$$

The friction torque generated by a ball-screw contact is:

$$Ms = Fs \cdot \left[\frac{d_m}{2} - \frac{d_w \cdot \cos\alpha}{2} \right] \quad (10)$$

The total tangential force between a ball and the nut Fn is the algebraic sum of the tangential contact forces in the rolling direction as Fn=FRn+FSn and results:

$$Fn = \frac{MCn + MCs + MERn + MERs + MB}{d_w} + FRn + FRs - \frac{(FRs + FRn)\cdot d_w \cdot \cos\alpha}{d_m} - \frac{FB}{2}. \quad (11)$$

The friction torque generated by a ball-nut contact is:

$$Mn = Fn \cdot \left[\frac{d_m}{2} + \frac{d_w \cdot \cos\alpha}{2} \right]. \quad (12)$$

For a number of z loaded balls, the total friction torque acting on the screw and on the nut is obtained by summing of the all friction torques in the ball-screw contacts, respectively:

$$MS = \sum_1^z Ms_i \; ; \quad MN = \sum_1^z Mn_i \; . \quad (13)$$

In a ball-screw system, neglecting the friction, to transmit an axial load F must acts on the spindle with an active torque MSa given by relation:

$$MSa = F \cdot Rs \cdot \frac{p}{\pi \cdot d_m} \; , \quad (14)$$

where p is the axial pitch of the screw.

Considering only the friction losses in ball-races contacts, the efficiency of the ball-screw system can be expressed by relation:

$$\eta = \frac{MSa}{MSa + MS} \; . \quad (15)$$

A relation for the global friction coefficient has been proposed. So, it can be determined a global friction coefficient in a ball screw - system, similarly with a rolling bearing, using the following relation:

$$\mu_{global} = \frac{MS}{Rs \cdot F} \; . \quad (16)$$

4. NUMERICAL RESULTS

A numerical program was developed in order to analyze the variation of the efficiency according to rotational speed of the screw and axial load.

Following geometrical parameters was considered: the average diameter of the screw d_m=40 mm; the ball screw d_w=3.175 mm; the pitch of the screw p = 5 mm; the number of active balls z=56; contact angle $\alpha=\pi/4$; ball roughness is $\sigma_b = 0.08\mu m$; screw and nut races roughness $\sigma_s = \sigma_n$ =0.3 μm friction coefficient betweens balls μ_b =0.1. The viscosity of the lubricant is considered as η_0 = 0.05 Pa.s. The contact load between balls is assumed to be FB=1/z Newtons. The dimensionless parameter Y is assumed to be 0.34, both for ball – screw and ball- nut contacts. The conformity of the screw and nut races was considered to have values of 0.515. The rotational speed n was considered between zero and 1000 rpm and axial load F was between 100 to 4000 Newtons.

The variations of the friction torque MS with rotational speed of the screw and contact load are presented in Figure 3. Increasing of the normal load leads to the increasing of the total friction torque. For small normal loads (Q=20 N) it can observe a continuum increase of the friction torque with speed. For high normal load (Q=100 N) it can be observed a Striebeck curve in variation of the friction torque with rotational speed. So, for low speed limits to mixed lubrication conditions in ball-races contacts can be developed with high value for the friction coefficient μ_m.

Increasing of the speed implies increasing of the lubricant film thickness and transfer to the mixed or EHD lubrication conditions.

The proposed analytical model gives for ball-screw efficiency values between 0.90 to 0.96, according to relation (15), depending on the geometrical and functional conditions.

In Figure 4 there is presented the variation of the ball-screw efficiency with rotational speed of the screw for different normal loads.

When the ball-screw system is low loaded (Q=20 N) important decreasing of the efficiency can be observed, for increasing of the rotational speed. By increasing of the axial load it can be obtained good values for the efficiency η=(0.93…0.95). Also, as result of a Striebeck behavior, a maximum efficiency can be obtained for (50 – 100) rot/min.

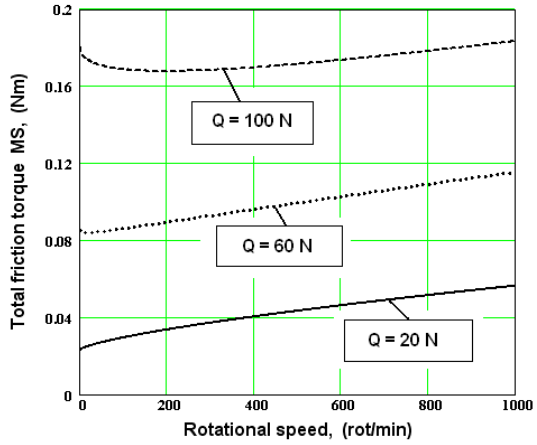

Figure 3. Variation of the total friction torque MS with rotational speed and normal load

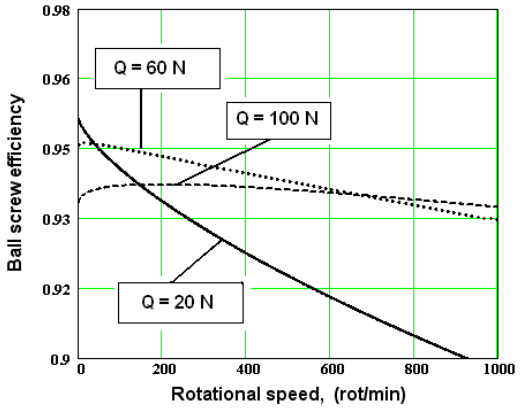

Figure 4. Variation of the ball-screw efficiency with rotational speed and normal load

The influences of the contact load Q and rotational speed on the efficiency in a ball-screw system are presented in Figure 5.

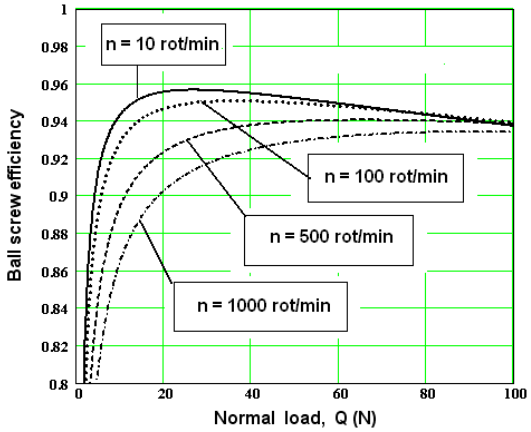

Figura 5. Variation of the ball-screw efficiency with contact load and rotational speed

It can be observed that increasing of the axial load (increasing of the contact load Q) lead to an increasing of the friction torque. The variation of the efficiency with the contact load has two zone: first zone correspond to low values of normal load (Q=0 to 20 N) when the efficiency increases from zero to 0.9 and the second zone with Q higher than 20 N with higher values for the efficiency (0.92…0.95), depending of the rotational speed.

It can be observed the presence of a maximum efficiency depending of rotational speed and load.

The proposed global friction coefficient according to the relation (16) has been analytical determined as variation of the rotational speed. Some numerical results are presented in Figure 6.

The global friction coefficient in a ball screw system has the similar values with a ball rolling bearing. In our investigation the values between 0.002 and 0.006 have been obtained. For normal load (Q>20 N) the global friction coefficient has very good values (0.002…0.004).

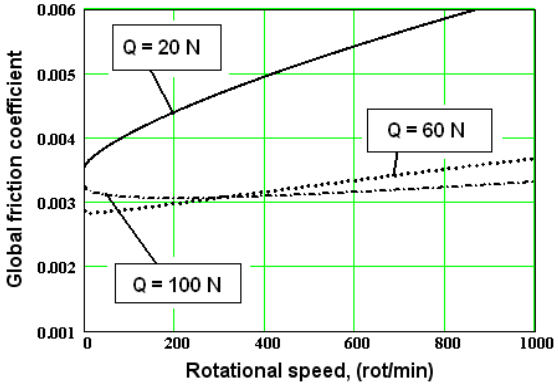

Figura 6. Variation of the ball-screw global friction coefficient with rotational speed and contact load

5. CONCLUSION

Based on the equilibrium of the forces and moments acting on the ball, the sliding forces between ball and both screw and nut in a ball - screw system was determined without an integrating of the shear stress on contact ellipses.

A general analytical model for friction torques and efficiency in a ball screw system has been developed. The analytical model includes influence of the rotational speed, axial load, lubricant viscosity and geometry of the ball-screw system. The developed model leads to realistic values both for the friction torque and for the efficiency of a ball-screw system.

A relation for the global friction coefficient has been proposed. So, it can be determined a global friction coefficient in a ball screw-system, similarly with a rolling bearing.

REFERENCES

1. Olaru, D.N., Lorenz, P., Rudy, D., Cretu, S., Prisacaru, Gh., 2002, "Tribology Improving the

Quality in the Linear Rolling Guidance Systems.Part 1 Friction in Two Contact Points Systems," *Proc. of the 13th International Colloquium on Tribology*, Esslingen (Germany), 15-17 January, (2002).

2. Olaru, D.N., Lorenz, P., Rudy, D., 2004, "Friction in the Circular–Arc Grooves Linear Rolling Guidance System," *Tribologie und Schmierungstechnik*, 2, pp. 9 –14.

3. Olaru, D.N., Puiu, G., Puiu V., 2004, "Friction in Ball-Screw System," *Proc. of International Conference VAREHD 12*, Suceava.

4. Puiu, V., 1999, "Ball Helical Transmission," *Buletinul Institutului Politehnic Iaşi*, vol.XLV (XLIX), fasc. 1-2, secţia V (Construcţii de maşini), pp.35-40.

5. Puiu, V., Olaru, D.N., 1999, "Film Thickness in Ball Screw", *Buletinul Institutului Politehnic Iaşi*, vol.XLV (XLIX), fasc. 3-4, secţia V (Construcţii de maşini), pp.17-20.

6. Purice, V., 1984, "Influenţa tipului de lubrifiant şi a parame-trilor funcţionali asupra momentului de frecare din şuruburile cu bile," *TRIBOTEHNICA'84*, vol. II, Iaşi, pp.105-110.

ISSN 1220 - 8434

ACTA TRIBOLOGICA
Volume 17, (2009), 30-33

Vytautas VASAUSKAS

Juozas PADGURSKAS

Raimundas RUKUIZA

[1] Department of Mechanical Engineering,
Lithuanian University of Agriculture ,
LITHUANIA

SURFACE MODIFICATION OF CARBON STEEL BY DEPOSITION OF FLUOR-OLIGOMERIC FILMS

The chemosorbic compounds with metal are composing after coating the surface with fluor-oligomeric material (FOM). Hardness, indentation and friction behaviour of FOM coat were investigated. Scratch adhesion and friction tests show that the fluor-oligomeric film decreases the micro-hardness of solid body and modifies the contact rheology by reducing the shearing force at the local contact. FOM coat shows good elasticity in rough contacts, but with a higher hardness it may be more suitable for abrasive applications, i.e. reduced plasticity in a given tribo-contact.
Keywords: fluor-oligomeric films, indentation, micro-hardness, chemosorbic compounds

1. INTRODUCTION

Growing attention to fluor-polymer and oligomeric films having the thickness from 0.1 up to 10 μm is recently given. The reason is their specific properties, such as good thermal stability, low coefficient of friction and simple coating of the friction surface [1,2]. Fluor-oligomeric materials (FOM), known under trade names as "FOLEOX" and "EPILOM", are liquid steamy oligomeric compounds of fluorine with oxygen and carbon and there are a kind of perfect self-lubricating material due to its low friction coefficient, good high-temperature stability and chemical stability [3]. This new family of composite materials frequently exhibits remarkable improvements of material properties when comparing to conventional micro- and macro-composite materials. The chemosorbic compounds with metal are composing after coating the surface with FOM. Surface modification should constitute a few mono-layers of the FOM polymer surface and the deeper layers (bulk material) should not be altered. This transfer into the top mono-layers (what is known as Rebinder effect) has different (generally desired) properties than the bulk material, which retains the original properties. Generally, chemical reactions that involve the incorporation of particular elements (fluorine atoms etc.) in tribo-film formation are invoked for modification processes [4]. The mechanical behavior, the elastic modulus and the hardness of thin coats is usually characterized through indentation hardness tests, particularly using depth-sensing indentation equipment. The maximal indentation depth, which eliminates the influence of the substrate to hardness measurement, can be quite small for very thin films. The aim of this investigation is to characterize the fluor-oligomeric coats as concerning their ductility, coat thickness and tribological properties.

2. EXPERIMENTAL PROCEDURE

The solutions of FOM (0.5…10% concentration) type FOLEOX were used for creating polymer coat on the metal surface. The specimen materials are carbon steel used for machine structures (carbon content 0.45%). Cylindrical samples of 30x30 mm in size of medium carbon steel grade AISI 1045 (DIN 1.1186) composition in wt % being (Fe, (0.37…0.44) C, (0.6…0.9) Mn, (0.19…0.23) Si), were cut, quenched and tempered for various hardness levels (40<HRC<63). The samples were grounded and mechanically polished to a surface roughness Ra of 0.2 μm. They were cleaned with acetone before testing. The mass of the FOM films in this study, depending of the thickness, was in the μg range. After the surface is coated with fluor-oligomeric coat, the chemosorbic bindings are created between metal surface and the film. The thickness of FOM layers was about 0.1…0.16 μm. Although the films allow water vapour diffusion, the films are both hydrophobic and not "wetted" when liquid waters contact these layers. The main goal of depth-sensing indentation is to obtain the elastic modulus and the hardness of the FOM film specimen by processing the experimental readings of indenter load and penetration depth. When the load is removed from the indenter there is some degree of recovery due to the relaxation of elastic strains within the material. The analysis of the initial

portion of this elastic unloading response gives us an estimation of the elastic properties of the coated material. Hardness tests were carried out with a Vickers pyramid indenter, using a Fischer HP 100 XY-PROS ultra-micro-hardness tester [5]. A diamond indenter of standard geometry, typically a 1360 square based pyramidal diamond (Vickers), is indented under a known load, into the surface of the sample. During tests, load – indentation depth – time data were recorded. Hardness measurements were performed under six different indentation loads, ranging from 0.1 to 1.0 N. At each load level, at least 10 measurements were done on the coatings. However, besides the properties of the coatings, the testing methods can also affect the performance of the coatings. Firstly, the fact that the scale of contact, being dominated by the film hardness at small scales as compared to the coating thickness and by the substrate hardness at large scales. Secondly, the stress-strain situation during indentation is triaxial. The scratch machine consisted of free lever arm with an indenter, attached onto one side. After applying the normal load to the indenter, the specimen, which was mounted on a stage, was moved at constant speed using a stepper motor. In this way scratches were produced on the surface of specimen. Vickers pyramid indenter and conical tungsten-carbide indenters of included angles of 90°, 120°, 160° and 170°, with 10 µm radii spherical tips were used for scratching. The range of normal load was 0…100 N; the range of scratch length varied between 1 nm and 10 mm; trial of friction - mono-pass.

3. RESULTS AND DISCUSSION

The depositing process was optimized according to the values for properties of hardness, adherence and wear measurements, using micro hardness and scratch tests.

Figure 1 shows the loading-unloading cycle obtained using a micro-indentation tester operating in the ramp mode and corresponding to Vickers contact geometry with non-coated sample and samples with fluor-oligomeric film. The load is incremented at constant speed up to the maximum load (F_{max}) and subsequently released at the same rate as in the loading cycle. The geometrical similarity of a pyramid Vickers indenter results in the quadratic relationship of the load F vs. the penetration depth h in the indentation loading, i.e. $F = k_1 h^2$. In contrast to loading, the unloading path follows the non-quadratic relationship of $F = \alpha(h - h_f)^m$, $(1.2 < m < 2.0)$, where h_f is the residual depth of the pyramidal impression after complete unloading [6]. In other words, the surface after being modificated by FOM films can be investigated in the elasto-plastic indentation regime and the locally distorted convex surface profile of the impression yields a non-quadratic F-h relationship with the exponent m less than 2.0 [7].

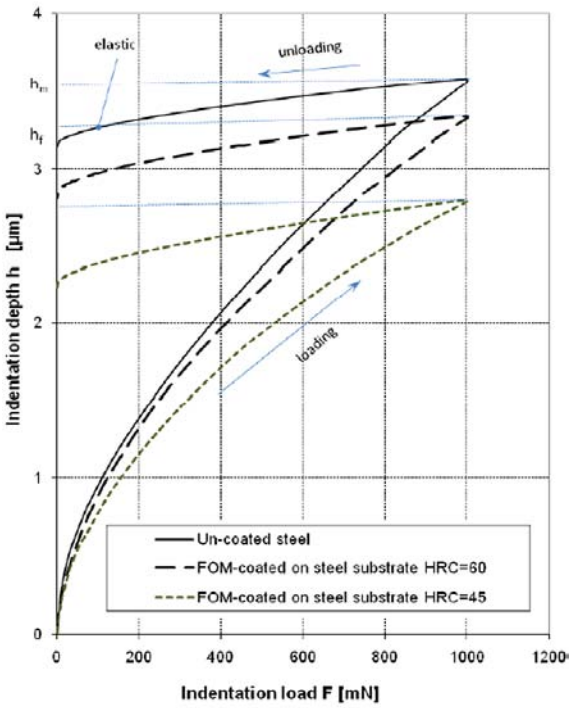

Figure 1. Typical loading and unloading curves of micro-indentation test cycle for un-coated sample and samples coated with fluor-oligomeric film. h_f is the residual indentation depth and h_m is the maximal depth of indentation

Figure 1 displays that each loading curve coincides with others in their common parts, indicating that the first assumption in the previous section, is reasonable. Experimental results showed that for all samples surface parameters remain constant for all the depths and the elastic properties of the samples are irrespective of the depth. This observation agrees with the fact that surface modified by FOM film has no significant influence on the elastic modulus of the surface region. By micro-hardness testing it is impossible to guarantee that the coating hardness will be measured independent of the substrate, particularly as the coating thickness is reduced. In order to give the most accurate results from indentation, the indenter penetration (1/7 of the indenter diagonal for a Vickers indenter) needs to vary between t/10 and t, where t is the coating thickness.

The difference in the hardness gradient causes variations such that a coating film with higher fluorine content may not always possess lower specimen hardness. Such attribute becomes noticeable when the coat is sufficiently thick. This quality can be interpreted as the combined effect of the decrease in the hardness due to the increase in the fluorine content and the increase in the hardness due to an increase in the film thickness. Surface modification by fluor-oligomeric film usually

introduces a hardness gradient in the near surface region of the material. The fluor-oligomeric treatment decreases the micro-hardness of solid body till 15% at 0.02…0.03 mm deep because of chemosorbic interaction with steel [6]. It is difficult to measure coating thickness which introduces the most significant error into the results. The unknown values of Young's modulus for many coatings are another source of error as in the assumption that the modeled scratch tests are conical when in fact a Vickers indenter is pyramidal. Quantitative measurements show that all coats displayed hardness values between 200 and 300 HV after preparation. The observed hardening loss process is assumed to be the result of a structure change, which is induced by fluor-oligomerisation and Rebinder effect process [9].

Fluor-oligomeric films formed by immersion into FOLEOX solution show a weaker scratch resistance than the films formed by dropping. It is possible to conclude that thickness of FOM film formed by immersion into solution is much thinner than that formed by the dropping the FOLEOX solution onto the surface of specimen. Frictional measurements of all material were carried out on the conventional hardness measurement tests. A simplified model is presented here for the case of analyzing the frictional force. Two hard tungsten carbides cones with various apex angles are pressed into a soft steel specimen surface, until plastic flow occurs. The torque required to slide the specimen relative to the cone indenters at low velocity is then measured. A small hole is provided at the center to eliminate the singularity that would otherwise exist there. The mean shear stress (τ) and normal stress (σ) may be estimated for different values of applied load.

Test results show clearly indicated deviation from Amonton's law as well as the reduction in coefficient of sliding friction with the increase in the applied load. It may be noticed that the static frictional force increases at first almost linearly with an increasing contact pressure and then it tends to approach a critical value, above a specific value of contact pressure. Results show that FOM layer formation occurs at low FOLEOX intensity. The film is of porous structure and adheres to the worn surface. The surface looks to be very oxidized and have a different morphology. The FOM film modifies the contact rheology, reducing the shearing force in the contact, facilitating sliding and decreasing the damage due to plastic deformation.

Typical morphology of wear scar surfaces with and without FOM composite coatings obtained from scratch testing are shown in Figure 2. The SEM micro-graphs of all the as-deposited coatings showed a combination of very fine powders and patterns of compacted debris along the side of the wear track. For both composites with and without coats, the wear path showed similar morphology with some regions along the wear track that are covered with a FOM film. The difference of surface conditions can be clearly seen. The worn surface of the scratch without FOM (fig. 2a) clearly shows flaking and delaminating of the surface.

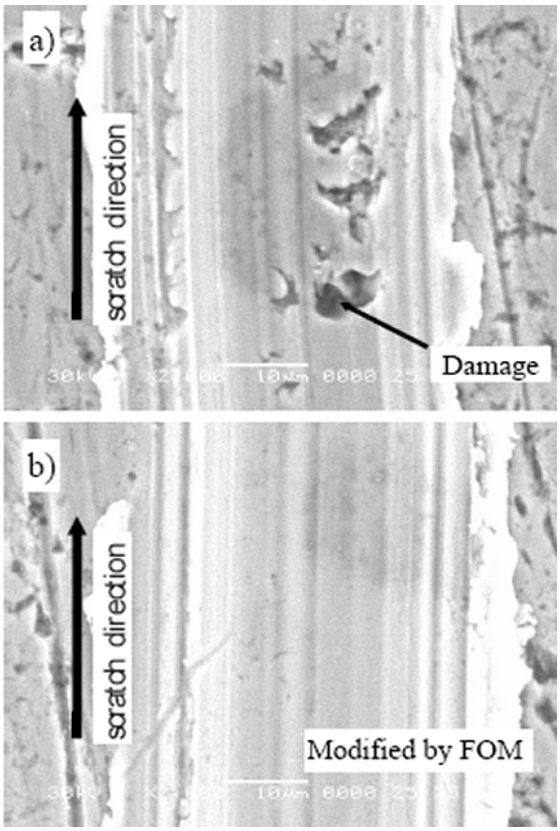

Figure 2. SEM micrographs obtained from the scar surface of FOM/steel coating after wear testing at 10 N load showing (a) un-coated sample, (b) FOM-coated sample

It could be seen the transition from where the coat undergoes no damage to where the coating adhesive delaminates from the surface, but otherwise it remains adhesively intact. It can be seen that micro-cracks were generated under the center of the intender tip and radiate outward at 45° angles. It results the removal of a small pieces of material, consequently leaving the substrate exposed and even damaged by the indenter (fig. 2a). Large wear fragments are stuck to the surface and the parts, which are close to flaking, also have a crude form. Those fragments are able to provide deep abrasive wear during the sliding contact. In the presence of FOM the wear particles, which are attached to the surface, are very thin. Figure 2b displays that FOM layer formation is taking place at low FOLEOX intensity. The film is porous and adhesive to the worn surface. The FOM film modifies the contact rheology, reducing the shearing force at the contact, facilitating sliding and decreasing the damage due to plastic deformation.

The surface modification by FOM coating shows good elasticity in rough contacts but with a higher hardness it may be more suitable for abrasive applications, i.e. reduced plasticity in a given tribo-contact.

4. CONCLUSIONS

With regard to the enhancement of the mechanical contact responses of substrate by thin fluor-oligomeric coatings we can do the following conclusions.

- The coating process should be optimized according to the values for properties of hardness, adherence and friction, measured using micro-hardness and scratch tests.
- For a displacement having the order of the coating thickness, the maximal residual displacement of indenter is reduced by ~30%.
- The fluor-oligomeric coat has a pronounced effect on hardness and dominates response at displacements ≤ t/10.
- Surface modification by fluor-oligomeric film usually introduces a hardness gradient in the near surface region of the material. The fluor-oligomeric treatment decreases the micro-hardness of solid body till 15% at 0.02…0.03 mm deep because of chemosorbic interaction with steel.
- Fluor-oligomeric films formed by immersion into FOLEOX solution show a weaker scratch resistance than the films formed by dropping. It is possible to conclude that thickness of FOM film formed by immersion into solution is much thinner than that formed by the dropping the FOLEOX solution onto the surface of specimen.
- Coated system, which has induced possible fracture, follows the substrate crack path in conditions of plastic yielding.
- FOM coating shows good elasticity in rough contacts but with a higher hardness it may be more suitable for abrasive applications, i.e. reduced plasticity in a given tribo-contact.

ACKNOWLEDGMENTS

The study was performed under INTAS financial support (Grant Ref. Nr 05-104-7540).

REFERENCES

1. Bhushan, B., Gupta, B.K., 1991, *Handbook of Tribology: Materials, Coatings and Surface Treatments*, McGraw-Hill, New York, USA.

2. Myshkin, N.K., Petrokovets, M.I., Kovalev, A.V., 2004, "Tribology of Polymers: Adhesion, Friction, Wear and Mass-Transfer," *Tribology International*, 38, pp. 910-921.

3. Isakovich, V.S., Struk, V.A., Gubanov, V.A., 1992, Troi-chanskaya, P.A. "The Influence of Hydrophobic Chemosorbic Films on the Tribotechnical Characteristics of Pair Metal-Metal and Polymer-Metal," *Friction and Wear*, 13, 2, pp. 306-310 (in Russian).

4. Rukuiza, R., Padgurskas, J., Vötter, M., Wollesen, V., 1999, "New Tribotechnical Materials for the Friction Pair Radial Lip Seal / Shaft," *Industrial Lubrication and Tribology*, 51, 5, pp. 233-238.

5. *** Evaluation Manual of Indentation Procedure, Helmut Fischer GmbH + Co, Sindelfingen, Germany, (2000).

6. Gore, G.J., Gates, F.D., 1997, "Effect of Hardness on Three Very Different Forms of Wear," *Wear*, 203/204, pp. 544-563.

7. Briscoe, B.J., 1996, "Scratching Maps for Polymers," *Wear*, 200, pp. 137-147.

8. Rukuiza, R., Padgurskas, J., 2007, "Influence of Fluor-Oligomeric Film on Tribological Properties in Local Contact Conditions," *Tribologie und Schmierungstechnik* (in press).

9. Rebinder, P.A., Likhtman, V., 1957, *Proc. of 2nd int. conf. Surface Activity*, III ed. J.H. Schulman, Academic Press, New York, USA, pp. 563.

ISSN 1220 - 8434

ACTA TRIBOLOGICA
Volume 17, (2009), 34-41

Andrei SZUDER[1]
e-mail: *szuder@ctanm.pub.ro*

Ioan D. MARINESCU[2]
T. G. MATHIA[3]
G. MEILLE[3]

[1] University Politehnica Bucharest, Center for Advanced Technologies, Bucharest,
ROMANIA

[2] University of Toledo, Toledo, Ohio,
USA

[3] Laboratoire de Tribologie et Dynamique des Systèmes- C.N.R.S.; École Nationale d'Ingénieurs de St. Etienne, École Centrale de Lyon, Ecully,
FRANCE

ABRASION IN FINISHING PROCESSES

The paper is an overview of the present state of the art and of the research and development results concerning the finishing abrasive processes.
Finishing processes are final machining processes which use fine grit abrasive as the cutting medium. The processes are widely used in industry in order to improve the surface topography to increase the bearing area and load-carrying capacity.
The main characteristic of finishing abrasive machining processes is that these processes are more random than many other machining processes. Tribology offers a good approach for describing the main characteristic of abrasive finishing processes and offers the ability to predict some of the outputs of the processes like abrasion rate or the surface quality.
The basic concepts and recent developments in lapping, polishing and fretting as well as the significance of surface metrology (especially the 3D methods) in finishing processes are presented.
Keywords: finishing, abrasion, lapping, polishing, fretting

1. INTRODUCTION

Abrasive manufacturing processes are probably less understood, published and educated for various scientific and economic reasons. On other side, economically the abrasive manufacturing process mostly is a final operation, therefore if correctly achieved is giving very high additional value. From energy point of view, the abrasive manufacturing procedure is one of more consuming. If one takes into consideration the ratio of the weight and the volume per amount of consumed energy is one of the highest.

The great difficulty facing the abrasion studies with abrasives lies in the great number of process interdependent variables and particularly in the abrasive variables of shape size and size distribution [1].

In most cases, the abrasive mode of surface finishing is a final one. In addition, the abrasive manufacturing process is also highly time consuming. Therefore, the abrasive process is probably the most expensive mode of industrialized machining and finishing of surfaces, frequently kept secret.

Abrasive machining processes are manufacturing techniques which employ very hard granular particles in machining, abrading, or polishing to modify the shape and surface texture of manufactured parts.

Abrasive finishing processes are accepted in a wide range of material applications and industries; typical examples are finishing of various components used in aerospace, automotive, mechanical seals, fluid handling, and many other precision engineering industries.

A wide range of such processes is mostly used to produce high quality parts to high accuracy and to close tolerances. Examples range from very large parts such as machine slideways to small parts such as contact lenses, needles, electronic components, silicon wafers, and ball bearings.

While accuracy and surface texture requirements are common reasons for selecting abrasive processes, there is another common reason. Abrasive processes are the natural choice for machining and finishing hard materials and hardened surfaces.

The manifestations of abrasive wear are the change of the surface roughness resulting from material removal and the change of the physical and chemical properties of the surface and subsurface with respect to those of the bulk. In addition to the mechanical and geometrical description, these deformations are accompanied by:

- the production of highly localized heat;
- the creation of excitations and defects in the material;
- the production of dangling bonds and trapped electrons;
- the emission of excited and reactive species into the gas phase (exo-emission).

All these phenomena result in a highly reactive surface accompanied by the formation of a

surface composition different from that of the bulk. Separation of charges also leads to the creation of intense electric fields at the surface of many insulating materials.

The abrasive processes may be categorized into one of following groups:

- grinding;
- lapping;
- polishing;
- honing.

This is not a completely inclusive list but usually the lapping, polishing and honing are considerate finishing processes and will be treated in this state of the art analysis

Honing is a process that employs bonded or fixed abrasives within the abrasive tool, whereas lapping employs free abrasive particles, often suspended in a liquid or a wax medium [2].

2. ABRASIVE MECHANISMS

The abrasive mechanisms occurring in a dry or humid environment result from the simultaneous actions of normal and tangential forces and are materialized by the development of ploughing grooves or scratches which are in some instances accompanied by Hertzian fractures.

The main characteristic of abrasive machining processes is that these processes are more random than many manufacturing processes

One classification scheme divides abrasive wear into two basic modes known as two-body abrasion and three-body abrasion. Another used approach involves division into three categories: gouging abrasion, high-stress abrasion and low stress abrasion. Whereas the two body/three body abrasion classification appears to be dominant in Europe, the gouging/high stress/low-stress abrasion approach appears to be favored in the US and Australia.

For the classification of the abrasive wear modes, we will use the most widely accepted terminology known as two-body abrasion and three-body abrasion.

The primary meaning of the two-body/three-body concept is to describe whether the abrasive particles are bound (two-body) or free to roll or slide (three-body).

3. TWO BODY ABRASION

The two-body abrasive wear is caused by abrasive particles or asperities which are rigidly attached (embedded) in the second body (Figure 1).

The relative motion between the abrasive and the workpiece is usually considered pure sliding

The abrasive particles in a two-body mechanism are able to cut deeply into the workpiece material, whereas in the case of three-body abrasion, the abrasive grains may spend only part of their time cutting into the material. Therefore, two-body abrasion is considered to produce wear rates three times bigger than in the case of three-body abrasion under the same loading condition [2].

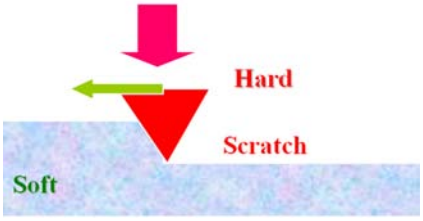

Figure 1. Two body abrasion

3.1 Three body abrasion

The three-body abrasion refers to wear caused by free and loose abrasive particles existing as interfacial elements between a solid body and a counterbody.

The free particles in a three-body wear mode may be intentionally added abrasives or be detached debris from the worn surface (Figure 3).

The three-body abrasion can be divided into "closed" and "open" groups. The closed group covers the cases of abrasives between closely mating surfaces and the open group covers the cases where there is a thick bed of abrasives.

The distinction between low-stress and high stress abrasion centers whether or not the abrasive particles are fractured during abrasion. This may be significant since fracturing generates fresh, sharp cutting edges and usually gives higher wear rates.

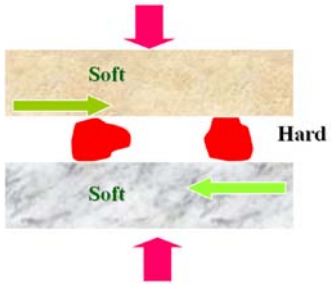

Figure 2. Three body abrasion

3.2 Lapping

In lapping, a free abrasive is introduced between a lap, which may be a cast iron plate, and the workpiece surface. The free abrasive is usually suspended in a liquid medium, such as oil, providing lubrication and helping to transport the abrasive. The lap and the abrasive are both subject to wear.

Each abrasive grain used for lapping has sharp irregular shapes and, when a relative motion is induced and pressure applied, the sharp edges of the grains are forced into the workpiece material.

The loose abrasive particles wear the surfaces by making indentations or causing the material to cut away very small particles. Even though the

abrasive grains are irregular in size and shape, they are used in large quantities and thus a cutting action takes place continuously over the entire contact surface.

To maintain the required geometry of the lap and of the workpiece surface, it is necessary to pay careful attention to the nature of the motions involved to average out the wear across the surface of the lap. Several laps may be employed and periodically interchanged to assist this process.

The size and size distribution of the abrasive are important factors in the surface obtained by lapping. The size of the abrasive is directly proportional to the material removal rate and surface roughness.

Larger grain sizes have a higher stock removal rate than smaller abrasive grains but the smaller abrasives produce a lower surface roughness than larger abrasive sizes.

Another important factor is the concentration of abrasive (the amount of abrasive per volume of carrier) which represents the number of grains in contact with the surface of the workpiece material. When the concentration varies, the load distribution changes. This means that with an increase in the number of grains, the effective load per grain decreases because of the larger number of contact points. If the size of the abrasive grains decreases below sub-micron sizes, the number of grains increases accordingly.

In lapping, the material removal mechanism includes rolling abrasives, sliding abrasives, and micro-cutting abrasives. It is a very complex mechanism that involves abrasive phenomena, brittle fracture, and plastic deformation. The predominant mode is dependent mainly on the size of the abrasive and the normal load.

Szuder [1] found that the in the three body abrasion (lapping) simulation the wear it is not due only to a micro cutting process, but mainly to a repeated plastic deformation process between contiguous built-up edges produces by repeated plastic deformations.

In the real lapping process the same phenomena may occur in the majority of the cases. The wear is induced by millions of plastically deformations produced by the tips of the rolling grits. Those plastically deformations produces bulges which are highly deformed and submitted continuously to new dynamical solicitations until they fail and wear debris are produced on the lapped surface.

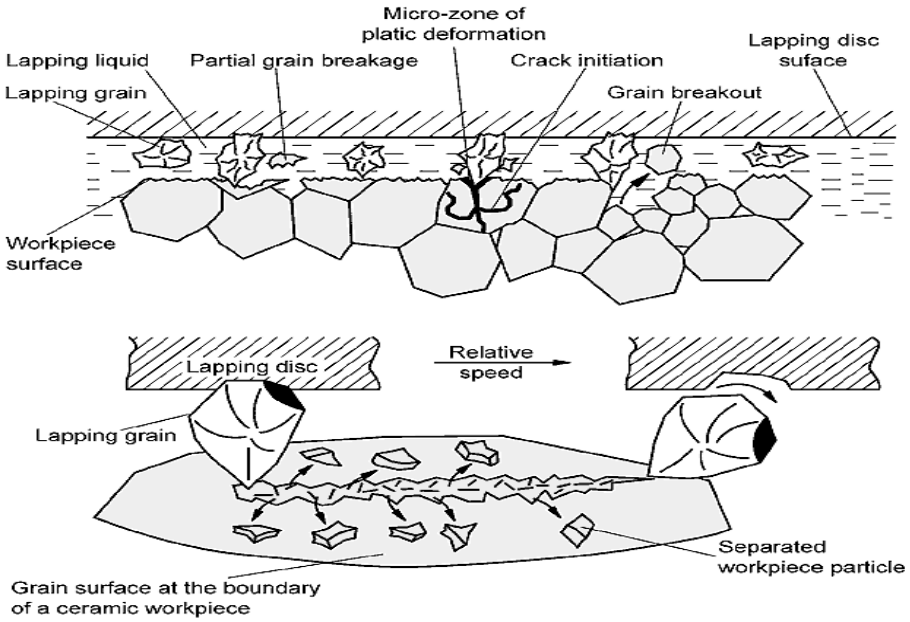

Figure 3. The lapping mechanism for ceramics [8]

Where a greater pressures are at play, a larger share of the normal load (W) is borne elastically (We) but still there is left a larger number of grains which deform plastically (Wp) (Figure 3).

With an increase of grain diameter there will be fewer grains in contact and these grains will evidence diameters of spaced out statistical distribution. According to the general rule, the number of plastically deforming grains increases with an increase in grain diameter up to a certain diameter or a certain range of diameters when their small number does not allow them to plastically bear the pressure.

In this case the hypothesis of rigid grains is no longer valid. Grains will crack until a new equilibrium sets in the more compact layer of abrasive grains whose diameters are closer. This is an explanation of "Critical Diameter" by elastic-plastic phenomena at the interface.

A possible explanation of constant increasing stock removal rates for the lapping oil as carrier may be the higher viscosity of the lapping oil retaining

more abrasive grains in the interface than the water or alcohol witch have lower viscosity and spread out the carrier and larger abrasive grains from interface [1,3].

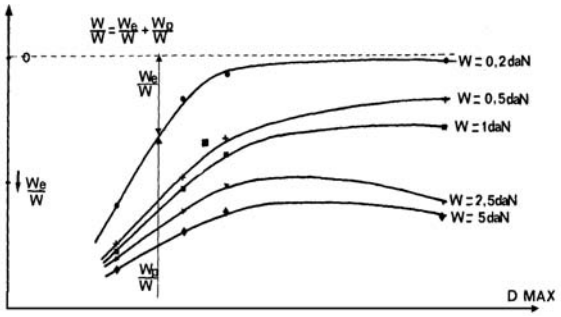

Figure 4. The dependencies of the Wp/W and We/W on W and D_{max}. Critical Diameter explanation [1]

3.3 Polishing

Polishing is one of the oldest manufacturing technologies used as a surface-smoothing operation; it mainly consists of removing or smoothing out grinding or lapping lines, scratches, and other surface defects in order to decrease the surface roughness. Although there are many operations to make a surface smooth, polishing remains the best method to obtain the finest surface. High accuracy and ultraprecision technology are indispensable ingredients of modern polishing, [2].

The primary difference between polishing and lapping is in the intent, rather than in the process. Because of this, high rates of material removal are not necessary. The aim of polishing is to achieve a desired surface finish. While lapping produces a gray nonreflective surface, polishing will generate a reflective or shiny surface. The degrees of reflectivity will vary in relation to the type of process used. Typical processes include hard and soft pad polishing, diamond abrasive/composite plate polishing, and optical pitch polishing.

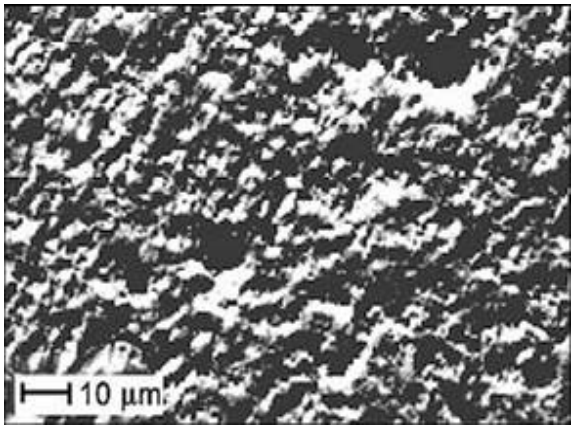

Figure 5. Lapped surface

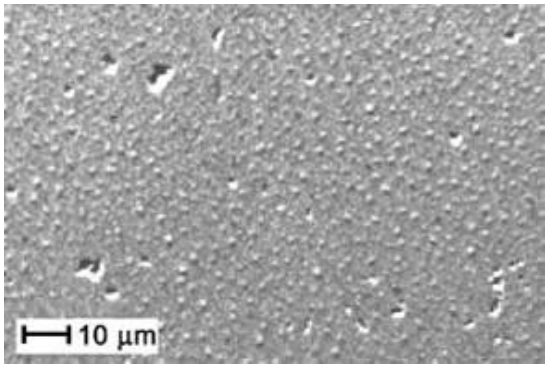

Figure 6. Polished surface

3.4 Honing

Honing is a very complex cutting process with a random phenomenon of detaching the chips, and a specific surface texture generation determined by the geometrical parameters of the abrasive grains the honing tool parameters and by the cutting process parameters.

Principal objectives of cylinder liner honing are:

- removal of ovality, deformations and scratch marks in the cylinder liner wall;
- producing a mesh of various depths in the material for the purpose of allowing the cylinder lube oil to remain in the mesh grooves for better lubrication;
- in a second step (plateau honing), achieving of a fine surface for piston ring contact;
- removal of the hardness in the liner wall surface.

This process is well mastered in most of applications from great size ship engines to small diameter for high speed sliding miniature aircrafts. In case of Formula I abrasive finishing process is different. The groove size and their orientations are different because first requirement is friction reduction and not a longevity of operational contact.

In honing, the abrasive particles are fixed in a bonded tool as in grinding. The honing process is mainly used to achieve a finished surface in the bore of a cylinder. The honing stones are pressurized radially outwards against the bore.

Honing is different than grinding in two ways. Firstly, in honing, the abrasive tool moves at a low speed relative to the workpiece. Typically, the surface speed is 0.2 m/s to 2 m/s. Combined rotation and oscillation movements of the tool are designed to average out the removal of material over the surface of the workpiece and produce a characteristic "cross-hatch" pattern favored for oil retention in engine cylinder bores.

Another difference between honing and grinding is that a honing tool is flexibly aligned to the surface of the workpiece. This means that eccentricity of the bore relative to an outside diameter cannot be corrected.

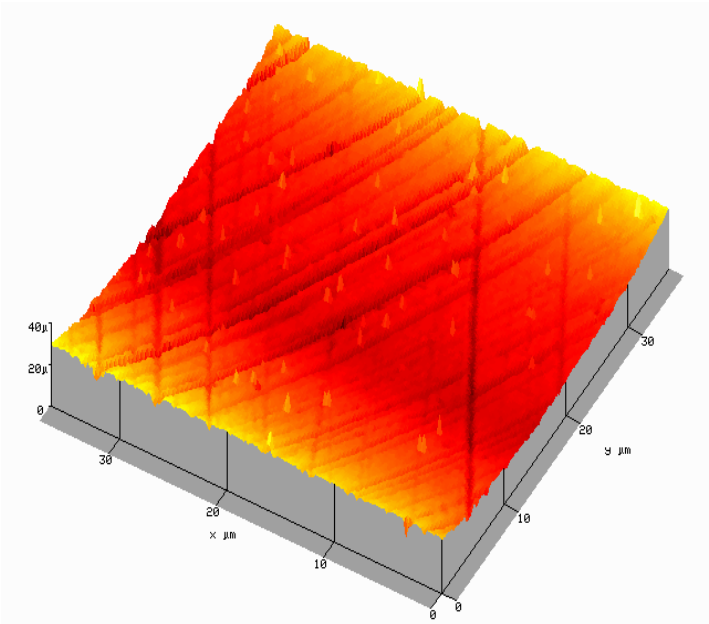

Figure 7. Typical 3D topography image showing dominating honing process [4]

SOMICRONIC

SURFASCAN®

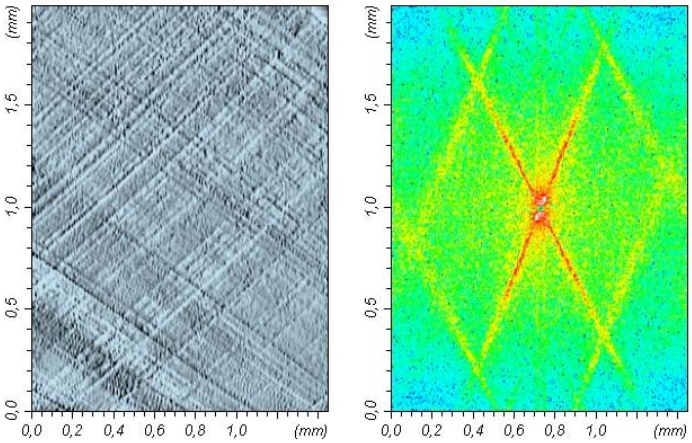

Figure 8. The anisotropy analysis tool helping in control quality of honing process showing almost perfect finishing [4]

One of the main purposes of the honing process is the specific honed surface texture, specially designed to retain during the operational life an important volume of lubricant. The lubricant volume is mainly determinate by the surface texture and the surface texture by the abrasive grain size utilized.

This problem has certain difficulties, attached to the complex phenomena appearing in honing processes.

Considering the above factors, research studies on surface generation by honing and a detailed analysis of the honing surfaces texture are important in modeling the process.

The following factors have been taking into consideration in computer simulation of honing process and experimental researches [6]:

- **bore geometry:** diameter, length;
- **cutting tool parameters**: ♦Macro parameters •width of lamella •length of lamella •number of lamellas for the honing head ♦Micro parameters •material of lamella •material of lint •minimum number of grain edges •maximum number of grain edges •dispersion of the number grain edges •maximum radius lamella •min. radius of lamella •disperse of radius •maximum inter granular disperse •minimum inter granular disperse

❑ **cutting regime parameters**: •rotation speed of the honing head •advanced speed •advanced length of the honing head •minimum length of inferior overtaking •maximum length on superior overtaking •angle between the trajectory and the generating line of the bore;

❑ **roughness criteria** :•R_{max} •R_z •R_a •V_u

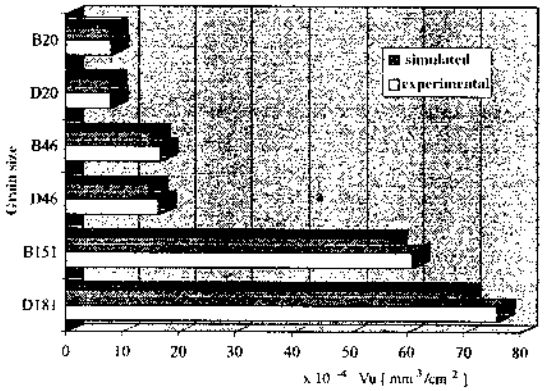

Figure 9. Abrasive grain size influence on oil volume stocked in surface texture [6]

The experimental values are greater than those obtained by the simulation program, due mainly to the plastic deformation of the micro channels borders, which was not taken into account in the simulation program. The difference between the experimental and simulated values is lower as the grains are smaller (Figure 9).

In the honing process the honing micro channels angle is due to the inclination angle of the helix as a result of the ratio between the axial speed and the peripheral speed of the honing tool.

Figure 10 presents the ideal dispersion of the abrasive grits on the tool for different types of honing (super finishing - M20, finishing - D46, roughing - B151, D181) for the 8 edges abrasive grits.

From those results and using the formula:

$$V_u = \frac{(100-B)(C-A)}{2000}\frac{mm^3}{cm^2}. \quad (1)$$

For the V_u the oil volume can be calculated and graphically represented as in Figure 11.

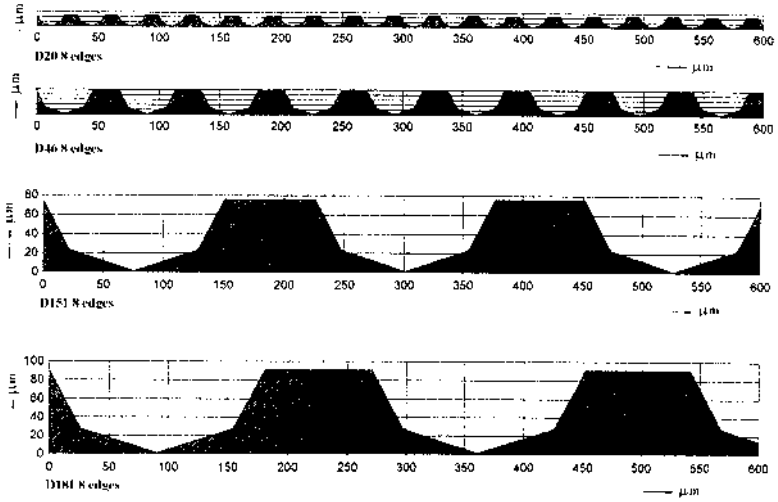

Figure 10. Dispersion of the abrasive grits on the tool for different types of honing grits [6]

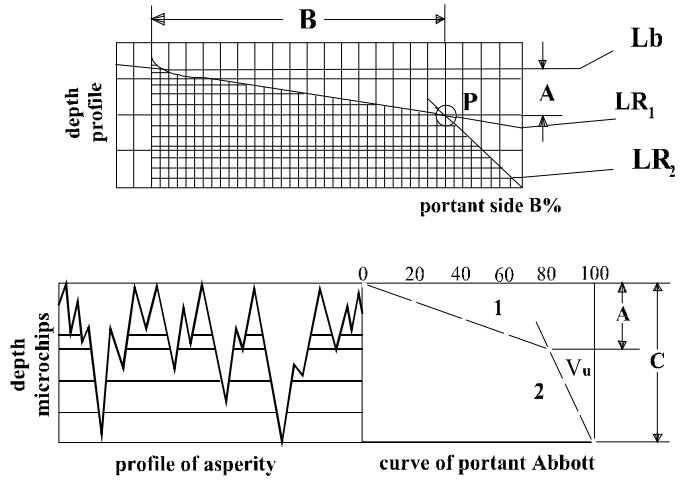

Figure 11. Surface topography diagrams an V_u calculation [6]

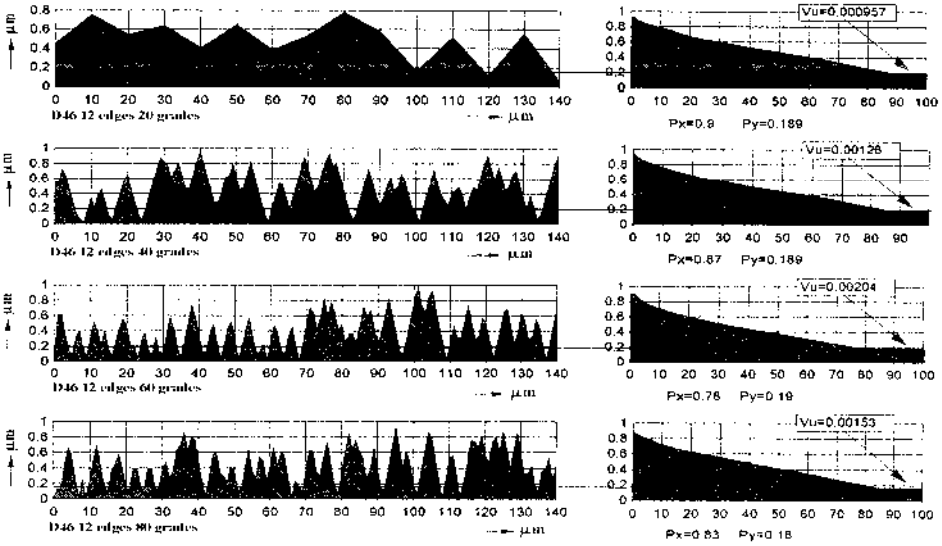

Figure 12. The simulated roughness of the surface, the Abbott curve and the V_u. [6]

Figure 12 presents in the same graph the simulated roughness of the surface, the Abbott curve and the V_u. for the D46 abrasive grits with different inclination angles. It can be noticed that the oil volume varies from 11.6 to 15.3 mm^3/cm^2.

3.5 Significance of surface metrology in finishing processes

The most important quantitative parameter in a surface finishing system is the roughness of the surface. Although it is somewhat obvious that the key to a flat surface is minimizing its surface roughness, a quantitative understanding of how roughness is changed by the finishing process is not perfectly understood.

Although much discussion has focused on the rate at which material can be removed from a surface in finishing processes, an important industrial consideration in the manufacturing process, comparatively little attention thus far has been devoted to determining surface roughness as a function of other finishing parameters.

Many functional aspects of engineering surfaces are determined by their morphology: their roughness, shape, organization of surface motifs etc. [1,2]. The measurement and characterization of these geometrical aspects is one field of morphological metrology.

The extraordinary development of various techniques (Atomic Force Microscopy, Phase Shifting Interferometry, Confocal Microscopy, Tactile Topometry) and metrology software, have their respective advantages and disadvantages specific applications, frequently without professional precautions. They make it possible to characterize in 3D surfaces whose amplitudes extend from 0.05 nm to 5 mm and scanning areas in the range of 1 µm to a few mm or event cm. We present some examples of problems solved thanks to the metrology of 3D topography of surfaces of different materials intended for various functions.

In metrology of surface morphology two main families of techniques can be considered, the first one requires a contact between a stylus tip and the surface, whereas the second one is a non-tactile technique, in which morphological information is obtained optically, without any contact between the sensor and the surface. The mechanical principle of the tactile technique is very simple: the vertical movements of a tip, which follows the roughness profile of a surface, are amplified and digitized to extract the usual roughness parameters for a profile. 3D morphology is obtained by collecting parallel scanning profiles with defined steps [1]. Several optical non contact systems are proposed, involving different physical phenomena: interferential hetero-dyne microscopy [3], defocalisation and confocal microscopy [4], roughness diffusion by reflection of monochromatic coherent beams [5,6], with various types of processes like phase shearing microscopy [7] and projected fringes. Typical ranges and resolution limits of the various techniques, in both vertical and horizontal directions, are different as schematically illustrated in Figure 13 for mentioned techniques.

An appropriate selection of expensive metrological equipment is a difficult task. Moreover, it is only possible to test the comparative capabilities of the metrological topological techniques by a complete analysis of different types of materials: homogeneous or heterogeneous, porous or continuous, structurally or/and topographically anisotropic, (with respect to the quality and the feasibility of determination of the significant morphological parameters). Here, comparative tests with the most commonly used 3D techniques are made on industrial finely polished flat but porous ceramic heterogeneous surfaces [5].

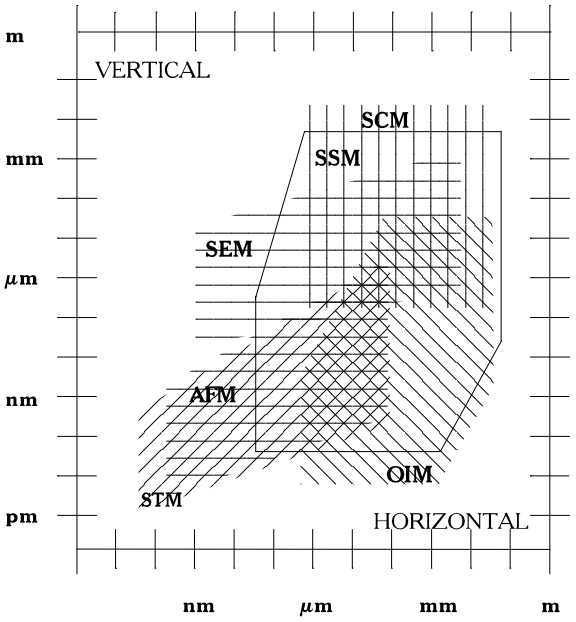

Figure 13. Ranges and resolution limits of different techniques: AFM- Atomic Force Microscopy, SCM-Scanning Confocal Microscopy, SSM-Scanning Stylus Microscopy, SEM-Scanning Electron Microscopy, STM- Scanning Tunneling Microscopy, OIM- Optical Interference Microscopy [4]

Measurements with AFM (Atomic Force Microscopy), SCM (Scanning Confocal Microscopy), SSM (Scanning Stylus Microscopy) and OIM (Optical Interferometric Microscopy) techniques which have recently become widespread have also been carried out, in order to take into global consideration the problem of micro-, macro- and meso-morphology's metrology of engineering surfaces [5,8].

Different tactile and optical 3D topometers were used, analyses were conducted on the measured textures using commercial surface French analysis soft-ware's Surfascan® V.2.6 from Somicronic and MountainsMap® 4.0 from Digital Surf includes a large number of 3D surface state parameters most of them being standardized. These parameters including the "14 Birmingham parameters" were proposed by the assembly composed of two educational institutions; University of Birmingham and Ecole Centrale de Lyon in collaboration with five industrial partners; Perthen, Exxon, Somicronic, Lucas Ltd and WBC [1]. These parameters are classified by family: amplitude parameters, hybrid parameters, spatial parameters, functional parameters, functional indices and volume parameters. Kurtosis of the height distribution – Sku, and Skewness of the height distribution – Ssk, and anisotropy characterizations were revealed most pertinent.

REFERENCES

1. Szuder, A., 2002, *Ingineria suprafetelor*, Ed. Tehnica, Bucuresti.

2. Marinescu, D.I., Rowe, W.B, Dimitrov, B, Inasaki, I, 2004, *Tribology of Abrasive Machining Processes*, William Andrew, New York.

3. Szuder, A, Marinescu, A, Popescu, M., 1986, "Study of the Influences of Flat Lapping," *Intern. Grinfing Conf*., June 10-12, Philadelphia, Pennsylvania. Society of Manufacturing Engineers. USA, MR 86-633.1-8.

4. Mathia T., 2007, "3D Surface Morphology Measurements in Abrasive Machining," *Bases & Techniques of Abrasive Machining Rzeszow*, Poland, 12-14, Novembre, Ed. E.Oczos & J.Burek.

5. Mathia, T. G., Ducret, S., Lanteri, P., Midol, A., Meille, G., 2007, "Improvement of Ski s Sole Performance via Specific Abrasive Finishing and Waxing Process Using Simultaneously: GPS² and Skiing Forces Metrologies," *Advances in Production Engineering*, pp. 360-369, 14-16 juin, Warsaw, Poland.

6. Szuder, A, Bardac, D, Palalau D, Bardac, D., 1998, "Considerations Concerning the Liquid Volume into the Honned Textures with Superabrasives," I.C.M.E. *CIRP International Seminar on Intelligent Computation in Manufacturing Engineering*, July 1-3, Capri , Italy, pp. 665-669.

7. Mathia T., Domeck, N., Leprat, E., 2006, "Why the 3D Metrology of Surfaces Morphology is Required?," *Scientific Bulletin of University of Bielsko-Biala*, vol. 22, pp.185-198.

8. Informationszentrum Technical Ceramics, Verband der Keramischen Industrie e.V, *Brevier Technical Ceramics*, Fahner Verlag 2007.

ISSN 1220 - 8434

ACTA TRIBOLOGICA
Volume 17, (2009), 42-45

Stefan GHEORGHE[1]

Cristina TEISANU[1]
email: *cteisanu@yahoo.com*

Andreas MERSTALLINGER[2]

Ion CIUPITU[1]

[1] University of Craiova, Faculty of Mechanics,
Dept. of Technologies & Materials,
ROMANIA

[2] Austrian Research Centre Seibersdorf,
AUSTRIA

THE INFLUENCE OF THE SINTERING ATMOSPHERES ON THE WEAR BEHAVIOUR OF COPPER BASED ALLOYS

The Powder Metallurgy (PM) technique allows the manufacturing of sintered self-lubricating materials having a high wear resistance. It is well known that the small and medium size bearings are processed by PM with better characteristics than those obtained by casting. The tested materials are Cu-based, having Sn, Zn, and Pb as alloying elements to improve the tribological properties. These alloys are designed to be used for manufacturing self-lubricating bearings. The alloy compositions were obtained by cold die compacting, using different pressures. The sintering was performed in vacuum. The wear test was performed for four ring samples on a ball on pin tester, the test atmosphere being vacuum and normal air.
Keywords: sintered bearings, sintering atmosphere, wear behaviour, linear wear

1. INTRODUCTION

Powder Metallurgy (PM) technology allows the control of the alloying elements content and obtaining of certain porosity which allows the absorption of the oil through the material pores; so, the parts can work without supplementary oil addition [1-3].

The tested material is the alloy grade CuSn5Zn5Pb4 without graphite, considered as a good antifriction sintered alloy.

The wear test was performed for ring samples with a ball pin and the atmospheres used were vacuum and air. The materials were tested at the Austrian Research Center Seibersdorf.

This is a large class of materials for these bearings processing and their selection depends on the working environment, relative speed shaft-bearing, specific pressure etc. The elaboration of the bearings by PM technique is a complex process, which depends on many factors such as: the type and morphology of powder particles, the chemical composition of the material, the alloying method, the compacting pressure, the sintering atmosphere, the sintering temperature, the cooling rate etc.

Bearings made of sintered bronze are still the most used parts in technical applications because of the availability of the copper powder and their very good tribological and self-lubricated properties. However, a substitution tendency of the tin powder with other chemical elements was noticed, due to very expensive and reduced amount of tin powder. Some of those materials are CuSnZn alloys with 1% graphite.

By Powder Metallurgy technology it is possible to obtain sintered materials for self-lubricating bearings having a high wear resistance and a porosity ranging between (15…30)%. This can be possible by different ways of driving the process cycle. The pore volume is impregnated with oil and during the bearing operation the oil is eliminated from pores, forming a thin film between the bush and the shaft walls. As the structure is porous these materials can be used in those conditions where the oil is not present. Because of these advantages powder-metallurgy bearings are superior to those conventionally made, for many applications [3-5].

Therefore these materials can be used in an completely dry atmosphere. But the oil from their pores improves the antifriction behaviour.

2. EXPERIMENTAL PROCEDURE

The tested materials are sintered copper based alloys having Sn, Zn and Pb as alloying elements to which 1% graphite was added in order to improve the tribological properties. These alloys are meant to be used for manufacturing self-lubricating bearings. The following sintered alloys:

- CuSn5Zn5Pb4 + 1% graphite (PBM 1),
- CuSn5Zn5Pb5 + 1% graphite (PBM 2),
- CuSn5Zn5Pb6 + 1% graphite (PBM 3),
- CuSn5Zn5Pb7 + 1% graphite (PBM 4),
- CuSn5Zn5Pb8 + 1% graphite (PBM 5),

were structural, mechanical and technological studied. Also, tribological tests were performed in order to

determine the amount of wear and the value of friction coefficient [1-3].

These materials were cold die compacted at two pressures, 165 MPa and 210 MPa, respectively (green state density = 6.9 g/cm^3), values which take into account the chemical composition of the alloys and the required mechanical and technological properties.

The sintering atmosphere was a high vacuum (10^{-4} atm) and hydrogen. The wear test was performed for ring samples with a ball pin and the atmosphere used was vacuum and air.

The material tested is the CuSn5Zn5Pb4 alloy grade without graphite, considered as a good antifriction sintered alloy.

To perform the wear test ring samples were obtain by PM technology with the following initial data:

- material–powder mixture of CuSn5Zn5Pb4;
- homogenization of the mixture with Turbula device;
- cold compaction with a pressure of 225 MPa (proportionally F = 38,000 daN);
- sintering at two temperatures, 805°C and 815°C in vacuum and hydrogen atmosphere;

The sintering cycle is presented in Figure 1.

Due to heavy wear loadings of the bearings it is necessary to accomplish the wear test of their materials.

The wearing can be expressed as a length, an area, a volume or a weight deterioration of the materials through friction process. Thus, the wearing and the friction phenomenon can not be separated and one of the results is the loss of mass.

There are known a lot of wear test methods like the macro and micro geometric dimensions measurement, the weighting method, the physical or chemical analysis of the lubricant and so on.

A technological test particular to self-lubricating materials is the wear test developed on the sintered bearing or on specific samples of the requested material. Because the quality of the oil can improve the wear resistance, the materials are indicated to be tested without oil in pores. In this case the $p \cdot v$ value is smaller than 1.8 MPa m/s, where p is the pressure and v is the relative sliding speed.

The wear test was performed for the ring samples with a ball pin and the atmosphere used was vacuum and air. The friction coefficient values are better for vacuum test than those performed in air for both samples sintered at 805°C and 815°C [4]. The best value is 0.11 for the sample sintered at 815°C and tested in vacuum.

The dependence of the sliding distance as a function of the friction coefficient shows a constant value after the beginning period.

The experimental conditions are:

- material of ball - 100Cr6;
- sliding speed of ball – 0.6m/s;
- load - 1N;
- sliding distance - 2000 m.

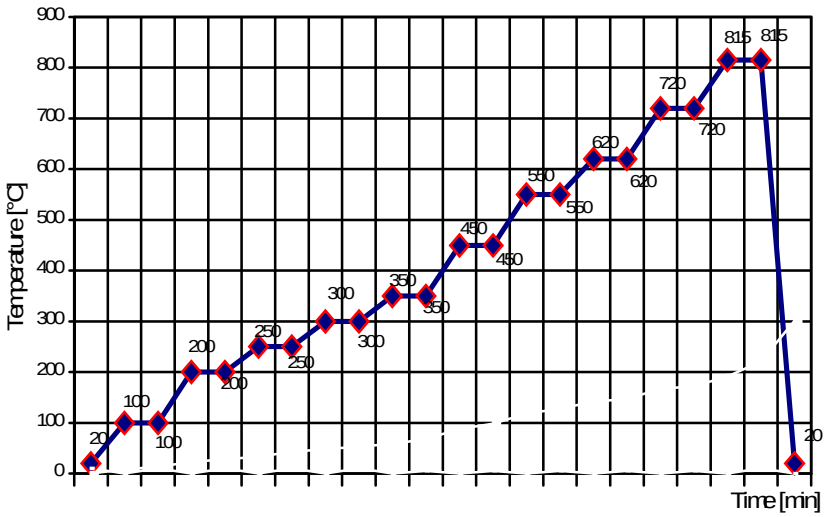

Figure 1. Sintering cycle for vacuum and hydrogen atmosphere, T = 815°C, heating velocity = 5°C/min

3. RESULTS AND DISCUSSION

During the wear test there are covered all three distinguished stages specific to wear evolution in time: running in wear, normal or steady wear and accelerated or damage wear.

As it may be seen in diagrams depicted in Figures 2 through 7, the wear increases rapidly in the first stage (running-in period) and then it remains almost constant in the steady period of functioning.

After finishing the wear test it was noticed that the wear value remains constant on the sliding distance of 2000 m, excepting a little increased pick characterising the starting point. This is also the moment when the friction is very intensive.

At the end of the wear test the materials did not failed, being capable to continue the running.

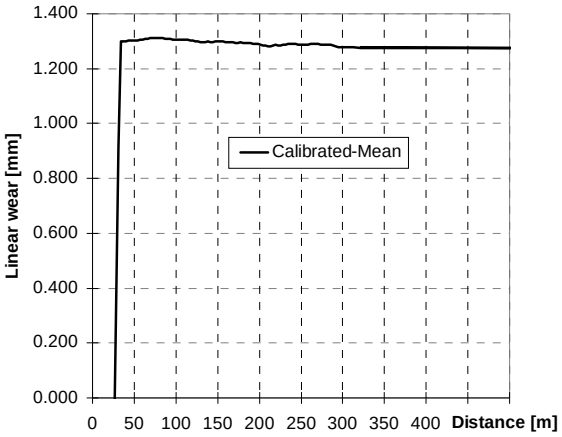

Figure 2. Linear wear for the ring sample sintered at 815°C and tested in vacuum

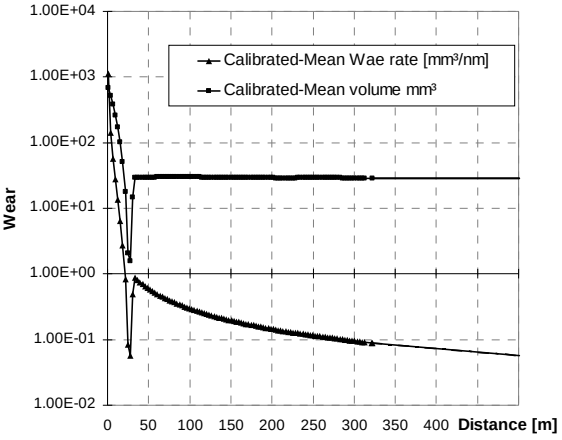

Figure 3. Calibrated mean wear rate and calibrate mean volume for the ring sample sintered at 815°C and tested in vacuum

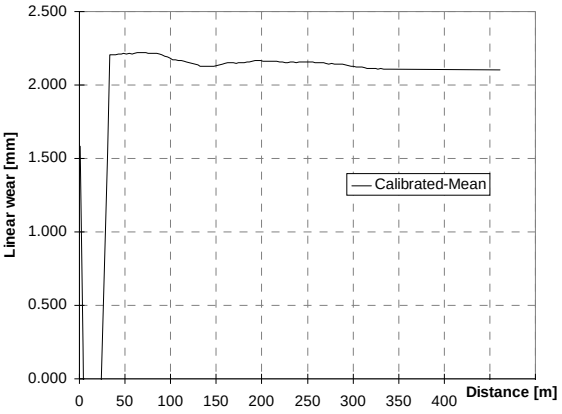

Figure 4. Linear wear for the ring sample sintered at 815°C and tested in air

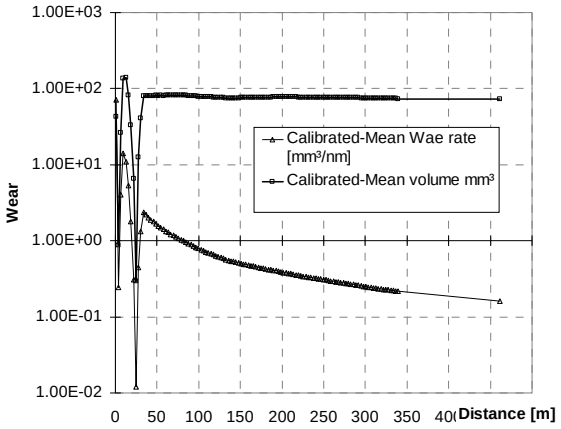

Figure 5. Calibrated mean wear rate and calibrate mean volume for the ring sample sintered at 815°C and tested in air

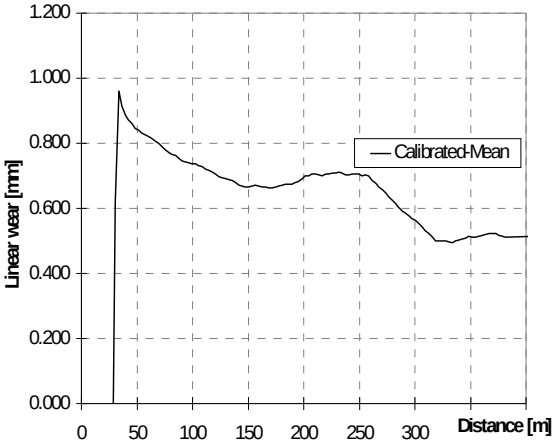

Figure 6. Linear wear for the ring sample sintered at 805°C and tested in air

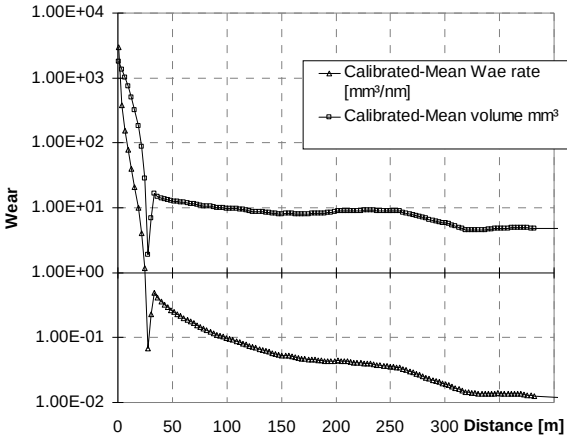

Figure 7. Calibrated mean wear rate and calibrate mean volume for the ring sample sintered at 805°C and tested in air

4. CONCLUSIONS

The samples sintered in hydrogen atmosphere present a very good tribologic behaviour comparable to those of the speciality literature.

The running in period of the sintered samples is very short being in normal functioning quite fast.

The lowest values of the wear rate are observed at the samples sintered at 805°C and wear tested in air.

REFERENCES

1. Gheorghe, St., Teisanu, C., and **Ciupitu, I.,** 2005, "Some Aspects Regarding Wear Test of Some PM Antifriction Copper Based Alloys," Proc. of the 4th Int. Conf. on Sci., Tech. and Applications of Sintering, 1, pp. 421-423.

2. Gheorghe, St., Teisanu, C., and **Ciupitu, I.,** 2005, "Some Aspects Regarding Wear Test of Some PM Antifriction Copper Based Alloys," *Third Int. Conf. on PM, RoPM*, 871.

3. Teişanu C., Gheorghe St., and **Ciupitu I.,** 2005, "Hardness Optimization of the Iron Base Self-Lubricating Bearings," Euro PM2005 - European Congress and Exhibition on Powder Metallurgy, Praga, Cehia, 2-5 october, vol.2, pg. 185-190.

4. Gheorghe, St., Ciupitu, I., Merstallinger, A., and **Kladler, G**., 2004, "Friction And Wear Behavior Of Iron-Copper Sintered Alloys," European Powder Metallurgy Association (EPMA), International Powder Metallurgy Congress & Exhibition, Euro PM2007, vol. 4, pp. 769-774.

5. Gheorghe, S., Ciupitu, I., Mangra, M., and **Teisanu, C.,** 2001, "Wear Resistant Alloys with Low Tin Content," European Congress and Exhibition on Powder Metalurgy, Nice, France, 22-24 October.

ISSN 1220 - 8434

ACTA TRIBOLOGICA
Volume 17, (2009), 46-51

G. MEILLE

T. G. MATHIA
e-mail: *Thomas.Mathia@ec-lyon.fr*

Laboratoire de Tribologie et Dynamique des Systèmes- C.N.R.S., École Centrale de Lyon, Ecully, **FRANCE**

STRATEGY FOR IDENTIFICATION OF WEAR MODE OF ENGINEERING SURFACES

Identification of engineering surfaces damage modes requires the selections of appropriate analytical techniques for characterisation of morphology, rheology as well as of physical & chemical properties. Different techniques of visual observations, based on optical and electronic microscopy, coupled with specific image analysis software are presented and discussed. The authors shear their experience in specific case studies.
Different strategies are discussed and numerous examples commented and illustrated for solving, choosing, and diagnosing various tribology problems by using contact mechanics, solid mechanics, system dynamics, physical chemistry, engineering materials science, lubricant chemistry, and metallurgy knowledge.
Below, a functional simplified diagram is presented, based on 30 years of experience and 1000 expertises. Some case studies are analysed in-depth.
Keywords: wear, expertise, diagnostic, analytical techniques, engineering surfaces

1. INTRODUCTION

1.1 Principal modes of wear

In materials science, wear represents all sorts of initial performances reduction of any system in terms of its functionality. From material engineering point of view it concerns any deformation, geometrical evolution or transfer or removal of material from a solid surface by the action of another solid, gas or liquid. The study of the processes of wear is part of the discipline of tribology. There are four principal widely recognized wear processes [1-3]:

1. adhesive wear;
2. abrasive wear;
3. corrosive wear;
4. surface and volume fatigue.

Voluntary we are not going to treat in detail mechanical and thermal failures like buckling, creep, fracture, fretting, yielding as melting and thermal shock. The definition of wear does not include loss of dimension from irreversible deformation, although wear has occurred despite no material removal occurs. Also this definition fails to include impact wear where there is no sliding motion or cavitations (also corrosion) where counter-body is a fluid or some gazes. Wear can possibly be better defined as a process in which interaction of surface(s) or bounding face(s) of a solid with the working environment results in the dimensional loss of the solid, with or without loss of material. Wear environment includes loads (mono or multi directional, reciprocating, rolling, impact), kinematics, speed, temperatures, counter - bodies (solid, liquid, gas), types of contact (single phase or multiphase in which phases involved can be liquid plus solid particles plus gas bubbles).

1.2 Adhesive wear

Adhesive wear is also known as scoring, galling, or seizing. It occurs when two solid surfaces slide over one another under pressure. Surface protuberances, or asperities, are plastically deformed and eventually welded together by high local pressure. As sliding continues, these bonds are broken, producing cavities on the surface, material transfer on the second surface, and frequently tiny, abrasive particles, all of which contributes to future wear of surfaces.

1.3 Abrasive wear

When material is removed by contact with hard particles, abrasive wear occurs. The particles either may be present at the surface of a second material or may exist as loose particles between two surfaces. For example abrasive wear can be measured as loss of mass by the Tabor Abrasion Test according to ISO 9352 or ASTM D 1044.

1.4 Corrosive wear

Often referred to simply as “corrosion”, corrosive wear is the deterioration of useful properties

in a ma-terial due to reactions with its environment. One form of high temperature corrosive (oxidative) wear can lead to the formation of compacted oxide layer glazes, which under certain circumstances reduces wear.

1.5 Surface or volume fatigue

Surface fatigue is a process by which the surface of a material is weakened by cyclic loading, which is one type of general material fatigue.

In standard wear test (e.g., those formulated by respective subcommittees under ASTM Committee G-2) relatively rare the real conditions of functional components can be reproduced, therefore expertise of engineering systems by the experts is very useful.

2. EXPERTISE AND EXPERT

There are broadly two approaches of expertise. The first understands expertise as an emergent property of communities of practice. In this view expertise is socially constructed; tools for thinking and scripts for action are jointly constructed within social groups enabling that group jointly to define and acquire expertise in some domain. In the second view expertise is a characteristic of individuals and is a consequence of the human capacity for extensive adaptation to physical systems and social environments. Many accounts of the development of expertise emphasizes that it comes about through long periods of deliberate practice. Expertise should be conducted by an expert or the team of experts. An expert is someone widely recognized as a reliable source of technique or skill whose faculty for judging or deciding rightly, justly, or wisely by various authorities and status by the public or/and their peers groups. An expert, more generally, is a person with extensive knowledge or ability in a particular area of study. Experts are called in for advice on their respective subject, but they do not always agree on the particularities of a field of study. Thus, instead of using rules he or she no longer remembers, as the knowledge engineers suppose, the expert is forced to remember rules he or she no longer uses. No amount of rules and facts can capture the knowledge an expert has when he or she has stored experience of the actual outcomes of tens of thousands of situations. An important feature of expert performance seems to be the way in which experts are able to rapidly retrieve complex configurations of information from long term memory. They recognize situations because they have broad knowledge. In line with the socially constructed view of expertise an expert can also be understood as a form of power. He must not be critical but exempted and free of any errors of judgment respecting totally confidentiality and established, signed before deontological chart rules.

An expert differs from the specialist in that a specialist has to be able to solve a problem and an expert has to know the different solutions. The concepts of experts and expertise are debated within the field of epistemology under the general heading of expert knowledge. The term is widely used informally, with people being described as 'experts' in order to bolster the relative value of their opinion, when no objective criterion for their expertise is available. The authors experience permitted, thanks to a great number of case studies, to establish some efficient low cost expertise's flow charts. Flowchart is a schematic representation of an algorithm or a process. A flowchart is one of the seven basic tools of quality control, which also includes the histogram, Pareto chart, check sheet, control chart, cause-and-effect diagram, and scatter diagram. They are commonly used in business/ economic presentations to help the audience visualize the content better, or to find flaws in the process. Alternatively, one can use Nassi-Shneiderman diagrams. Our simplest one is illustrated on Figure 1.

2.1 Motivations for strategy optimisation

There are few fundamental origins of motivations for establishment of optimal strategy or strategies for identification of wear mode or modes of engineering surfaces. The first is purely scientific, philosophical and logic selection of analytical tools and simulators. The second one is technological, where the process of design, technological data of machining, of manufacturing; of assembling and quality control is known, the expertise is easer, faster and more pertinent. The last motivation but not slightest is economical one, in terms of time and cost.

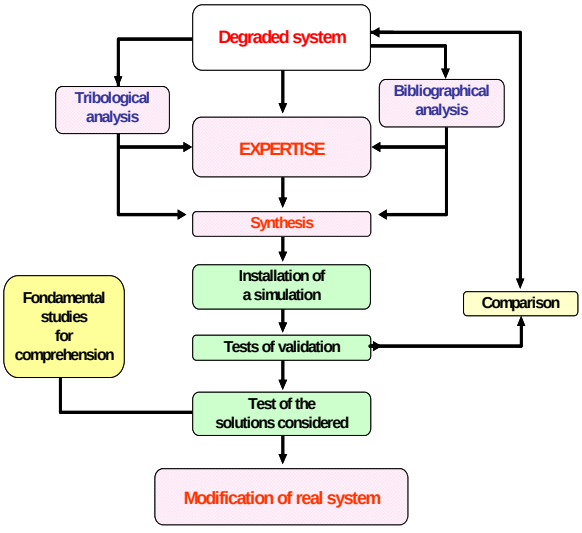

Figure 1. Flow chart diagram of optimal strategy for identification of wear mode of engineering surfaces

2.2 Identification of required tools

Most important aspect of required tools criteria identification is the compromise between the equipment and the sought task. The metrology aspects as transfer function of the apparatus, its range

of measurement and the resolution, fidelity, reproducibility and calibration must be considered. Never the time of tools employment and cost balance can be mistreated.

3. TRIBOLOGICAL ANALYSIS

3.1 Knowledge management of existing information

The deep collection of existing data and information using modern tools of business intelligence and knowledge management contributes to establishment of a successful and more efficient strategy. Data mining has been defined as "the nontrivial extraction of implicit, previously unknown, and potentially useful information from data" and "the science of extracting useful information from large data sets or data bases".

Data mining involves sorting through large amounts of data and picking out relevant information. It is usually used by business intelligence organizations, and financial analysts, but is increasingly used in the sciences to extract information from the enormous data sets generated by modern experimental and observational methods.

Usually the expert uses personal data and goes through own, free structured or unstructured data mining very rapidly with high fidelity of pertinent information selection.

3.2 Analytical tools

Principal frequently used tools are for a few families of engineering surfaces and bulk properties investigations and their characterisations are:

- Visual examinations by optical and electronic microscopy.
- 3D morphology characterisations using different topography measurement techniques (tactile, optical etc.).
- Rheological characterisations (elastic modulus, hardness, visco-elastic behaviour, toughness).
- Residual stresses.
- 3D polytomography (X, gamma rays, acoustic).
- GPS (Geometrical Product Specifications).
- Others specifically selected depending on requirements.
- Chemical compositions of superficial and bulk part of material.

Most of data are graphical or pictorial, therefore for practical use extremely detailed operating and metrological specifications have to be textually associated.

3.3 Strategies for synthesis

- Intermittent reports
- Individual and personalised meeting exchange of expertise results with client
- Proposal part conclusions
- Final report

3.4 Strategies for simulation

Few strategies of simulations exist. The sensors implementations on real systems are the best solution particularly if different variables and parameters are interactive. Sensors implementation can modify conditions of simulations. In case of limitation of sensors number it can be difficult to determine pertinent parameters. Individual elements simulation is less complicated. Feasibility of tribometer tests without knowing their own transfer function is an important problem too. Over or understate scale simulations in term of time, size environmental conditions etc can conduct to wrong speculations, hypothesis and therefore conclusions.

4. CASE STUDIES

4.1 First - Fretting case of great displacements

When in case of fretting study focus is on surfaces morphology, the evolution presented in the flow chart can be proposed.

4.2 Surface measurements

The rapid development of modern surface morphology measurement techniques and equipment has been accompanied by an increasing number of surface roughness and waviness parameters. Nowadays there is a large number of 2D and 3D parameters to characterise surface profiles [4-6].

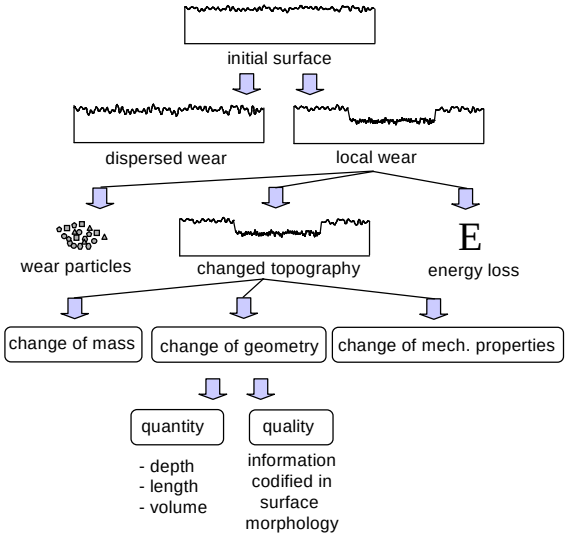

Figure 3. Generic of wear process

To measure the evolution of the surface morphology, the Somicronic-Hommel Surfascan S-M2 tactile profilometer and Veeco Wyco NT3300 light interferometer have been applied. NanoTest rig from Micro Materials has been used to produce a wear track and measure the surface 3D plots presented in Figure 4. In this study, parameters AR and W were selected due to their correlation to fretting wear scar morphology presented in Figure 5. Typical geometry of fretting scar on TiN coating with AR and W parameters interpretation is presented in Figure 6.

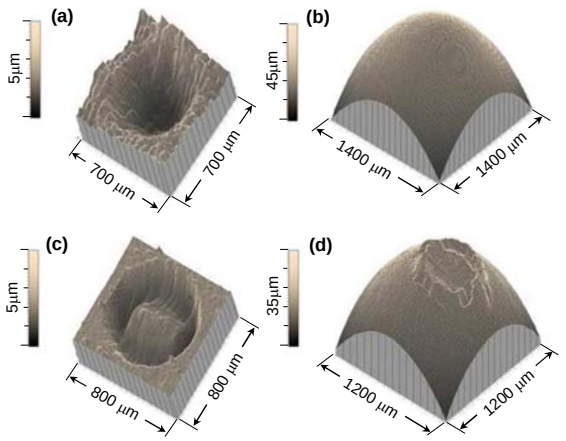

Figure 4. 3D topographical measurements of simulating fretting tests

4.3 Criteria for tests validations and test of retained solutions

In case of fretting tests, French motifs standard has been very efficiently used, thanks to the use of the parameter W, effectively easy to measure and well adapted to identification of transitional stages and the recognition of local destruction of protective coating shown on Figure 6.

4.4 Tests of validation

Industrial standardised test and scientific are not every time perfectly correlated. It is very useful to compare carefully the results from standardised methods advanced many years before and today's scientific well metrologically established scientific measurements. Frequently surprising of conclusion differences push to deep elucidations.

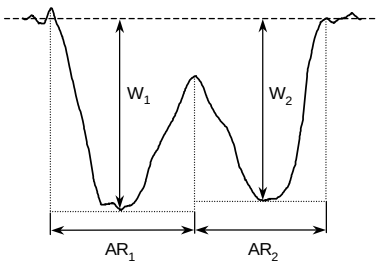

$$AR = \frac{AR_1 + AR_2}{2}$$

$$W = \frac{W_1 + W_2}{2}$$

Figure 5. Extracted axial profile of the fretting wear scar on TiN coating with AR and W morphological parameters

4.5 Comparisons with initial results of the analysis.

This stage of expertise depends very much on available budget of time and finances. It is detailed below in second case of study.

4.6 Second - Wear of male splined shaft and sleeve bushing

This stage of expertise depends very much on expert knowledge. It is detailed below in next case of study.

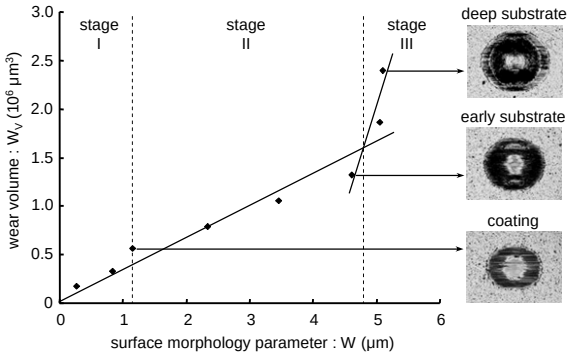

Figure 6. Fretting wear scar volume as a function of W surface parameter

4.7 Third – thermal degradation

Melting bubbles easily recognized on SEM images occur. Extractional sudation of Pb from matrix Cu-Pb under friction and thermal constrains are seen in Figures 10 and 11. The wear is due essentially to inefficient lubrication and misalignment of bearing parts.

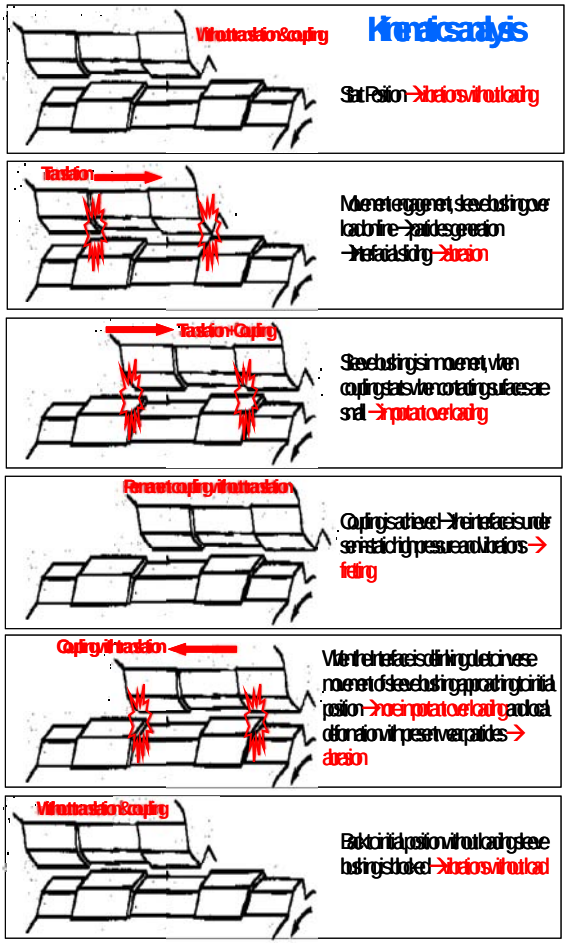

Figure 7.a. Complete kinematics analysis is evidently demonstrated via microscopic visual observations

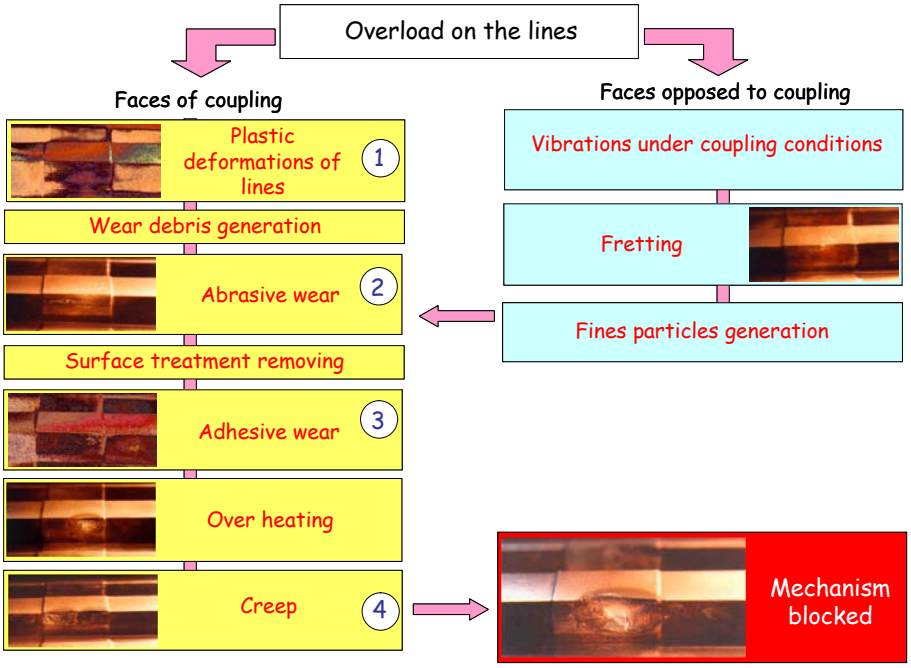

Figure 7.b. From simple well analysed and elucidated optical observations basic conclusions can be stated

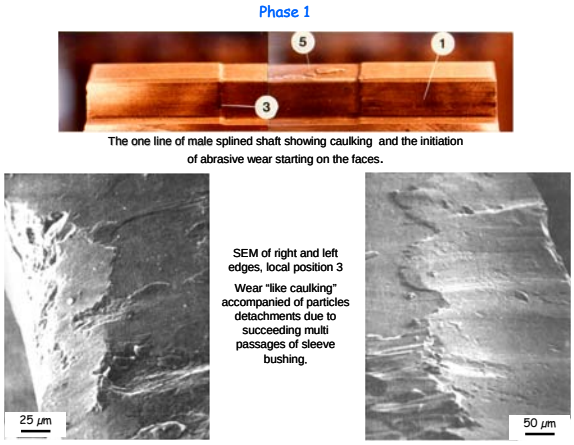

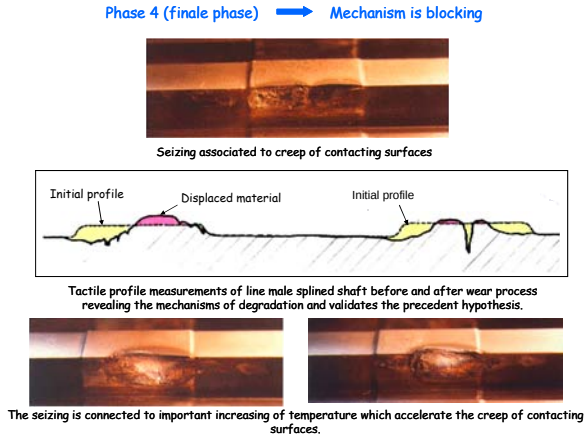

Figure 9. In final phase seizure and creep is depicted

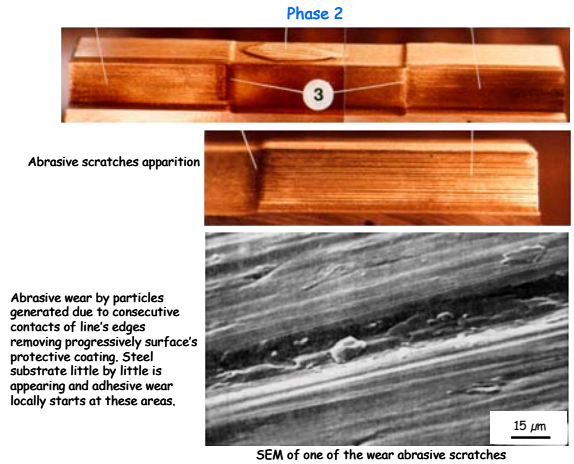

Figure 8. From visual (optical & SEM) images one can conclude that anti-adhesion coating has been removed

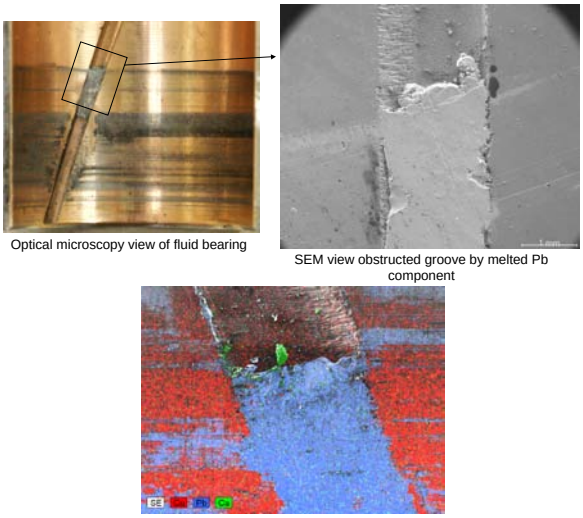

Figure 10. Optical & SEM views following of mapping of chemical compounds

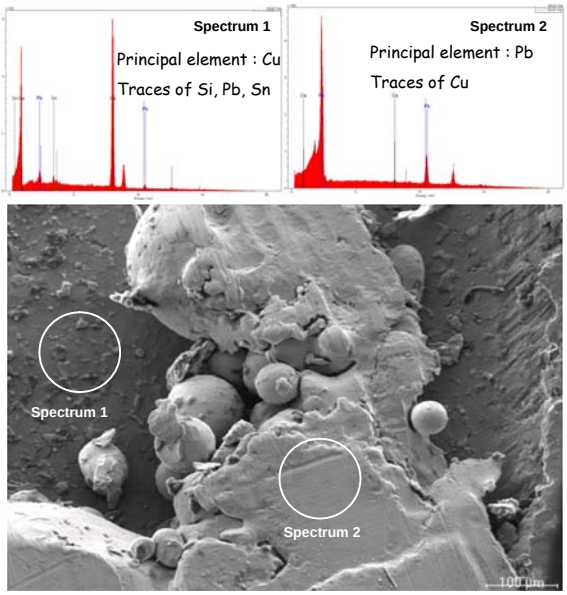

Figure 11. SEM (Scanning Electron Microscopy) view of thermal degradation due to extreme conditions of friction in case of pseudo-alloy (Cu-Pb-Sn) bearing associated with EDS (Energy Dispersive Spectrometry)

5. CONCLUDING REMARKS AND SUGGESTIONS

Only very professional and well oriented investigations following deep elucidation based on "retour d'expérience" can help in efficient investigations in strategy of wear mode of engineering surfaces. There is not time and space for free improvisations. The term cindynics (from the Greek kindunos, "danger") is currently used in frame of science (science of risks study and its reduction). It is generally used in case of risks preventions, which is the case of strategy the authors have developed associated with preclusions in great number of risk's domains like feasibility, industrial manufacturing, commerce, economy up to environmental policy.

ACKNOWLEDGEMENTS TO INDUSTRIAL PARTNERS

The authors wish to express theirs appreciation to the Centre National de la Recherche Scientifique and to the clients from French, Italian, Japanese, U.K. Swedish, American, German industries helping in improvement of our strategy of tribological expertise keeping our confidence since so many years. References of the companies for confidential reasons are not plainly mentioned.

REFERENCES

1. Chattopadhyay R., 2001, "Surface Wear-Analysis, Treatment and Prevention," ASM-International, OH, USA.

2. Germain, M. L., 2006, *Development and preliminary validation of a psychometric measure of expertise: The Generalized Expertise Measure (GEM)*, Unpublished Doctoral Dissertation. Barry University, Florida.

3. Swanson, R. A., and **Holton, E. F.,** 2001, *Foundations of Human Resource Development*, San Francisco: Berrett-Koehler Publishers, Inc.

4. Liskiewicz, T., Mathia T., Fouvry, S., and **Neville A.,** 2007, "Systematic Morphological Approach for Analysing Fretting Worn Surfaces," *33rd Leeds – Lyon Symposium on Tribology*, Leeds, Royaume-Uni, 12-15 September, *TriboTest Journa*l, John Wiley & Sons, Ltd, nr. 13, pp. 139-150.

5. Chattopadhyay, R., 2004, *Advanced Thermally Assisted Surface Engineering Processes*, Kluwer Academic Publishers, MA, USA (now Springer, NY).

6. Blunt, W., Dong, P., Luo, N., Mathia, T., Stout, K J., Sullivan, P. J., and **Zahouani, H.,** 2004, *Surface Topography*, Stylus Publishing Press.

ISSN 1220 - 8434

ACTA TRIBOLOGICA
Volume 17, (2009), 52-57

Ivan SOVILJ-NIKIC[1]
Bogdan SOVILJ[1]
Miran BREZOCNIK[2]
Sandra SOVILJ-NIKIC[1]
e-mail: *sandrasn@EUnet.yu*

Vlastimir PEJIC[3]

[1] Faculty of Technical Sciences, Novi Sad,
SERBIA
[2] Faculty of Mechanical Engineering, Maribor,
SLOVENIA
[3] Technical Faculty, Doboj,
BOSNIA AND HERZEGOVINA

ANALYSIS OF INFLUENCE OF GEAR HOB GEOMETRIC PARAMETERS ON THE TOOL LIFE USING A GENETIC ALGORITHM

Hob milling is one of the most complex machining processes. It is used at the mostly in operation of serration of spur wheels thanks to the high productivity of the process. Complicated cinematic and geometric relations between gear hob and work-piece raise some problems which disable optimal use of the tool and the machine. Optimization of working processes is based on reliable mathematical formulas which define the process in dependence on its parameters. In this paper, reliable tool life function of gear hob in the dependence on geometric parameters using a genetic algorithm was determined.
Keywords: wear, gear hob, genetic algorithm, tool life, optimization

1. INTRODUCTION

One of the basic trends in the development of modern mechanical engineering is to improve efficiency of metal machining. Successful solving of these aims is connected with investigation of working conditions of cutting tool as one of the most important links in the chain of machining process. Also, it is needed to investigate the physical phenomenon connected with machining process. The use of optimal geometric parameters of cutting piece of cutting tool and optimal working conditions provides minimal cost of the products and maximal work productivity. Gear hobs are used to manufacture gear serration with straight, slant and helical teeth, as well as to manufacture worm wheels for external conjugation with involute profile.

Taking significance of geometric parameters of gear hob into consideration for economy and productivity during processing of gear serration, within this paper the investigation is directed to the application of artificial intelligence in order to determine optimal geometric parameters of gear hob. High quality cutting tools are necessary for economical production. Production of these tools requires comprehensive study, computation and construction of each specific case.

There are a lot of factors influencing hob milling process. The great number of factors and their interactions make investigation of wear process difficult. They are h_i - width of concentrated wear on the transition between outlet flank and tip of tooth, h_t - width of wear zone along the blade, h_u - width of concentrated wear on the transition between inlet flank and tip of tooth (Figure 2).

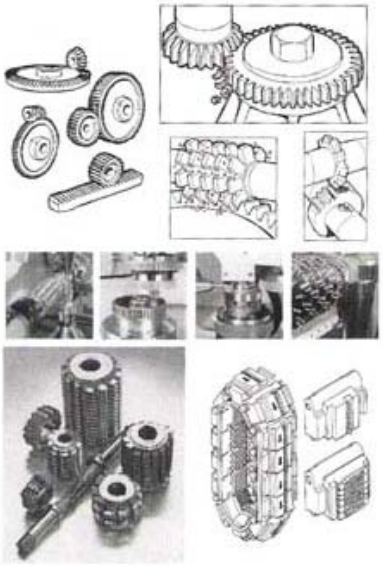

Figure 1. Products with serration and tools for serration processing

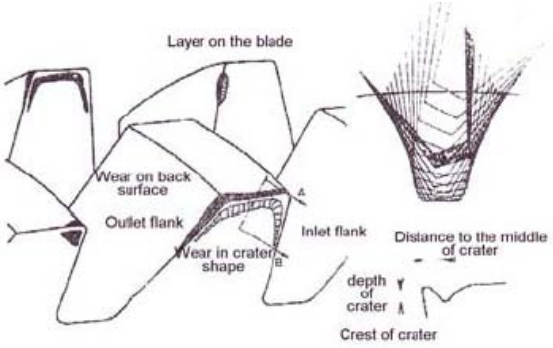

Figure 2. Distribution of wear

In Figure 3, the factors influencing wear during hob milling process are given. In the Figure 4 the possible reasons for fracture of gear hob tooth are shown. Three parameters of wear on the back-surface of tool can be defined. As above mentioned, there are numerous geometric parameters of gear hob and cutting geometry which are very important for hob milling process. Rake-angle, radial relief-angle and radius of face of a tooth as elements of cutting geometry have also influence on the development of wear process of gear hob. It can be concluded that is very important to determine optimal values of rake-angle, radial relief-angle and radius of face of a tooth. In this paper, on the basis of experimental investigations, mentioned parameters will be determined using genetic algorithm.

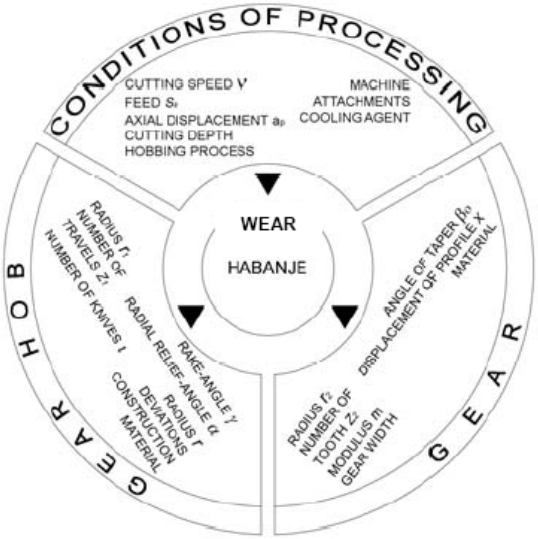

Figure 3. Factors influencing wear during hob milling process

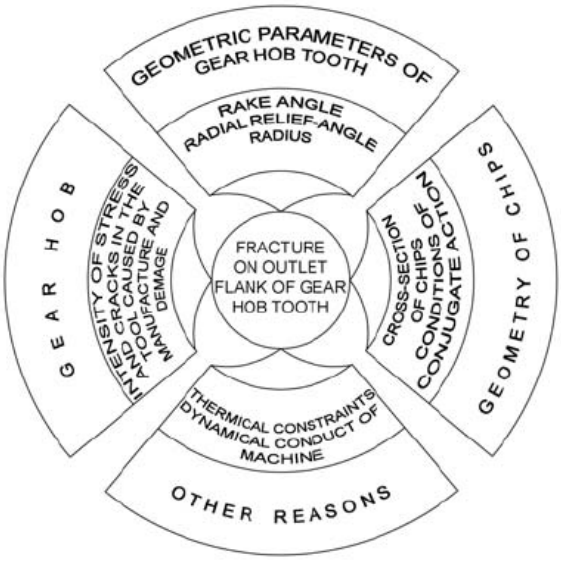

Figure 4. Possible reasons for fracture of gear hob tooth

2. DETERMINATION OF TOOL LIFE FUNCTION AND OPTIMAL GEOMETRIC PARAMETERS USING GENETIC ALGORITHM

Optimization is defined as a science which is occupied with determination of "the best" solution of a mathematical defined problem. Aim of optimization is to minimize negative effects (efforts, costs etc.) or to maximize positive effects (gains). Basic notions of techno-economical optimization are: aims, objects, methods and conditions (Figure 5).

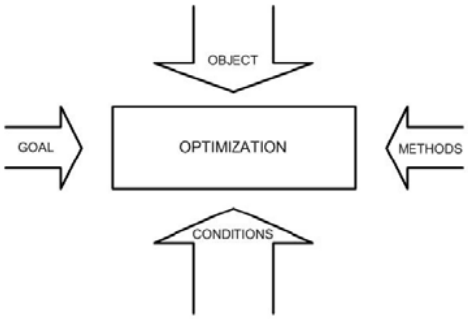

Figure 5. Basic notions of techno-economical optimization

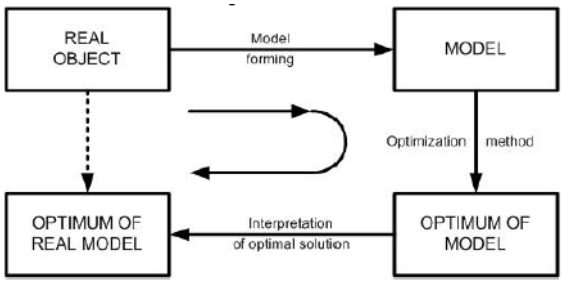

Figure 6. Optimization scheme of real object

Optimization aim is presented through the optimization criteria or optimization function (fitness function). This aim on the observed object is realized by some optimization method. Forming of mathematical model of given object represent important and often the most difficult phase in the decomposed optimization process. In the Figure 6, a scheme of real object optimization using model is given. Mathematical model has to be reliable; it describes features of some object approximately reflecting the most important characteristics of given real object.

Taking into consideration the character of optimization problems and available data at the beginning of optimization process, in this paper genetic algorithm is chosen for solving the problem. Genetic algorithm consists of several steps whose performing lead to the solution of optimization problem. In the Figure 7, the structure of genetic algorithm is shown.

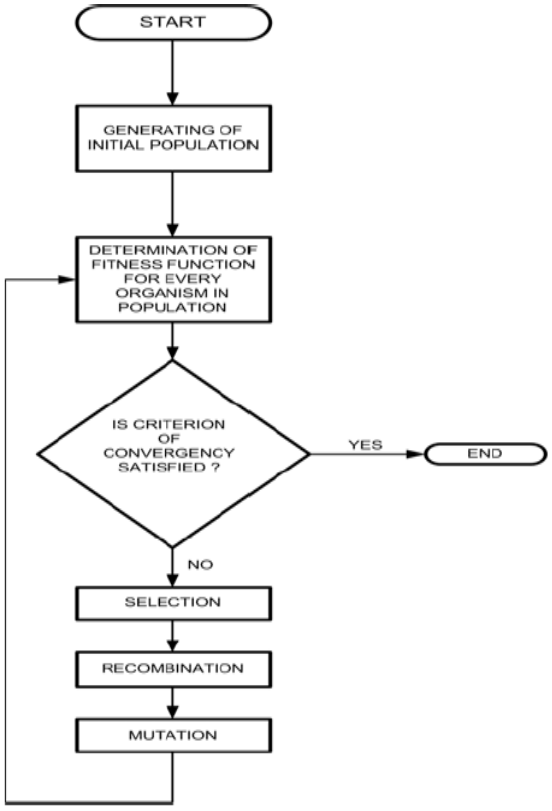

Figure 7. Structure of genetic algorithm

In this paper, in order to model the tool life function L of a single tooth gear hob, the model of second order was used:

$$L = k_o + k_1\gamma + k_2\alpha + k_3 r + k_4\gamma\alpha + k_5\gamma r + k_6\alpha r + \\ + k_7\gamma\alpha r + k_8\gamma^2 + k_9\alpha^2 + k_{10} r^3. \quad (1)$$

Optimization aim using genetic algorithm is to obtain values of coefficients k_o, k_1, k_2, k_3, k_4, k_5, k_6, k_7, k_8, k_9, k_{10}, such that the difference between experimental and predicted values should be minimal.

First step in the determination of an appropriate model using genetic algorithm is to generate initial population P(t) randomly. Population P(t) consists of organisms. Every organism represents one of the possible problem solutions and it contains genes that are real constants: k_o, k_1, k_2, k_3, k_4, k_5, k_6, k_7, k_8, k_9, k_{10}.

The absolute deviation D(i,t) of individual model i (organism) in generation time t was introduced as the fitness measure. It is defined as:

$$D(i,t) = \sum_{j=1}^{n} \left| E(j) - P(i,j) \right|, \quad (2)$$

where E(j) is the experimental value for measurement j, P(i,j) is the predicted value returned by the individual model i for measurement j, and n is the maximum number of measurements. Equation (2) is standard raw fitness measure for solving regression problems proposed by Koza [13]. The aim of the optimization task is to find such model that equation 2 would give an as low absolute deviation as possible. However, because it is not necessary that the smallest values of the above equation also means the smallest percentage deviation of this model, the average absolute percentage deviation of all measurements for individual model i is defined as:

$$\Delta i = \frac{D(i,j)}{\left| E(j) \right| \cdot n} \cdot 100\% . \quad (3)$$

After generating the initial population, iterative procedure of genetic operations (reproduction, crossover and mutation) applies to individuals until convergence criteria would not be satisfied. Two parents are selected randomly and they create their two offspring in the crossover operation. Crossover enables to exchange information between different potential solutions. In this paper decade encoding and real arithmetic crossover is applied. Crossover is performed between two parental genes with identical indexes. These parental genes are selected randomly, too. Offspring genes are formed as:

$$OFFSPTRING1 = \frac{\lambda_1 \cdot PARENT1 + \lambda_2 \cdot PARENT2}{2};$$

$$OFFSPTRING2 = \frac{\lambda_2 \cdot PARENT1 + \lambda_1 \cdot PARENT2}{2} \quad (4)$$

Coefficients λ_1 and λ_2 are selected randomly in the range [0.1].

After crossover, the next operation is mutation. One individual is selected randomly and one of its genes, which will be altered, is also selected. Mutation introduces new genetic material into population. Initial population which consists of 100 organisms was generated randomly. In the initial generation values of coefficients [k_0, k_{10}] were selected in the range [-10, 10] randomly.

In order to mitigate negative features of elitism and to accelerate performing of genetic algorithm in the great extent, probability of reproduction is 0.1. In this paper tournament selection is applied to select potential parents. Probability of recombination is 0.3. Within tournament selection participants of the tournament can also be participants of some other tournament. In other words, an individual which was not the best individual in the tournament can be as an selected individual for recombination in some other tournament until 30% of population which give their offspring would not be selected. Recombination of only one gene realizes between 10% pairs of

individuals and in 90% recombination carries out on several genes.

Probability of mutation is 60%. Mutation of only one gene realizes at 50% individuals and remaining individuals have mutation on more than one gene. Procedure of civilization generating was developed to 5,000-th generation and then it was stopped temporary. If the average deviation Δ(i) of assumed model (organism) in the population is less than 4% evolution of population would be continued to 20000-th generation. On the contrary, process would be stopped. After each phase of training the accuracy of the best models is tested with the help of initial data. Five independent civilizations were used during modeling.

3. EXPERIMENTAL RESULTS

Investigations were carried out on the gear hob machine MODUL-ZFWZ-250X5AVE produced by STARKSTROM - Anlagenbau, KarlMarx, Germany. In the investigations, special designed and constructed single tooth tool manufactured at Faculty of Technical Sciences in Novi Sad was used (Figure 8).

Figure 8. Single tooth gear hob

Optimization of geometric parameters of cutting tool precedes internal optimization, i.e. optimization of cutting regimes. In order to determine the optimal cutting geometry, it is necessary to provide rational working conditions. In other words, it is needed to determine cutting speed, feed and axial displacement in order to carry out experimental investigations of cutting tool geometry.

Obtained experimental results are shown in the Table 1. For each experimental point, values of characteristic wear (h_u, h_t, h_i) are obtained by measurements. On the basis of analysis, wear criterion of single tooth tool was adopted. It is width of wear zone on the outlet flank h_i=0.6 mm. For each experimental point, the curves of wear process development are drawn. In Figure 9, the curve for the fourth experimental point is given.

4. ANALYSIS OF OBTAINED RESULTS

Using genetic algorithm some possible models satisfying the chosen criterion, were obtained. Therefore, they represent a potential solution of the problem.

Table 1. Experimental conditions and obtained results

REGIME OF PROCESSING					
v = 98.125(m/min), sa = 2.0(mm/ob), ap = 0.63(mm), b = 54mm					
MO Č4721					
h_i=0.6(mm)					
Order of experiment realization	Number of experimental points	Cutting geometric parameters			Experimental results of
		g[o]	a[o]	r (mm)	L(m)
1	7	0	20	0.75	73
2	4	0	8	0.55	29
3	1	12	8	0.55	39
4	6	12	20	0.75	99
5	15	6	14	0.65	64
6	2	12	20	0.55	68
7	3	0	20	0.55	60
8	18	3	15	0.63	79
9	5	12	8	0.75	41
10	16	6	17	0.66	91
11	17	4	16	0.65	91
12	8	0	8	0.75	39
13	14	6	14	0.818	60
14	20	7	18	0.67	93
15	10	16.092	14	0.65	53
16	13	6	14	0.482	48
17	19	8	18	0.7	93
18	12	6	24.092	0.65	81
19	11	6	3.908	0.65	34
20	9	-4.092	14	0.65	41

The characteristics of one of these models of tool life function are:

$$\begin{aligned} L_{opt} &= 3.47514 + 4.84292\gamma + 0.00449625\alpha + \\ &+ 23.1512r - 0.195747\gamma\alpha - 5.9446\gamma r + \\ &+ 0.36683\alpha r + 0.323794\gamma\alpha r - 0.0495238\gamma^2 + \\ &+ 0.0859158\alpha^2 + 18.7778r^2 \end{aligned} \quad (5)$$

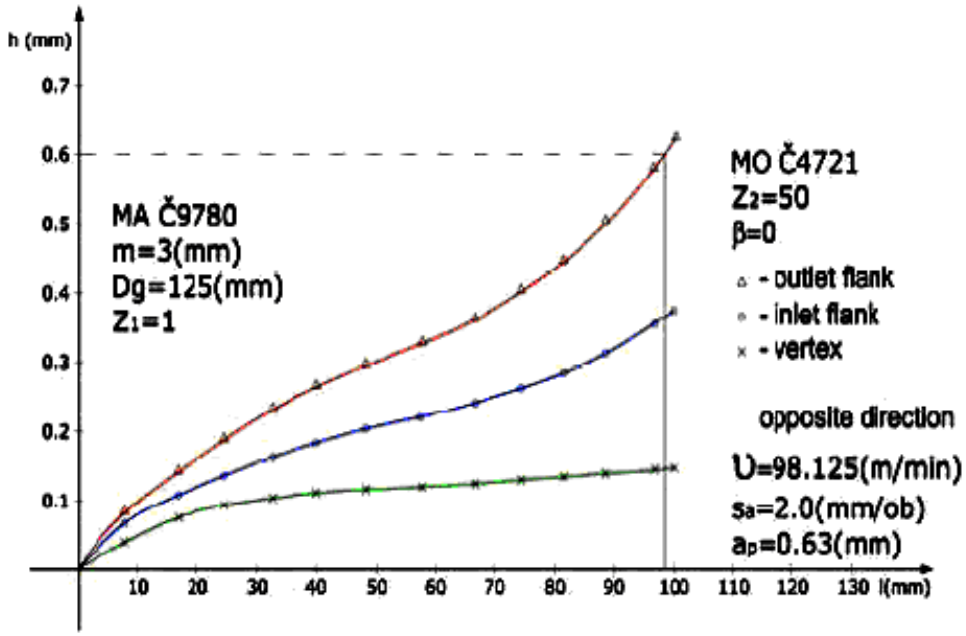

Figure 9. Development of wear process on single tooth gear hob

Table 2. Experimental values of tool life and predicted values of tool life

Order number of measurement	Experimental results	Results predicted by model	D (i)	Δ (i)
1	73.000	71.360	1.640	2.247
2	29.000	29.037	-0.037	0.128
3	39.000	39.091	-0.091	0.234
4	99.000	80.146	18.854	19.045
5	52.000	52.025	-0.025	0.048
6	68.000	67.891	0.109	0.161
7	60.000	60.380	-0.380	0.633
8	41.000	41.140	-0.140	0.342
9	39.000	39.137	-0.137	0.350
10	60.000	59.985	0.015	0.025
11	53.000	52.942	0.058	0.109
12	48.000	45.124	2.876	5.991
13	81.000	88.396	-7.396	9.131
14	34.000	33.154	0.846	2.487
15	41.000	41.019	-0.019	0.047

Total absolute difference of the best individual is 40.977. The deviation of the best individual in percentages: 2.7318. The generation with the best individual: 18885.

In Table 2, the experimental obtained values of tool life and the model predicted values of tool life are given. Also, absolute values and percentage values of the difference between experimental and predicted results are shown. Predicted results refer to the best individual in the generation. On the basis of shown results one can see that the deviation between experimental and predicted results is less than 10% in all measurements, except in the fourth measurement. In some measurements this deviation is less than 1%.

Because of this significant difference of successfulness Δ(i) between fourth measurement and the others, it can be concluded there is some possibility for existence of errors during the measurement, manifesting in tool and working piece materials, human factor, vibrations of machine tools and some other stochastic disturbances. Also, on the basis of this difference of Δ(i) it can be concluded that a quality of solution obtained using genetic algorithm depends on the reliability of the data which are used in the optimization.

In Figure 10, the diagram showing the tendency of organism improvement through the generations is given. On the diagram one can see that the successfulness of the best organism increases rapidly at the beginning, in other words the values of successfulness measure decrease rapidly. After 1500 generations this trend starts to decrease more and more, and it exceeds into stagnation. Finally, it achieves the largest successfulness in the 18,885-th generation in which the organism with average deviation Δ(i,t)=2.7318% was obtained.

After achievement of the largest successfulness, it decreases. Identical value of the largest successfulness will appear in later generations again, but the number of its appearance is almost insignificant with constant tendency to successfulness reduction, i.e. increasing of Δ(i).

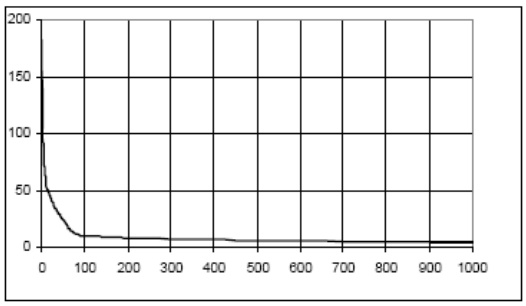

Figure 10. Average percentage deviation of the best models

Variety of individuals in the population was very large with permanent oscillating in all generations (Figure 11). On the basis of the best model, the determination of maximum tool life and optimal geometric parameters was performed.

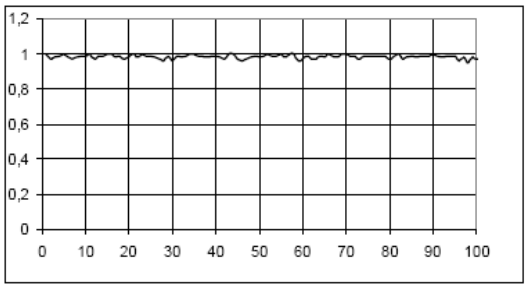

Figure 11. Variety curve of the population

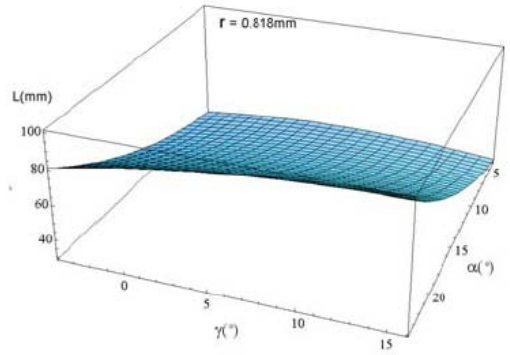

Figure 12. Dependence of tool life on geometrical parameters of gear hob

Using mathematical methods maximal tool life L=105.836 mm was determined. Geometric parameters that provide global maximum for the given model are r = 0.818 mm, α = 24.092º, γ = 16.092º.

5. CONCLUSION

There are numerous controlled and uncontrolled factors influencing hob milling process. Because of these factors this kind of processing is very complex.

The great number influencing factors and the interaction among these make difficult to investigate and define mathematically the process of hob milling.

Optimization of fitness function using genetic algorithm needs much less information about fitness function and it does not need satisfying of some conditions like classical methods, for instance function differentiability and continuity. In this paper the optimal geometry of blade was researched. Obtained results enable the construction, manufacture and application of gear hobs which give better techno-economical effects.

REFERENCES

1. Brezočnik, M., 2000, Uporaba genetskega programiranja v inteligentnih proizvodnih sistemih, Fakulteta za strojništvo, Maribor.

2. Koza, J.R., 1992, *Genetic programming*, The MIT Press: Massachusetts.

3. Sovilj-Nikić, I., 2007, Primena genetskog algoritma u optimizaciji geometrijskih parametara odvalnog glodala, Diplomski-master rad, Fakultet tehničkih nauka, Novi Sad.

ISSN 1220 - 8434

ACTA TRIBOLOGICA
Volume 17, (2009), 58-62

Antonio TACHE[1]

Carmen TACHE[2]

[1] PETROM SERVICE S.A. Bucharest,
ROMANIA
[2] VALAHIA University of Targoviste,
ROMANIA

THERMAL ASPECTS REGARDING THE DRILLING PROCESS

The more important parameters for understanding the problem of tool wear are the contact pressure distribution and the real contact area.
When hard particle slide on the edge of the cutting tool, the plastic deformation appear and make microwaves as results of the contact pressure. The contact area it is establish and the contact pressure decrease when is obtain the limit fatigue strength (ps). At this stress, the external force is taking over by elastic deformation.
Beginning to the proposed model, when a hard particles sliding to the edge of the cutting too, it is determined the variation of some parameters: contact pressure, the critical attack angle, global wear intensity.
Keywords: drilling process, heat flux, work piece, cutting tool

1. INTRODUCTION

When two surfaces are in contact and when contacting asperities are in relative motion, an amount of mechanical work is required to over come in friction.

Most of this frictional work transforms into heat during a sliding contact. The temperature at the sliding interface rises due to the work done by the external force.

The temperature distribution is a function of the speed, load, material properties, the surface topography and the environment.

The temperature rise due to frictional contact also changes the material properties. In general, material field strength decreases as temperature increases.

When the normal load acting at the interface is large and the contact pressure is very large, the real area of contact is nearly equal to the apparent area of the contact and the heat transfer is one dimensional.

This situation exists at the chip tool interface in metal cutting. If surface fielding causes material to flow and results in chip wear, the tribocutting mechanism can be defined.

The concept of energy partition was developed by Block (1938) [1]. The fraction of heat generated at the sliding interface goes into each one of the sliding bodies.

Major sources of energy dissipated in cutting are shear energy in work piece and friction energy of chip with the tool and the work piece with the tool [2].

Usually, the theoretical models not considering the friction between drill flank surface and work piece.

The temperature distribution in each body due to the heat conducted into the solid it is assumed that the interfacial temperature is the same for both bodies [3].

This paper proposes analyze of the heat fluxes repartition on the chip-work piece-drill, during the cutting process.

2. THE HEAT REPARTITION BETWEEN WORK PIECE AND CHIP

For analyze the energy partition between tool, chip and work piece, it is considered the following cutting model (Figure 1).

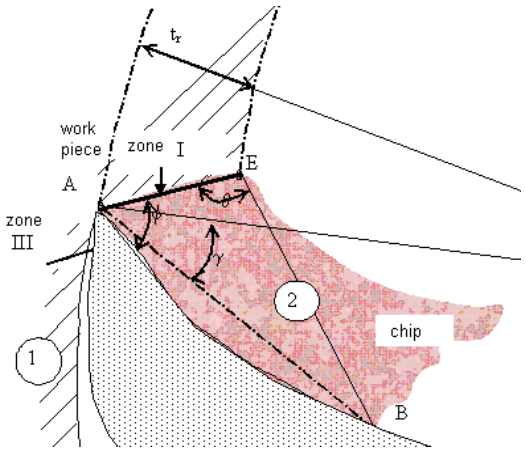

Figure 1. Cutting model by drilling

Considering ε_I as the fraction from the energy generated in the shearing area I that dissipates through chip, then $(1-\varepsilon_1)q_1$ is the fraction which dissipates through work piece [2,4]. The growth of chip's medium temperature $(T_{2-1}-T_0)$ due to mechanical work generated in the shearing plane is determined from the condition of thermo-conductibility of a part of the heat through chip:

$$T_{2-1} = \frac{\varepsilon_I q_1}{\rho_2 c_2 v_2} + T_0 = \frac{\varepsilon_1 u_s}{\rho_2 c_2} + T_0, \quad (1)$$

where v_2 is the speed of the chip, ρ_2 is the density of the chip's material, c_2 is the specific heat, $(\rho_2 c_2)$ volumetric specific heat and T_0 is the environment temperature.

It is defined the temperature parameter T_{a21}:

$$T_{a21} = T_{2-I}\frac{\rho_2 c_2}{\varepsilon_I f_H \tau_f} = \frac{\sin(\varphi+\gamma)}{(1-0.5t_{ar})t_{ar}} EA_a . \quad (2)$$

Therefore, in Figure 2 it is presented the variation of the temperature parameter T_{a21} in relation with the adhesion coefficient f.

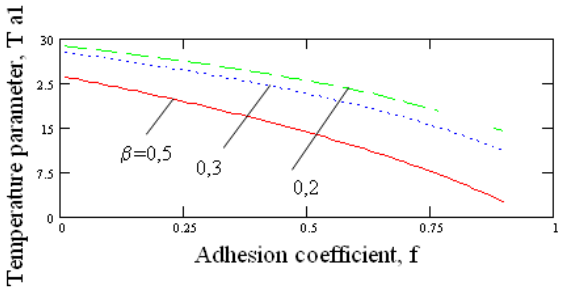

Figure 2. Variation of adhesion coefficient with T_{a1}

The equation of the thermal energy for the heat conduction in the work piece has the following form:

$$\frac{\partial^2 T_1}{\partial y^2} = \frac{1}{a_1}\frac{\partial T_1}{\partial t}, \quad (3)$$

where: T_1 is the temperature, y is the Cartesian coordinate of the work piece, (Figure 3), t time, and a_1 is the thermal diffusivity of the work piece material, $a_1 = \lambda_1/\rho_1 c_1$ (ρ_1- worked material density, c_1-worked material specific heat).

The heat source from the shearing plane AE is mobile related to the work piece during the drilling process. The medium speed can be developed as a function of the angular speed of the drill (ω), the current radius on the conic area of the cutting edge (r) and the relative radial advance ($t_a = t_r/r$) or $t_{aR}=t_r/R$.

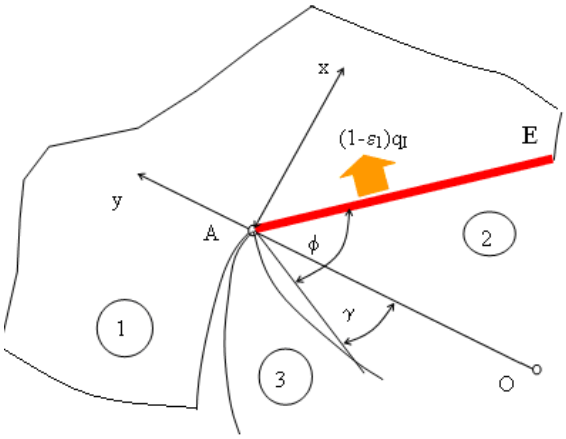

Figure 3. The contact between work piece (1), drill (3), chip (2)

$$v_m = r\omega(1-0.5t_a) = V(r_a - 0.5t_{aR}), \quad (4)$$

where: V is the circumferential speed of the drill; R – external radius of the drill; r_a- radius of the current point in the conic area; t_{aR}-relative advance.

Thereby, during time t, the heat source is advancing along x direction with the space:

$$x = v_m t, \quad (5)$$

and equation (3) becomes:

$$\frac{\partial^2 T_1}{\partial y^2} = \frac{v_m}{a_1}\frac{\partial T_1}{\partial x}. \quad (6)$$

The increasing of the temperature due to mobile source AE (Figure 3) can be calculated by integrating the differential equation (6).

For the points on the work piece which are placed right in the vicinity of the AE surface, the following interrelation can be written:

$$x = y \cdot tg(\varphi - \gamma). \quad (7)$$

In this case, the solution of equation (6) is:

$$T_1 = s_1 e^{m_1 y} + s_2, \quad (8)$$

where: $m_1 = \frac{v_m \rho_1 c_1}{\lambda_1} tg(\varphi-\gamma)$, s_1 and s_2 constant parameters which can be evaluated from the following limit conditions:

$$\lambda_1 \left.\frac{\partial T_1}{\partial y}\right|_{y=0} = -(1-\varepsilon_I)q_I; \quad (9)$$

$$T_1\big|_{y=t_{r1}} = T_0. \quad (10)$$

Temperature spreading in the worked piece, on AE surface, is:

$$T_1 - T_0 = \frac{-(1-\varepsilon_1)q_1}{v_m c_1 \rho_1 \cot an(\varphi-\gamma)}\left[e^{m_1 y} - e^{m_1 t_r}\right]. \qquad (11)$$

Maximum temperature occurs at surface $y = 0$.

For the shearing plane, the work piece temperature is equal with the chip's temperature. In this hypothesis (Block Hypothesis) by equalizing (2) and (11) equations, partition factor of the thermal energy ε_1 can be determined:

$$\varepsilon_1 = \frac{A}{1+A}, \qquad (12)$$

where A is the geometrical and thermal dimensionless parameter of the drilling process:

$$A = \frac{\rho_2 c_2}{\rho_1 c_1}\frac{t_r}{AE} tg(\varphi-\gamma) e^{m_1 t_r}\left(e^{m_1 y - m_1 t_r} - 1\right). \qquad (13)$$

Lubrication state of the drill, evaluated by the chip-cutting tool adhesion coefficient (f), is significantly influencing the heat partition coefficient (Figure 4). Also here is to be highlighted a maximum of the partition coefficient, function of f, for different points on the shearing plane.

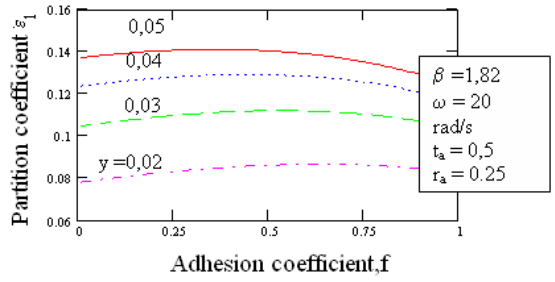

Figure 4. Variation of partition coefficient ε_1 function of f

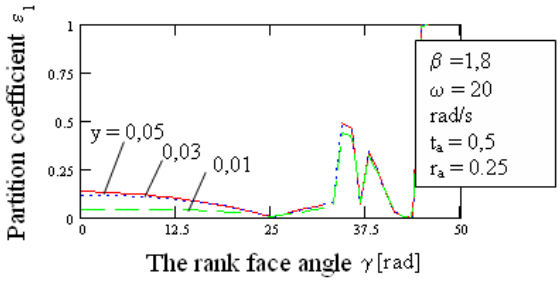

Figure 5. Variation of partition coefficient ε_1 function of γ

The strongest influence on the partition coefficient of the heat, generated in the chip creation plane, belongs to the chip bearing surface angle (γ). This variation is shown in Figure 5. Is to be noticed that for angles above 26°, the partition coefficient is rapidly increasing and it doesn't depend on point's position on the shearing plane.

Concurrently, from Figure 5, it is noticeable that for higher values of the bearing surface angle, the coefficient of partition of the heat generated in the shearing plane, in the chip, has several maximums and minimums.

This theoretical oscillatory variation is demonstrating the possibility that chip is not created in certain geometrical conditions, material and adhesion characteristics of the chip. A fake "peak" creation is possible, and obviously, with another "pseudo-chip".

3. THE HEAT REPARTITION BETWEEN CHIP AND DRILL

The friction couple between the chip and the drill's spire is a contact with both elements of the couple in movement, but with relative movement, because the chip's speed is different, as vector quantity, from the centrifugal speed of the drill's spire in selected points.

In this case the hypothesis considered to be correct is of the thermal effect of a mobile source (the chip), with sliding speed equals to the difference between chip's speed and drill's spire speed. Heat source is of a rectangular shape, dimensioned $d=d_1+d_2$ (Figure 1) and the conic length of the edge.

Sliding speed of the chip relative to the drill, in a considered point on the conic edge of the drill represents exactly the chip's medium speed.

If ε_{II} is the fraction from q_{2m} which penetrates the chip, the augmentation of the temperature can be determined using the temperature equation for a rectangular shaped source.

For the chip-drill spire contact, the medium temperature can be calculated using equations [5]:

$$T_{2-3} = \frac{\varepsilon_{II}\cdot q_{2m}\cdot d}{2\lambda_2}\left(\frac{v_{mas}\cdot d}{2a_2}\right)^{-1/2} + T_0, \qquad (14)$$

when $v_t = \frac{v_{mas}\cdot d}{4a_2} > 10$, where v_t is the speed parameter and a_2 – thermal diffusivity at the chip's material.

$$T_{2-3} = 0.95\frac{\varepsilon_{II} q_{2m} d}{2\lambda_2} + T_0, \qquad (15)$$

when $v_t < 0.5$.

From thermal point of view, the chipping speed can be considered high when v_t >10, low, when v_t<0.5 and moderate for speed parameters between 0.5 and 10.

If chip's medium speed (v_{mas}) and contact length of the chip with drill's spire are inputted into speed parameter expression (v_t), for some point on the conic area (r_a), can be obtained the drill's centrifugal speed, named cutting speed, wherefore the thermal regime is considered high, low, or medium:

$$v_{bM} = \frac{40\,a_2}{R \cdot v_{mas} \cdot d}. \qquad (16)$$

In Figure 6 it is shown the fluctuation of the cutting speed function of adhesion coefficient f.

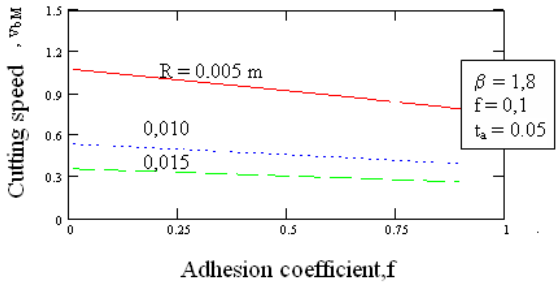

Figure 6. Variation of cutting speed v_{bM} function of f

By no dimensioning the chip's surface temperature (14) or (15) in relation with peripheral (circumferential) speed of the drill, and with thermo-physical characteristics of the worked material, is to be obtained:

$$T_{a23} = \frac{T_{23}\lambda_2}{\varepsilon_{II} R^2 \omega \tau_f} = \frac{1}{2} q_{a2m} A B_a r_a v_t^{-1/2}, \qquad (17)$$

for $v_t \geq 10$;

$$T_{a23} = \frac{T_{23}\lambda_2}{\varepsilon_{II} R^2 \omega \tau_f} = \frac{0,95}{2} q_{a2m} A B_a r_a \quad , \qquad (18)$$

for $v_t \leq 0.5$.

For speed parameters between the two limits (10 şi 0.5) is proposed a linear variation of the dimensionless temperature T_{a23}.

From this condition, it is deducted the linear expression of the temperature:

$$T_{a23} = (299.838 - 29.968 v_t)\, q_{a2m} A B_a r_a, \qquad (19)$$

for $0.5 \leq v \leq 10$.

In Figure 7 it is presented the variation of the dimensionless chip temperature T_{a23} function of adhesion coefficient, f.

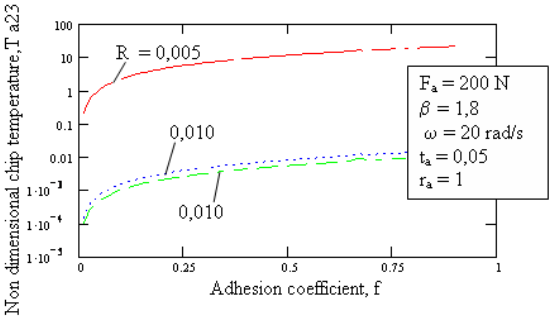

Figure 7. Variation of non-dimensional chip temperature T_{a23} function of f

The medium temperature of the chip's surface being in contact with cutting tool's face, is given by the sum of the medium temperature of the whole chip ($T_{2\text{-}1}$), generated by the heat in the shearing plane, and the medium temperature of the surface ($T_{2\text{-}3}$), generated by the friction between chip and the drill's spire. Thus,

$$T_2 = T_{2-1} + T_{2-3} = \\ = T_{a2-1} \frac{\varepsilon_I f_H \tau_f}{\rho_2 c_2} + T_{a2-3} \varepsilon_{II} R^2 \omega \tau_f \,/\, \lambda_2. \qquad (20)$$

The thermal regime of the drill can be determined considering the chip as the heat source. For the drill's spire, the heating source is stationary. In this hypothesis, the temperature is determined with the solution provided by Carlslow and Jaeger [2], [6]:

$$T_3 = 0.95(1-\varepsilon_{II}) q_{2m} \frac{d}{2\lambda_3} + T_{0'}, \qquad (21)$$

where $T_{0'}$ is the environment temperature.

By a dimensioning, this temperature will have the form:

$$T_{a3} = \frac{T_3 \lambda_2}{(1-\varepsilon_{II}) R^2 \omega \tau_f} = \frac{0,95}{2} q_{a2m} A B_a r_a. \qquad (22)$$

Equalizing the medium temperature of the chip's surface (20) with drill's spire surface temperature, (21) and considering the adimensioning, it is deducted the heat fraction generated by friction between the chip and the drill (ε_{II}), in the chip [7]:

$$\varepsilon_{II} = \frac{T_{a3} - T_{a2-1} \dfrac{\varepsilon_I \cdot f_H}{\rho_2 \cdot c_2} \dfrac{\lambda_2}{R^2 \omega}}{T_{a2-3} + T_{a3}}. \qquad (23)$$

The variation of this factor in relation with the adhesion coefficient is graphically shown in Figure 8.

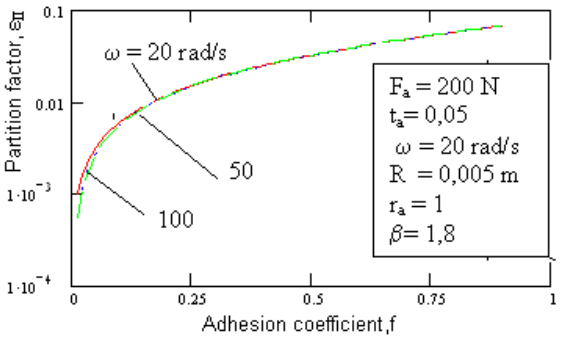

Figure 8. Variation of partition factor ε_{II} function on f

Figure 9 represents the fluctuation of the partition coefficient ε_{II} function of the angular speed ω.

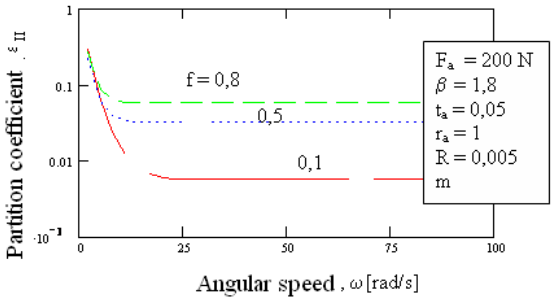

Figure 9. Variation of partition factor ε_{II} function on ω

4. CONCLUSIONS

1. Heat flow generated in the chip creation area decreases with the drill's sharpening angle and with the adhesion coefficient, and increases with the angle of departure.

2. The relative speed of the chip in relation with the variable peripheral (circumferential) speed of the drill is the main source of the heat flow generated at the chip-chip bearing surface interface.

3. Heat flow between the chip and the chip bearing surface decreases with the cutting angle and it has a maximum with the chip-drill adhesion coefficient variation.

4. It was defined and deducted the heat partition factor between the work piece and the chip and between the chip and the drill, for Block hypothesis.

5. The heat partition factor proves the statistical weight of heat spreading through chip, for different geometries of the drill (angle of throat, angle of clearance) and different work conditions (drill rotation speed, adhesion state).

REFERENCES

1. Carslaw, H.S., Jaeger, J.C., 1959, *Conduction of heat in Solids*, Oxford, at the Clarendon Press.

2. Suh, N.P., 1986, *Tribophysics*, Prentice-Hal, Englewood Cloffs.

3. Bos, J., Moes, H., 1995, "Frictional Heating of Tribological Contacts," *Journal of Tribology*, vol.117, pp. 263-268.

4. Tudor, A., Tache, C., 1999, "Friction Energy Partition in the Cutting Process," *Proc. of Intern. Conf. on Coatings in Manufacturing Engineering*, October 14-15, Thessaloniki, Greece.

5. Bos, J., Moes, H., 1995, "Frictional Heating of Tribological Contacts," *Journal of Tribology*, vol. 117, pp. 263-268.

6. Tian, X., Kennedy, F., E., 1994, "Maximum and Average Flash Temperatures in Sliding Contacts," *ASME Journal of Tribology*, vol. 116, pp. 167-174.

7. Tache, I.A., 2006, PhD Thesis, Universitatea Politehnica Bucuresti, Facultatea de Mecanica si Mecatronica, pp. 92-116.

ISSN 1220 - 8434

ACTA TRIBOLOGICA
Volume 17, (2009), 63-68

Leonard PASTRAV
e-mail: *cezar.pastrav@mech.kuleuven.be*

Siegfried JAECQUES
e-mail: *siegfried.jaecques@mech.kuleuven.be*

Michiel MULIER
e-mail: *michiel.mulier@uz.kuleuven.be*

Georges VAN DER PERRE
e-mail: *georges.vanderperre@mech.kuleuven.be*

Catholic University of Leuven,
BELGIUM

THE DETECTION OF INSERTION ENDPOINT AND STABILITY ASSESSMENT OF CEMENTLESS HIP STEMS BY VIBRATION ANALYSIS: A PER-OPERATIVE PILOT STUDY

The stability of an implant in bone is directly related to the quality of the contact at the bone-implant interface. The assessment of the primary stability of cementless implants still remains a subjective factor in total hip replacement (THR) and, as a consequence, the excessive press-fitting of a THR component can be the cause of intra-operative fractures. Objective information about the stability of implant-bone structures can be obtained using methods based on vibration analysis. After extensive in vitro studies a per-operative protocol was designed to detect the insertion endpoint and/or to assess the stability of custom made hip prostheses. The frequency response function evolution during the hip stem insertion in the femur was studied. The experiments were performed in per-operative conditions.
Keywords: cementless hip implant, implant-bone contact, implant stability, vibration analysis, frequency response function

1. INTRODUCTION

Initial stability seems to be very important for any prosthetic implant but the objective assessment of this parameter for cementless hip stems remains a challenge. Surgeons rely mainly on experience to evaluate the extent of stem stability and the insertion end point. Excessive press-fitting of a total hip replacement (THR) component, Figure 1, can cause intra-operative fractures with an incidence of up to 30% in revision cases [1].

Different methods based on vibration analysis have been successfully used to determine bone mechanical properties in vitro as well as in vivo [2-6], to monitor the fracture healing [7-9], to quantify fixation of dental implants [10,11], and to assess mechanical properties of the hip stem/femur structure, both in vitro and in vivo [12-16].

In a previous study [17], it was confirmed that the imperfections in the contact between a THR prosthetic stem and a femur can most sensitively be detected by observing shifts in the resonance frequency of the higher vibration modes of the femur/prosthesis system. This observation is in agreement with the work of Qi et al who state that the most sensitive frequency band for observing defects in the femur/prosthesis contact is placed above 2500 Hz [18].

Figure 1. Total Hip Replacement (THR)

An experimental study [19] performed on artificial human femora (Sawbone® nr. 3306, Left Large Composite Femur, www.sawbones.com) has shown that the evolution of the frequency response function (FRF) can be used to detect the insertion end point as well.

This paper presents the per-operative protocol derived from the previous in vitro studies and partial results obtained in a pilot experimental study performed in per-operative conditions.

2. MATERIALS AND METHODS

The per-operative protocol was designed to detect the insertion endpoint and/or to assess the stability of cementless custom made hip prostheses (Advanced Custom Made Implants, Leuven, Belgium). The surgeon inserts the implant in the femoral canal through hammer blows. After each blow, the FRF of the implant-bone structure is measured directly on the prosthesis neck in the range 0-12.5 kHz. Only the 0-10 kHz interval is used for analysis. The FRF change indicates stiffness evolution of the implant-bone structure and, as a consequence, the implant stability evolution. The hammering is stopped when the FRF graph does not change noticeably anymore. Extra blows will not improve prosthesis stability but will increase fracture risk.

The prosthesis neck is attached to a shaker (Bruel & Kjaer model 4810) using a stinger provided with a clamping system. The excitation is realized by white noise in the range 0-12.5 kHz. The input force and the response acceleration are measured with an impedance head (PCB Piezotronics model nr 288D01) mounted between the shaker and the stinger. The experimental setup is shown in Figure 2.

The FRF was measured and recorded by a Pimento vibration analyzer (LMS International) connected to a portable computer provided with the appropriate software (Pimento 5.2, LMS International).

The vibration analyzer generates the excitation signal which is amplified and sent to the shaker. The vibration analyzer, the portable computer and the amplifier were installed in the surgical theatre but outside the so-called laminar flow area, Figure 3. Different insertion stages are shown in Figure 4.

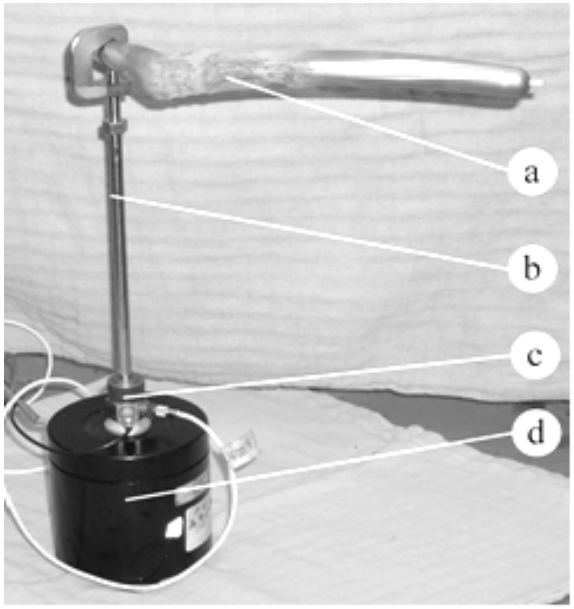

Figure 2. Experimental setup
(a) hip stem, (b) stinger and clamping system, (c) impedance head, (d) shaker

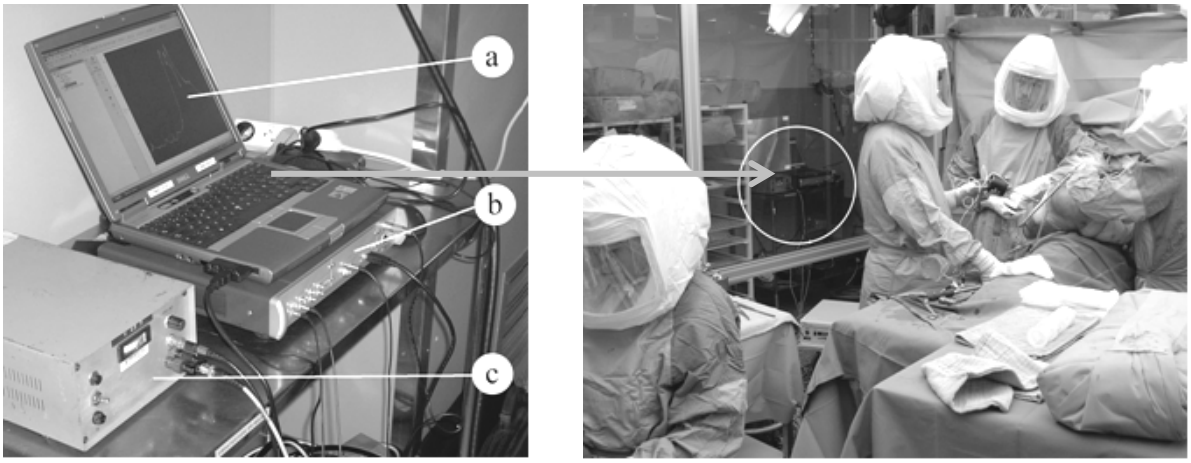

Figure 3. Measuring hardware (left) and surgical theatre (right)
(a) portable computer, (b) vibration analyser Pimento, (c) power amplifier

The Pearson's correlation coefficient was used to compare the similarity of two FRF graphs. Due to the fact that there is no linear dependence of one graph with respect to the other, the two graphs are identical if the correlation coefficient is 1.

The normalized cross correlation function calculated between two successive FRF graphs was used to assess the direction and the magnitude of the FRF graph shift. The abscissa of the maximum value of the cross correlation function indicates the displacement direction.

A positive value means that the current FRF graph is shifted to the right with respect to the previous FRF graph. The maximum value of the cross correlation function indicates the similarity of the two FRF graphs. When two graphs are identical, the cross correlation function becomes the autocorrelation function and its normalized maximum has the coordinates $x = 0$ and $y = 1$.

Volunteer patients were included in this study after informed consent and approval by the institutional review board.

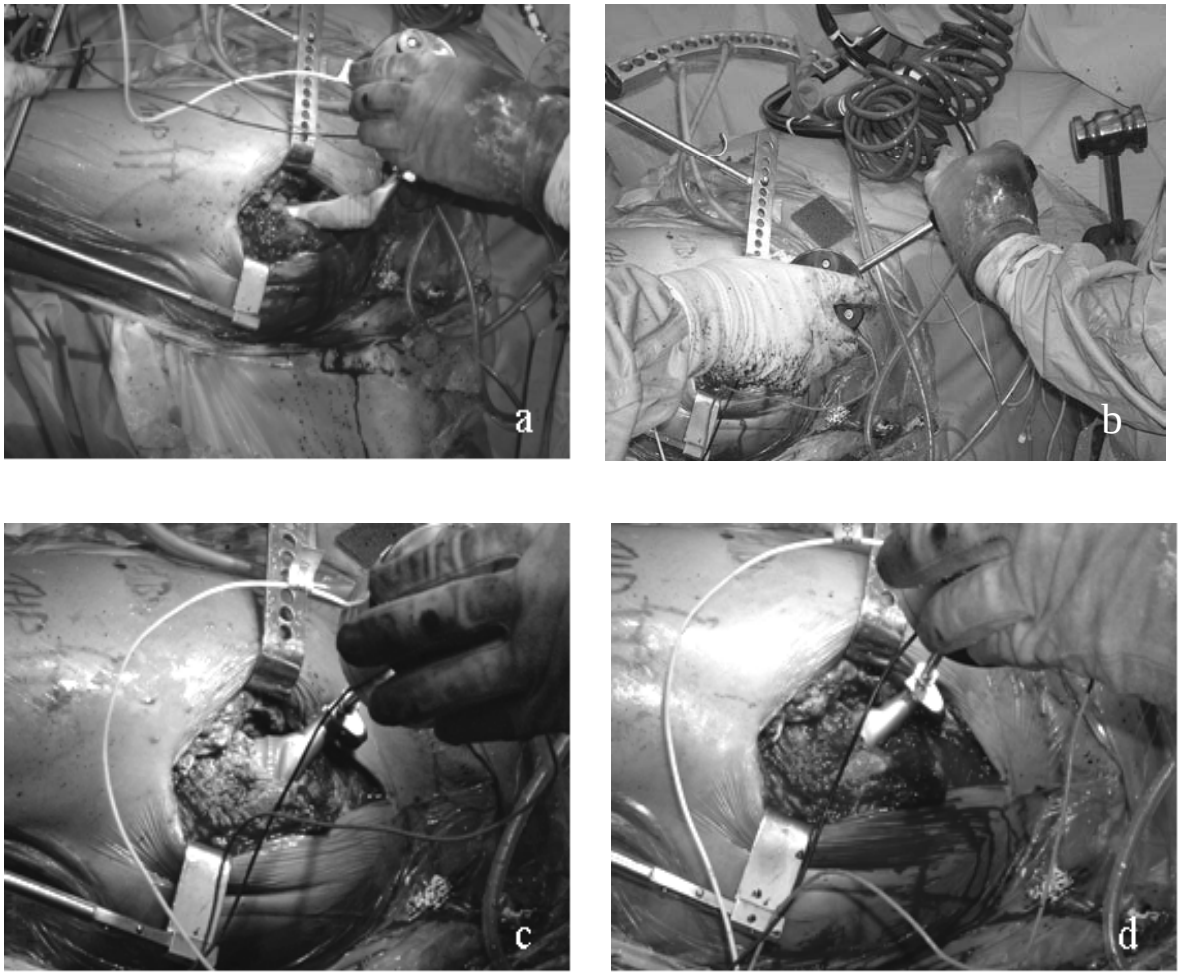

Figure 4. Hip stem insertion
(a) the beginning, (b) hammering, (c) an intermediate stage, (d) the final stage

3. RESULTS

Eleven cases of cementless stems were studied and a typical example is presented in Figure 5. Figures 5.a to 5.d show the FRFs calculated for two successive insertion stages. Stage 0 corresponds to the FRF calculated after the stem was introduced in femur by hand. Stage 1 corresponds to the FRF calculated after the first hammer blow series, stage 2 after the second hammer blow series and so on. The surgeon needed 5 stages (0…4) to completely insert the stem in this case.

The evolution of Pearson's correlation coefficient (R) calculated for two successive FRFs is represented in Figure 5.e. The normalized cross correlation function was also calculated for the last three successive FRF pairs and presented in Figure 5.f. The evolution of the maximum values of the cross correlation function can be observed in Figure 5.g. Figure 6 shows a similar case with four insertion stages (0…3).

The final Pearson's correlation coefficients calculated for all the eleven cementless cases are shown in Table 1.

During the insertion procedure, changes of boundary conditions and implant stability between different stages are reflected by the FRF evolution and the most sensitive frequency band is above 4 kHz.

Table 1. Pearson's correlation coefficients calculated between FRFs corresponding to the final two insertion steps

Case number	1	2	3	4	5	6	7	8	9	10	11	Average
R	0.997	0.999	0.992	0.999	0.999	0.998	0.955	0.998	0.964	0.994	0.999	**0.990**

* In cases 7 and 9, the insertion was stopped early because of suspected bone fragility.

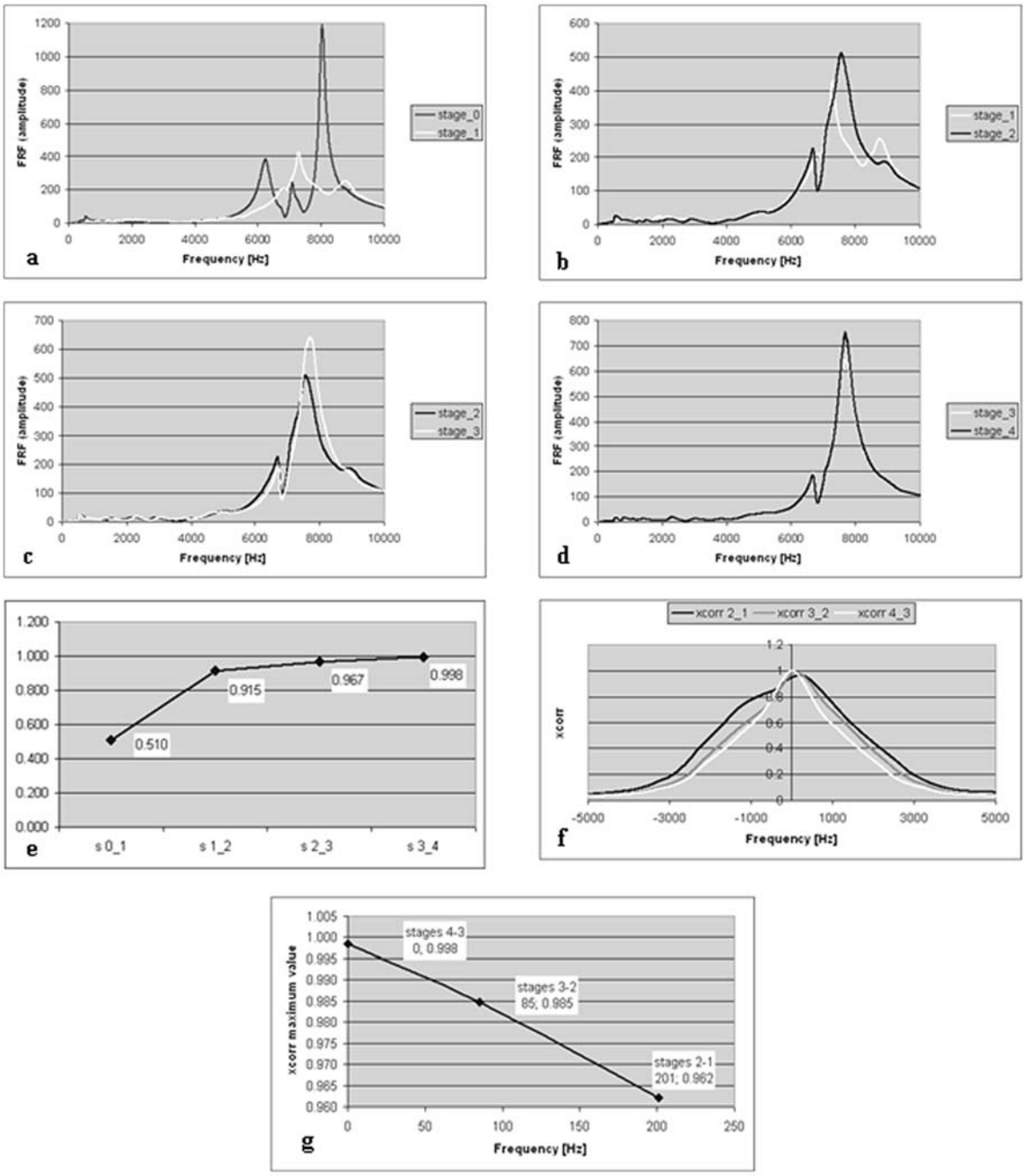

Figure 5. Cementless stem (example case 1)
(a-d) FRF graphs for successive insertion steps; (e) Pearson's correlation coefficients for the FRF pairs of Figures 5.a-5.d; (f) Normalized cross correlation functions calculated for the FRF pairs represented in Figures 5.b-5.d; (g) Maximum values of the cross correlation functions represented in Figure 5.f

4. DISCUSSION AND CONCLUSIONS

The structures analyzed in this study are composed of stinger, hip stem and femur. Since during the insertion process the single variable element is the contact between the stem and the femur, a logical conclusion would be that the resonance frequencies of the studied structures are influenced only by this variable.

A FRF shift to the right indicates an increasing stiffness [20] of the stem-bone connection, thus an increasing stability of the implant. If the FRF does not change between two successive insertion stages, then the mechanical properties of the structure did not change by the additional hammer blows, thus the stem-bone connection is stable and the insertion end point is reached.

During the operation, the surgeon corroborates the information obtained by direct visual and tactile observation, with the information furnished by vibration analysis, in order to take optimal decisions.

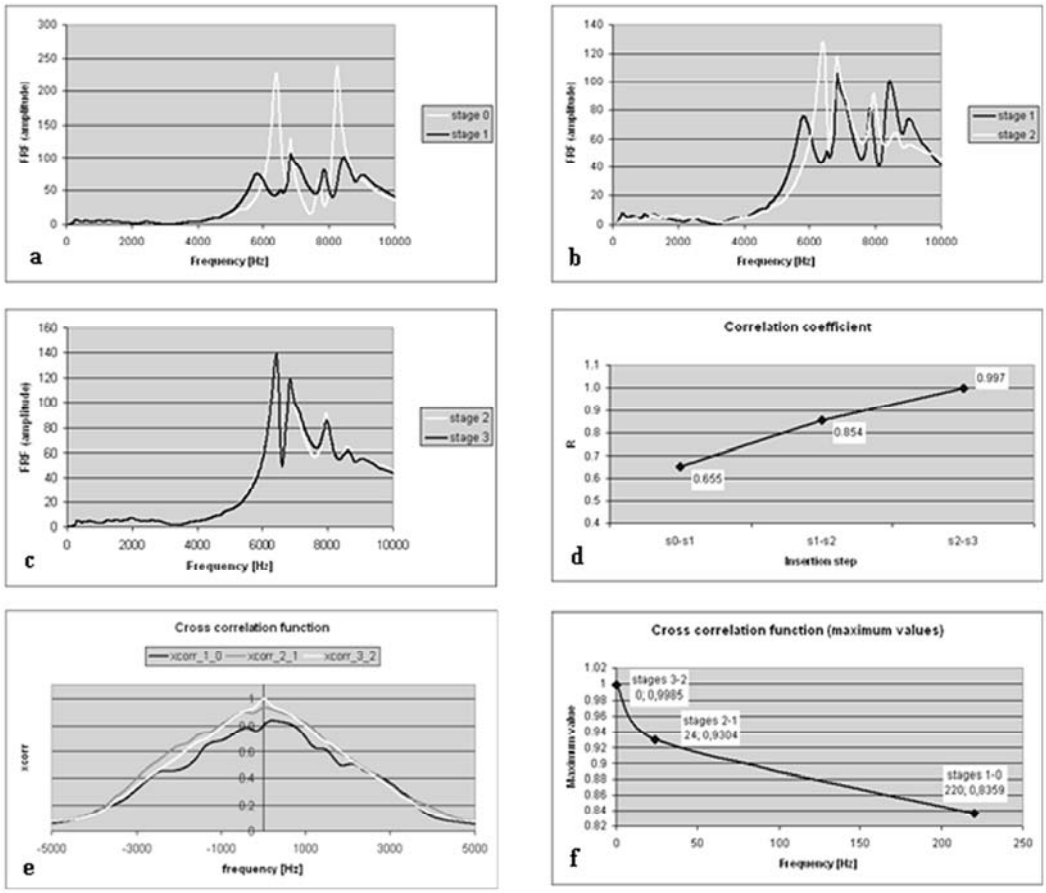

Figure 6. Cementless stem (example case 2)
(a, b, c) FRF graphs for successive insertion steps; (d) Pearson's correlation coefficients calculated for the FRF pairs represented in Figures 6.a-6.c; (e) Normalized cross correlation functions calculated for the FRF pairs represented in Figures 6.a-6.c; (f) Maximum values of the cross correlation functions represented in Figure 6.e

In a previous in vitro study [21] the criterion $R=(0.99 \pm 0.01)$ of Pearson's correlation coefficient between FRFs for successive insertion stages was used as a quantitative threshold to stop the cementless stem insertion process. In per-operative conditions, the correlation coefficient between the last two FRFs was above 0.99 when the surgeon stopped the insertion, in nine of eleven cases, (Table 1). In the other two cases, when the surgeon decided to stop the insertion because of suspected bone fragility, the final correlation coefficient reached lower values (0.955 and 0.964, as underlined in Table 1).

Although the FRF evolution is a good indication concerning the stability evolution, in some cases the FRF graph changes are complex and difficult to evaluate directly, like in Figure 6.b. However, the cross correlation function graphs presented in Figures 5.f and 6.g indicate a general shift of the FRF graph to the right after each insertion stage, except for the last one when the FRF graph did not show any noticeable changes in its shape and position.

Custom made hip stems are designed to fit and fill as much as possible the femoral cavity to obtain a good stability. Their geometry is variable depending on the patient's femur characteristics. This variability complicates the comparison between the stabilities of different stems and the establishment of a general scale to evaluate the stability and further evolution of custom hip implants. However, the follow-up of patients as part of an ongoing clinical study, and the analysis of a large number of FRF graphs could allow a classification depending on stem geometry, femur properties and implant-bone contact characteristics. The final FRF graphs are not an absolute indication of stability, but represent important information concerning the best stability that could be obtained in each case.

ACKNOWLEDGEMENTS

This research was partially funded by K.U.Leuven research council (project OT/03/31). Hip prostheses provided by courtesy of Advanced Custom Made Implants, Belgium.

REFERENCES

1. Meek, R. M., Garbuz, D. S., Masri, B. A., Greidanus, N. V., and **Duncan, C.P.,** 2004, "Intraoperative Fracture of the Femur in Revision Total Hip Arthroplasty with a Diaphyseal Fitting Stem," *J. Bone Joint Surg [Am]*, 86A(3):480-5.

2. Lowet, G., Van Audekercke, R., Van Der Perre, G., Geusens, P., Dequeker, J., and **Lammens, J.,** 1993, "The Relation Between Resonant Frequencies and Torsional Stiffness of Long Bones in Vitro. Validation of a Simple Beam Model," *J. Biomechanics*, 26, pp. 689-696.

3. Lowet, G., Van Der Perre, G., 1996, "Ultrasound Velocity Measurement in Long Bones: Measurement Method and Simulation of Ultrasound Wave Propagation," *J. Biomechanics*, 29: 1255-1262.

4. Nokes, L. D. M., 1999, "The Use of Low-Frequency Vibration Measurement in Orthopaedics," *Proc. Instn. Mech. Engrs*., 213H: 271-290.

5. Van Der Perre, G. and **Lowet, G.,** 1996, "In Vivo Assessment of Bone Mechanical Properties by Vibration and Ultrasonic Wave Propagation," *Bone*, 18:29S-35S.

6. Roberts, S. G., Hutchinson, T. M., Arnaud, S. B., Kiratli, B. J., Martin, R. B., and **Steele, C. R.,** 1996, "Noninvasive Determination of Bone Mechanical Properties Using Vibration Response: A Refined Model and Validation in Vivo," *Journal of Biomechanics*, 29(1): 91-98.

7. Van der Perre, G., 1985, "Monitoring of Fracture Healing by Vibration Analysis and Other Mechanical Methods," (Eds. G. Van der Perre and A. Borgwardt-Christensen), *Proceedings of the Specialists Consensus Meeting*, Leuven.

8. Nikiforidis, G., Bezerianos, A., Dimarogonas, A., Sutherland, C., 1990, "Monitoring of Fracture Healing by Lateral and Axial Vibration Analysis," *J. Biomechanics*, 23:323-330.

9. Nakatsuchi, Y., Tsuchikane, A., Nomura, A., 1996, "Assessment of Fracture Healing in the Tibia Using the Impulse Response Method," *Journal of Orthopaedic Trauma*, 10 (1): 50-62.

10. Meredith, N., Shagaldi, F., Alleyne, D., Sennerby, L., Cawley, P., 1997, "The Application of Resonance Frequency Measurements to Study the Stability of Titanium Implants during Healing in the Rabbit Tibia," *Clinical oral implant research*; 8: 234-243.

11. Pattijn, V., Van Lierde, C., Van der Perre, G., Naert, I., Vander Sloten, J., 2006, "The Resonance Frequencies and Mode Shapes of Dental Implants: Rigid Body Behaviour Versus Bending Behaviour. A Numerical Approach," *Journal of Biomechanics*, 39 (5): 939-947.

12. Van der Perre, G., 1984, "Dynamic Analysis of Human Bones," *Functional Behaviour of Orthopedic Biomaterials*, Vol I: P. Ducheyne and G.W. Hastings, Eds., CRC Press, Boca Raton, 99-159.

13. Rosenstein, A. D., McCoy, G. F., Bulstrode, C. J., McLardy-Smith, P. D., Cunningham, J. L., and **Turner-Smith, A. R.**, 1989, "The Differentiation of Loose and Secure Femoral Implants in Total Hip Replacement Using a Vibrational Technique: An Anatomical and Pilot Clinical Study," *Proc. Instn. Mech. Engrs.*, 203: 77-81.

14. Collier, R. J., Donarski, R. J., Worley, A. J., and **Lay, A.,** 1993, "The Use of Externally Applied Mechanical Vibrations to Assess Both Fractures and Hip Prosthesis," *Micromovement in Orthopaedics*, A.R. Turner-Smith, Ed., University Press, Oxford, 151-163.

15. Li, P. L. S., Jones, N. B. and **Gregg, P. J.,** 1996, "Vibration Analysis in the Detection of Total Hip Prosthetic Loosening," *Med. Eng. Phys*.; 18: 596-600.

16. Georgiou, A. P., and **Cunningham, J. L.,** 2001, "Accurate Diagnosis of Hip Prosthesis Loosening Using a Vibrational Technique," *Clinical Biomechanics*, 16: 315-323.

17. Jaecques, S. V. N., Pastrav, C., Vegehan, E., and **Van der Perre, G.,** 2004, "Analysis of the Fixation Quality of Cementless Hip Prostheses Using a Vibrational Technique," *Proceedings of ISMA2004 International Conference on Noise and Vibration Engineering*, September 20 - 22, Eds. P. Sas and M. De Munck, K.U. Leuven, Belgium, ISBN 90-73802-82-2, pp. 443-456.

18. Qi, G., Mouchon, W. P., and **Tan, T. E.,** 2003, "How Much can a Vibrational Diagnostic Tool Reveal in Total Hip Arthroplasty Loosening," *Clinical Biomechanics*, 18: 444-458.

19. Pastrav, L. C., Jaecques, S. V. N., Deloge, G., Mulier, M., and **Van Der Perre, G.,** 2005, "A System for Intra-Operative Manufacturing and Stability Testing of Hip Prostheses," *Proceedings of XIIIth International Conference on New Technologies and Products in Machines Manufacturing and Technologies* (TEHNOMUS XIII), May 6-7, University "Stefan cel Mare", Suceava, Romania, Published by University of Suceava, Ed. I. Dumitru, ISBN 973-666-154-7, pp. 505-510.

20. Heylen, W., Lammens, S., and **Sas, P.,** 1997, *Modal Analysis Theory and Testing*, Katholieke Universiteit Leuven, Departement Werktuigkunde, Leuven.

21. Jaecques, S., Pastrav, L. C., Mulier, M. and **Van der Perre, G.,** 2005, "Determination of THR Stem Insertion Endpoint by Vibrational Analysis," R. Cabral, M. Cassiano Neves, C. Camilo, Eds., *Transactions of the EORS*, Vol. 15, p. 92, ISBN:90-9018444-9, published by Soc. Portuguesa de Ortopedia e Traumatologia.

ACTA TRIBOLOGICA VOLUME 17, 2009

CONTENTS